



UNIVERSITEIT VAN PRETORIA
UNIVERSITY OF PRETORIA
YUNIBESITHI YA PRETORIA

MSC 422

2013

Samantha Ayres

10261720

Supervisor: Professor J.P. Meyer

THE
INFLUENCE OF
SURFACE
ROUGHNESS
ON THE
TRANSITIONAL
FLOW REGIME



INDIVIDUAL COVER SHEET FOR PRACTICALS / INDIVIDUELE DEKBLAD VIR PRAKTIKA

Module code / Modulekode: MSC 422		Module: PROJECT	
Practical number: Praktikum nommer:		Date of submission: Datum van inhandiging: October 2013	
Student / Student	Initials / Voorletters SR	Surname / Van AYRES	Student number / Studentenommer 10261720

<p>Declaration:</p> <p>1. I understand what plagiarism is and am aware of the University's policy in this regard.</p> <p>2. I declare that this practical report is my own, original work.</p> <p>3. I did not refer to work of current or previous students, memoranda, solution manuals or any other material containing complete or partial solutions to this assignment.</p> <p>4. Where other people's work has been used (either from a printed source, Internet, or any other source), this has been properly acknowledged and referenced.</p> <p>5. I have not allowed anyone to copy my work/report.</p>	<p>Verklaring:</p> <p>1. Ek begryp wat plagiaat is en is bewus van die Universiteitsbeleid in hierdie verband.</p> <p>2. Ek verklaar dat hierdie praktikumverslag my eie, oorspronklike werk is.</p> <p>3. Ek het nie gebruik gemaak van huidige of vorige studente se werk, memoranda, antwoord-bundels of enige ander materiaal wat volledige of gedeeltelike oplossings van hierdie werkstuk bevat nie.</p> <p>4. In gevalle waar iemand anders se werk gebruik is (hetsy uit 'n gedrukte bron, die Internet, of enige ander bron), is dit behoorlik erken en die korrekte verwysings is gebruik.</p> <p>5. Ek het niemand toegelaat om my werk/verslag te kopieer nie.</p>
<p>Signature of Student Handtekening van Student</p>	

ECSA OUTCOME 4: INVESTIGATIONS, EXPERIMENTS AND DATA ANALYSIS		Max mark	Mark awarded	Yes	No
Did the student:					
1	Plan and conduct his/her investigation/experiment in an appropriate and scientific manner?	10		√	×
2	Perform the necessary analyses and interpretations and/or derived valid information from the data?	50		√	×
3	Draw conclusions based on the evidence or data obtained?	20		√	×
4	Communicate the purpose, process and outcomes/conclusions in a technical report in a coherent manner?	20		√	×
Total for outcome 4 (minimum of 50% to pass)		100			
Is the student capable of applying research methods, planning and conducting investigations and experiments using appropriate equipment – if the answer is "NO" a mark of less than 50% must be awarded				√	×

Marked by	
Signature	
Date	

Abstract

Title: The influence of surface roughness on the transitional flow regime.

Author: S. Ayres

Student number: 10261720

Supervisor: Professor J.P. Meyer

Year: 2013

The transitional flow regime is the region where the Reynolds number changes from laminar to turbulent flow. In round tubes, this region exists between Reynolds numbers of 2 100 and 2 300. Very little information exists currently, to accurately predict the heat transfer, and flow instability and uncertainties exist in this region. The purpose of this study was to accurately take heat transfer and pressure drop measurements at different heat fluxes for water in order to determine the effect of surface roughness on the transitional flow regime. The heating mode used was a constant heat flux, and a square inlet configuration was used. A simulation was performed to determine an applicable diameter which is suitable for experimentation, in order to determine the effect of surface roughness. Experiments were then conducted between Reynolds numbers of 1 125 to 12 700, at Prandtl numbers between 6.25 and 8.1. This was performed on heat fluxes from 5 600 to 11 300 W/m². The surface roughness of the tube was 0.6 mm. It was concluded that surface roughness decreases the heat transfer coefficient and thus the Nusselt number. The transition region occurs much earlier in a roughened tube. Friction factor results could not be found due to faulty equipment and thus pressure drop measurements could not be taken.

Acknowledgements

I would like to thank Professor J.P. Meyer for his guidance and supervision throughout this research project. I would like to also thank Nicola Kotzé, Thabang Mofokeng and Marelize Everts for their help with this project.

Table of Contents

Abstract.....	i
Acknowledgements.....	ii
List of Figures.....	vi
List of Tables.....	viii
Nomenclature.....	ix
Greek Letters.....	x
Subscripts.....	x
Chapter 1.....	1
Introduction.....	1
1.1 Background.....	1
1.2 Previous Work.....	2
1.3 Problem Statement.....	2
1.4 Objective.....	3
1.5 Scope of Work.....	3
1.6 Outlay of Report.....	3
Chapter 2.....	5
Literature Study.....	5
2.1 Introduction.....	5
2.2 Numbers.....	5
2.3 Types of Inlets.....	7
2.4 Work by Ghajar.....	9
2.5 Work by Meyer.....	14
2.6 Conclusion.....	18
Chapter 3.....	19
Design.....	19
3.1 Introduction.....	19
3.2 Calculations.....	19
3.3 Simulation.....	21
3.4 Experimental Design.....	22
3.5 Experimental Setup.....	23
3.8 Conclusion.....	31
Chapter 4.....	32

Data Analysis and Validation.....	32
4.1 Introduction	32
4.2 Data Reduction.....	32
4.3 Data Acquisition	35
4.4 Validation	36
4.5 Uncertainties.....	37
4.6 Conclusion	37
Chapter 5.....	38
Results.....	38
5.1 Introduction	38
5.2 Smooth Tube Results	38
5.3 Validation	45
5.4 Rough Tube Results.....	46
5.5 Comparison between smooth and rough tube.....	54
5.6 Summary, Discussion and Conclusions	55
Chapter 6.....	58
Summary, Conclusions, Recommendations and Limitations.....	58
6.1 Summary	58
6.2 Conclusions	58
6.3 Recommendations	60
6.4 Limitations.....	61
References	62
Appendix	A1
Appendix A: Protocol	A1
Appendix B: Protocol/Research Project Compliance Matrix	B1
Appendix C: Progress Reports.....	C1
First Progress Report.....	C1
Second Progress Report	C2
Appendix D: Meeting Log.....	D1
Appendix E: Sample Calculations	E1
Smooth Tube.....	E1
Rough Tube	E3
Insulation	E4
Appendix F: Spreadsheet Examples.....	F1

Appendix G: Data Sheets	G1
Appendix H: Article	H1

List of Figures

Figure 1: Square-edged inlet.....	7
Figure 2: Re-entrant inlet.....	8
Figure 3: Bell-mouth inlet	8
Figure 4: Fully developed inlet.....	8
Figure 5: Schematic of calming section.....	24
Figure 6: Thermocouple placement along the tube	26
Figure 7: Wrapping of the test section showing how crossing over of the thermocouple stations was performed	26
Figure 8: Pressure tap	27
Figure 9: Location of pressure taps.....	27
Figure 10: Schematic of the experimental setup.....	29
Figure 11: Test section	30
Figure 12: Thermocouple placement (A to M).....	30
Figure 13: Mean fluid temperatures and surface temperatures along a tube for the case of a constant surface heat flux.....	33
Figure 14: Comparison between adiabatic experimental results and existing correlations	36
Figure 15: Graph of local Nusselt number versus position along the smooth tube for various Reynolds number. This graph shows the results of the 5 600 W/m ² surface heat flux test.	39
Figure 16: Graph of local Nusselt number versus position along the smooth tube for various Reynolds number. This graph shows the results of the 8 300 W/m ² surface heat flux test.	40
Figure 17: Graph of local Nusselt number versus position along the smooth tube for various Reynolds number. This graph shows the results of the 11 300 W/m ² surface heat flux test.	41
Figure 18: Graph of average Nusselt number versus Reynolds number for the smooth tube for three different heat fluxes: 5 600, 8 300 and 11 300 W/m ²	42
Figure 19: Graph of average Nusselt number versus Reynolds number for the smooth tube for two different heat fluxes: 5 600 and 11 300 W/m ²	42
Figure 20: Temperature distributions for 5 600 W/m ² smooth tube test, at a Reynolds number of 1 125.	43
Figure 21: Temperature distributions for the 5 600 W/m ² smooth tube test, at a Reynolds number of 8 650.	43
Figure 22: Temperature distributions for the entire temperature scale, for the 5 600 W/m ² smooth tube test, at a Reynolds number of 8 650.	44
Figure 23: Graph of Colburn j-factor as a function of Reynolds number for the smooth tube. The heat fluxes depicted on the graph are 5 600 and 11 300 W/m ²	44
Figure 24: Heat transfer validation for the smooth tube for a heat flux of 5 600 W/m ²	46
Figure 25: Graph of local Nusselt number versus position along the rough tube for various Reynolds number. This graph shows the results of the 5 600 W/m ² surface heat flux test.	47
Figure 26: Graph of local Nusselt number versus position along the rough tube for various Reynolds number. This graph shows the results of the 8 400 W/m ² surface heat flux test.	48
Figure 27: Graph of local Nusselt number versus position along the rough tube for various Reynolds number. This graph shows the results of the 11 200 W/m ² surface heat flux test.	49
Figure 28: Graph of average Nusselt number versus Reynolds number for the rough tube for three different heat fluxes: 5 600, 8 400 and 11 200 W/m ²	49

Figure 29: Temperature distribution for 5 600 W/m ² rough tube test, for a Reynolds number of 1 280.	50
Figure 30: Temperature distribution for 5 600 W/m ² rough tube test, for a Reynolds number of 9 090.	50
Figure 31: Graph of Colburn j-factor as a function of Reynolds number for the rough tube. The heat fluxes depicted on the graph of 5 600, 8 400 and 11 200 W/m ²	51
Figure 32: Graph of Colburn j-factor versus Reynolds number for three heat fluxes, on a logarithmic scale. The heat fluxes depicted on the graph of 5 600, 8 400 and 11 200 W/m ²	52
Figure 33: Graph depicting the relationship between the measured Nusselt number and the theoretical Nusselt number for three heat fluxes. The heat fluxes on the graph are: 5 600, 8 400 and 11 200 W/m ²	53
Figure 34: Graph of average Nusselt number versus Reynolds number for the smooth and rough tubes	54
Figure 35: Graph of Colburn j-factor as a function of Reynolds number for the smooth and rough tube. The heat fluxes depicted on the graph of 5 600 and 11 300 W/m ² for the smooth tube, and 5 600, 8 400 and 11 200 W/m ² for the rough tube.	55
Figure 37: Thermal resistance of the smooth and rough tubes.....	56

List of Tables

Table 1: Typical ranges of Prandtl numbers for common fluids	6
Table 2: Reynolds number range for isothermal conditions, when considering pressure drop	10
Table 3: Transition Reynolds numbers for friction coefficient	11
Table 4: Transition region for diabatic heat transfer measurements.....	11
Table 5: Constants for correlation equation of inlet type influence	12
Table 6: Effect of heating on Reynolds number range for the transition region.....	13
Table 7: Coefficients for correlation equation.....	13
Table 8: Ranges and constants for corrected correlation equation	13
Table 9: Correlation equation ranges	13
Table 10: Transition range for different inlets (Meyer & Olivier, 2010)	15
Table 11: Properties of different enhanced tubes tested.....	15
Table 12: Reynolds number ranges for enhanced tubes with different inlet types	16
Table 13: Electrical calculations for different heat fluxes.....	25
Table 14: Property uncertainties	37
Table 15: Equipment uncertainties.....	37
Table 16: Smooth tube electrical input quantities	38
Table 17: Smooth tube energy balances.....	38
Table 18: Correlations used for heat transfer validation.....	45
Table 19: Rough tube electrical input quantities.....	46
Table 20: Rough tube energy balances.....	47

Nomenclature

A_s	Surface area	m^2
A_c	Cross-sectional area	m^2
C	Specific heat	$J/kg \cdot K$
c_f	Friction coefficient	
d, D	Diameter	m
D_h	Hydraulic diameter	m
g	Gravitational acceleration	m/s^2
Gr	Grashof number	
h	Convection heat transfer coefficient	$W/m^2 \cdot K$
I	Electric current	A
k	Thermal conductivity	$W/m \cdot K$
L	Length	m
L_c	Corrected length	m
m	Mass	kg
\dot{m}	Mass flow rate	kg/s
Nu	Nusselt Number	
p	Perimeter	m
P	Pressure	Pa
Pr	Prandtl number	
\dot{q}	Heat flux	W/m^2
Q	Total heat transfer	J
\dot{Q}	Heat transfer rate	W
$r_{c,r}$	Critical radius of insulation	m
R, r	Radius	m
R	Thermal resistance	K/W
R_c	Thermal contact resistance	$m^2 \cdot K/W$
R_f	Fouling factor	
R-value	R-value of insulation	
Ra	Raleigh number	
Re	Reynolds number	
St	Stanton number	
t	Time	s
T	Temperature	$^{\circ}C$ or K
T_b	Bulk fluid temperature	$^{\circ}C$ or K
T_s	Surface temperature	$^{\circ}C$ or K
U	Overall heat transfer coefficient	$W/m^2 \cdot K$
V	Voltage	V
V	Volume	m^3
V	Velocity	m/s
V_{avg}	Average velocity	m/s
\dot{W}	Power	W

Greek Letters

α	Thermal diffusivity	m^2/s
ΔP	Pressure drop	Pa
ΔT_{lm}	Log mean temperature difference	
ϵ	Emissivity	
ϵ	Roughness size	m
η_{fin}	Fin efficiency	
η_{th}	Thermal efficiency	
μ	Dynamic viscosity	$\text{kg}/\text{m}\cdot\text{s}$
ν	Kinematic viscosity	m^2/s
ρ	Density	kg/m^3
θ	Dimensionless temperature	

Subscripts

atm	Atmospheric
avg	Average
b	Bulk
cond	Conduction
conv	Convection
e	Exit conditions
i	Inlet, initial conditions
o	Outlet conditions
s	Surface
surr	Surroundings
sat	Saturated
sys	System

Chapter 1

Introduction

1.1 Background

Due to the increasing energy demands which are required globally, efficiencies of systems need to increase in order to ensure maximum usage of the available energy. There is an increasing need for the operation of heat exchangers in the transitional region of flow. This is due to the fact that efficiencies of the heat exchangers are increased by increasing the surface area. This causes a decrease in the flow rates in each tube which requires operation in the transitional flow regime, instead of in the turbulent flow region. This implies that the power requirements of the pump and the compressor decrease as well. Currently, there is a lack of information and knowledge concerning this region and therefore predictive methods cannot be used.

The transitional flow regime is the region in which the Reynolds number changes from laminar to turbulent flow. Generally, heat exchanger designers work outside of this region due to the instabilities and uncertainties which exist. Also, predictions cannot be made with respect to the heat transfer (represented by the Nusselt number, Nu) as a function of mass flow rate (Reynolds number, Re). Experimentation will allow for the acquisition of data and therefore relationships can be developed for the transitional flow regime. This will allow for the operation of heat exchangers in the transition region.

It is generally accepted that transition occurs between Reynolds numbers of 2 100 and 2 300 in round tubes (Cengel & Ghajar, 2011). This depends on the type of inlet used as well as the tube augmentation. Due to the uncertainty, heat exchanger designs are either equipped for laminar or turbulent flow.

Heat exchangers are used to either cool or heat a fluid by a pipe or system of pipes. Fluid flows through the pipes where heat is transferred to or from the fluid. The fluid may have a phase change where it boils or condenses (Borgnakke & Sonntag, 2009).

When considering the heat transfer with respect to heat exchangers, conduction and convection are important. Conduction is “the transfer of energy from the more energetic particles of a substance to the adjacent, less energetic ones as a result of interactions between the particles” (Cengel & Ghajar, 2011). This heat transfer mechanism involves direct physical contact, and no motion. Convection occurs as a result of the contact between a solid surface and the adjacent liquid or gas in motion. It is a combination of fluid motion and conduction. The fluid motion enhances the heat transfer. This is because the warmer and cooler areas of the fluid are brought into contact with one another, therefore creating a higher rate of conduction heat transfer, at more locations in the fluid. Convection is thus, a more efficient means of heat transfer than conduction. For this reason, heat exchangers make use of fluid flow (Cengel & Ghajar, 2011).

Convection heat transfer depends on the following properties of the fluid:

- Dynamic Viscosity μ
- Thermal Conductivity k
- Density ρ
- Specific heat c_p
- Fluid Velocity V
- Geometry and roughness of the solid surface

Important relationships exist between the Reynolds number and the Nusselt number, as well as between the Colburn 'j' factor and the pressure drop (f). These relationships are to be determined with respect to the transitional flow regime.

1.2 Previous Work

Two research groups have done significant work on heat transfer and pressure drop measurements in the transitional flow regime. They are the groups of Professor Afshin Ghajar of Oklahoma State University, and the group of Professor Josua Meyer of the University of Pretoria. Work has been done on the transitional flow regime with respect to the type of inlet, the augmentation techniques of the tube (as tube enhancements) and the use of multi-walled carbon nanotubes.

Ghajar and co-workers (Madon 1992; Tam 1994 & 1997; Cengel 2011; Tam H.K. & Tam, L.M. 2013) dealt with the effect of the inlet type on the heat transfer and pressure drop measurements when considering the transitional flow regime. Constant temperature and heating conditions were investigated. The inlet types investigated were square-edged, re-entrant and bell-mouth inlets.

Meyer and co-workers (Olivier 2010; McKrell & Grote 2012; Batema, 2012) dealt with the effect of tube augmentation on the heat transfer and pressure drop measurements. Essentially augmentation of the tube involved internal helical fins, in order to increase the surface area and therefore the heat transfer rate. These experiments were performed on square-edged, re-entrant, bell mouth and hydro-dynamically fully developed inlet types.

Meyer *et al.* (2012) dealt with the effect of multi-walled carbon nanotubes on heat transfer and pressure drop characteristics in the transitional flow regime. These multi-walled carbon nanotubes increase the thermal conductivity of the fluid, and therefore the heat transfer.

1.3 Problem Statement

All of the previous work performed on the transitional flow regime has dealt with inlet effects, the heating mode, the addition of fins (heat transfer enhancement) and nanomaterials. However, it is known that tube roughness (Cengel & Ghajar, 2011) has a significant influence on the transitional flow regime. Thus far, the influence of tube roughness on heat transfer has not been investigated. Last year an attempt was made by Everts (2012) to determine this effect in a Research Project at the University of Pretoria. The measurements could not be complete successfully as a result of instrumentation problems.

1.4 Objective

The objective of this project is to take heat transfer measurements and pressure drop measurements at different heat fluxes for water in a smooth tube and a rough tube, over the transitional flow regime. The two tube diameters should be the same and the heating mode should be a constant heat flux. The inlet should be a square edge inlet. The specific objective of this project is to determine the effect of surface roughness on the transitional flow regime. One tube will be smooth, and one will be roughened using sand.

1.5 Scope of Work

A simulation model must be developed in order to achieve the desired conditions. This simulation will determine the equipment required, and specifically, the length and diameter of the tube for the test section. This must aid an experimental set-up which can be developed and built. Experiments are to be conducted on one tube diameter. The equipment needed to build and test the experimental setup will be determined using this simulation, for example, the length of the thermocouple wire required, as well as the current flowing through these wires and the voltage drop across the test section.

Accurate heat transfer and pressure drop measurements must be taken and compared to the simulation model and any previously published results. These results will also be compared to two other students' results, which are completing the same project, but with different tube diameters. Graphs showing the relationship between Nusselt number and Reynolds number must be drawn up, as well as graphs showing the relationship between pressure drop (f) and heat transfer (Colburn 'j' factor). These graphs will be used to determine the effect of surface roughness on the transitional flow regime.

1.6 Outlay of Report

The next chapter in this report is the literature study which was performed in order to understand the theoretical background behind this project, as well as to discuss previous work which has been completed with respect to the transitional flow regime. Through this, a theoretical background was known which enabled the continuation of the research project. Chapter 3 deals with the experimental setup of this project. It discusses the calculations which were performed in order to determine what equipment is necessary for the successful construction of the test section.

Chapter 4 discusses data reduction, analysis and validation. This is an important chapter in this project because it shows which equations are used in order to obtain the required results and whether or not these results are similar to that of theory. This chapter discusses the calibration procedure.

Chapter 5 discusses the results obtained once the experiment has been performed and completed, and has graphs which show the correlations of the Nusselt number versus Reynolds number, and the friction factor versus Reynolds number. The Colburn 'j' factor is also found and discussed. The final chapter of this report, Chapter 6, discusses the conclusions from the results and the project, in its

entirety, and gives possible recommendations and limitations for this experimental investigation. The Appendix is the final section of the report and includes the protocol, compliance matrix, sample calculations, and data sheets used for this research project.

Chapter 2

Literature Study

2.1 Introduction

This literature study will discuss the research and investigations which has already been completed with respects to the transitional flow regime. A brief background will first be discussed, with respects to some of the important aspects which need to be understood when considering this transitional flow regime.

2.2 Numbers

2.2.1 Reynolds Number

The dimensionless Reynolds number was derived by Osborne Reynolds (1842 – 1912). It is essentially based on the ratio of inertia forces to viscous forces in a fluid (Cengel & Ghajar, 2011). Transition depends on many effects (for example roughness and inlet type), but primarily on the Reynolds number parameter. If the transition is occurring, intermittent turbulent fluctuations will occur in bursts. This is due to the fact that the “increasing Reynolds number causes a breakdown or instability of laminar motion” (White, 2011).

Reynolds number can be calculated using the following equation:

$$Re = \frac{\rho V d}{\mu} = \frac{V d}{\nu}$$

Laminar flow occurs at low Reynolds numbers (typically less than 1 000) and turbulent flow occurs at high Reynolds numbers (usually around 10 000). The Reynolds number at which flow becomes turbulent is termed the critical Reynolds number (Re_{cr}). This, however, is dependent on flow geometry, surface roughness and the level of fluctuations in the inlet stream (White, 2011). For the purpose of this research, the transitional region is under consideration. The transition zone occurs between 2 100 and 2 300 in round tubes.

Usually, the transition region of 2 300 – 10 000 applies to very steady flow and uniform entry flow with a round entrance.

2.2.2 Nusselt Number

The Nusselt number was found by Wilhelm Nusselt (1882-1957). It is also a dimensionless number like the Reynolds number. This number is a function of the heat transfer coefficient, and can be defined as:

$$Nu = \frac{h L_c}{k} = \frac{h D}{k}$$

This number represents the enhancement of heat transfer through a fluid layer as a result of convection relative to conduction across the same fluid layer. A larger Nusselt number ensures more effective convection. If $Nu = 1$, pure conduction exists across the fluid layer (Cengel & Ghajar, 2011).

2.2.3 The Prandtl Number

The Prandtl number was discovered by Ludwig Prandtl (1875-1953). It too is a dimensionless parameter and accounts for “the relative thickness of the velocity and thermal boundary layers” (Cengel & Ghajar, 2011). A very high thermal conductivity results in a very low Prandtl number. It is important for heat convection and can be defined as:

$$Pr = \frac{\mu c_p}{k}$$

It is essentially the ratio between molecular diffusivity of momentum and molecular diffusivity of heat or the ration between dissipation and conduction. The Prandtl number for fluids has a range between 0.01 to greater than 100 000. For gases, the Prandtl number is about 1. The table below contains Prandtl numbers for various fluids (Cengel & Ghajar, 2011).

Fluid	Pr
Liquid metals	0.004 - 0.030
Gases	0.7 - 1.0
Water	1.7 - 13.7
Light organic fluids	5 – 50
Oils	50 – 100 000
Glycerin	2000 – 100 000

Table 1: Typical ranges of Prandtl numbers for common fluids

2.2.4 Grashof Number

The Grashof Number is also a dimensionless parameter. It is the ratio between the buoyancy force and the viscosity force and is important for natural convection. The Grashof number can be defined as:

$$Gr = \frac{\beta \Delta T g L^3 \rho^2}{\mu^2}$$

The Grashof number is, in natural convection, what the Reynolds number is, in forced convection. It essentially determines whether laminar or turbulent flow exists (in natural convection).

2.2.5 Reynolds Analogy

Reynolds analogy is defined as:

$$C_{f,x} \frac{Re_L}{2} = Nu_x \quad (Pr = 1)$$

Or as:

$$\frac{C_{f,x}}{2} = St_x \quad (Pr = 1)$$

Where 'St' is the Stanton number. The Stanton number is also a dimensionless number, which is a heat transfer coefficient. It is defined as:

$$St = \frac{h}{\rho c_p V} = \frac{Nu}{Re_L Pr}$$

The modified Reynolds analogy, also known as the Chilton-Colburn Analogy is described as:

$$C_{f,x} \frac{Re_L}{2} = Nu_x Pr^{-\frac{1}{3}}$$

Or:

$$\frac{C_{f,x}}{2} = St_x Pr^{\frac{2}{3}} = j_H$$

Where j_H is termed the Colburn j-factor, also a dimensionless parameter, and was found by Allan Philip Colburn.

2.3 Types of Inlets

The type of inlet used in this application, affects the transition region from laminar to turbulent flow. The effect of the inlets will be discussed further on in this thesis; however, it is important to note the different types and their geometries.

There are three inlets which are most commonly used, the square-edge, re-entrant and bell-mouth inlet. Another type exists, the hydro-dynamically fully developed inlet. This inlet is not used often in practice. Figures are given for each type of inlet (Meyer & Olivier, 2010).

The square-edged inlet is when the tube end is flush with the tube-sheet face. This type of inlet causes a sudden contraction of the flow due to the decrease in area.

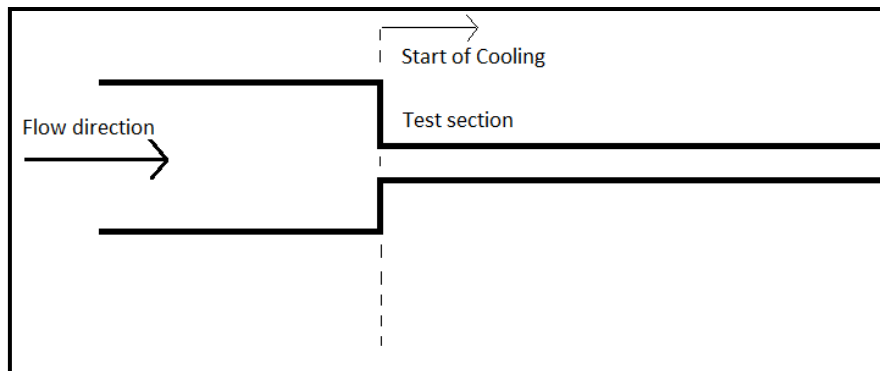


Figure 1: Square-edged inlet

The re-entrant inlet is when the tube extends beyond the tube-sheet face and into the heat or distributor. It makes use of the square-edge inlet, except with the lengthening of the tube into the inlet.

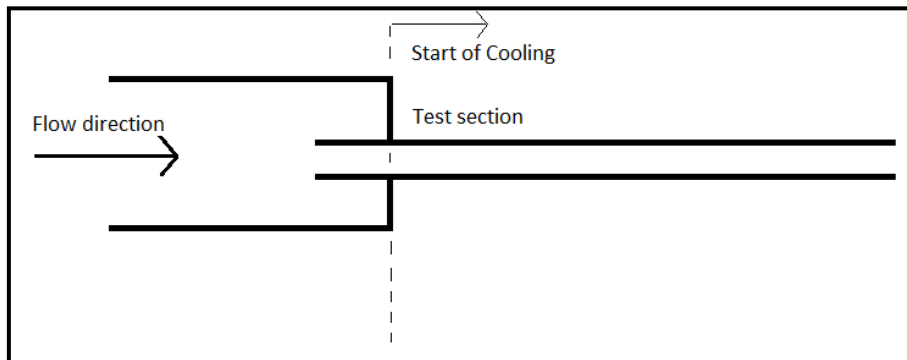


Figure 2: Re-entrant inlet

The bell-mouth inlet contains a tapered entrance of tube from the tube-sheet face, in which the cross sectional area gradually decreases. This inlet is used to reduce fouling, but it is seldom used in heat exchangers. This inlet allows for a smooth and gradual contraction of flow.

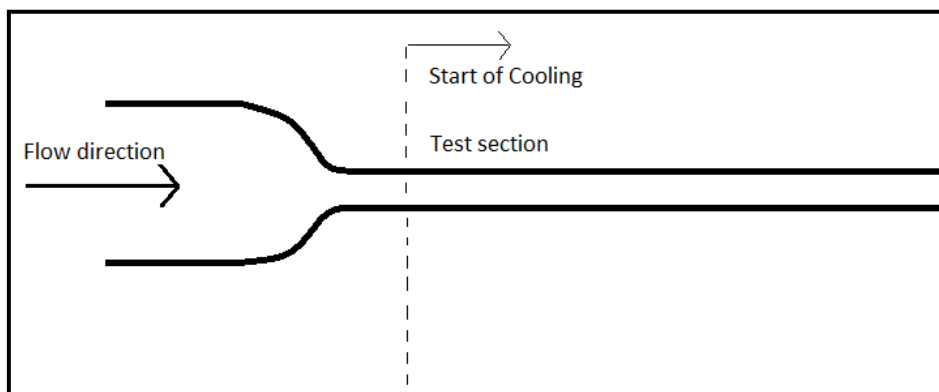


Figure 3: Bell-mouth inlet

The hydro-dynamically fully-developed inlet occurs when the inlet has the same diameter as the tubing of the test section. This allows for the inlet flow to already be developed, whereas with the other three more commonly known types, the velocity profile is always developing at the inlet.

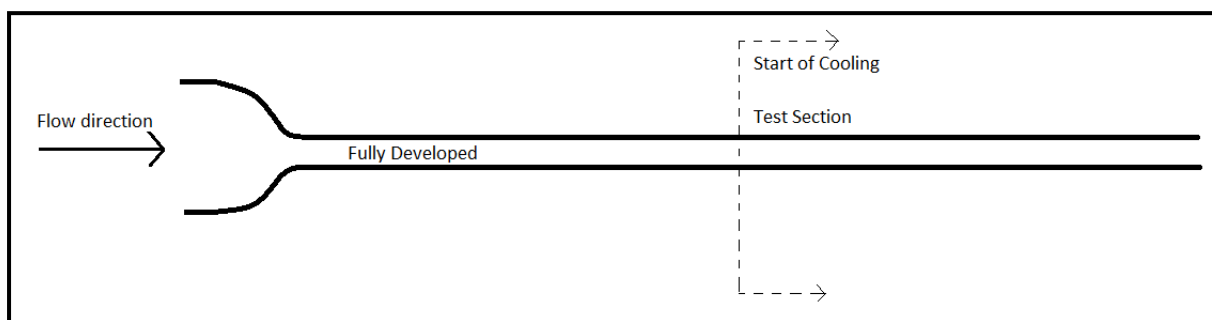


Figure 4: Fully developed inlet

2.4 Work by Ghajar

Ghajar and his team of co-workers have investigated the effect of the inlet configuration on the pressure drop under constant temperature and heating conditions, for the fully developed transition region. This has been experimentally tested on circular tubes, using transitional forced and mixed convection heat transfer methods. Correlations for the friction coefficient and Nusselt number, as a function of the Reynolds number have been drawn up, which are both practical and easy to use (Cengel & Ghajar, 2011).

Adiabatic Pressure Drop Measurements

The pressure drop measurements taken during the experiments carried out by Ghajar and Madon were done to calculate the friction factor for a database which could be used across all flow regimes with respect to the inlet type. Skin friction factor (c_f) considers pressure arising from shear stress only. This is fully developed friction. The apparent friction factor (f_{app}) refers to the entrance region friction factor. This is the friction caused by the momentum flux and well as the shear stress. The apparent friction factor is always greater than the skin friction factor (Ghajar & Madon, 1992).

For the inlet, it was found that the following range exists for the transition region:

- Re-entrant: $1\ 980 < Re < 2\ 600$
- Square-edged: $2\ 070 < Re < 2\ 840$
- Bell-mouth: $2\ 125 < Re < 3200$

It was found that, at a range of 1 980 to 2 125, the data closely followed that of the laminar skin friction coefficient, and at a Reynolds number greater than the range of 2 600 to 3 200, depending on inlet type, the data closely mimics that of the turbulent skin friction coefficient line. The experimental results were within $\pm 5\%$ of the established correlations. Correlations were found for the fully developed transition region and are summarised below (Ghajar & Madon, 1992).

Re-entrant

$$c_{f,tr} = -9.88 \times 10^{-3} + 1.15 \times 10^{-5}Re - 1.29 \times 10^{-9}Re^2$$

Where: $1\ 950 < Re < 2\ 650$

Square-edged

$$c_{f,tr} = -2.56 \times 10^{-2} + 2.49 \times 10^{-5}Re - 4.25 \times 10^{-9}Re^2$$

Where: $2\ 055 < Re < 3\ 140$

Bell-mouth

$$c_{f,tr} = -8.03 \times 10^{-3} + 1.05 \times 10^{-5}Re - 1.47 \times 10^{-9}Re^2$$

Where: $2\ 075 < Re < 3\ 450$

An isothermal experiment was also carried out when the effect of heating on the fully developed friction factor was investigated. The results found for the transition region Reynolds number range are summarised in the table below (Cengel & Ghajar, 2011).

Inlet type	Reynolds number range
Re-entrant	2 870 < Re < 3 500
Square-edged	3 100 < Re < 3 700
Bell-mouth	5 100 < Re < 6 100

Table 2: Reynolds number range for isothermal conditions, when considering pressure drop

Diabatic Pressure Drop Measurements

The purpose of this experimentation was to create a database for pressure drop across all flow regimes in the fully developed region. This database could then be used for future applications, where flow exits in the transition region. The measurements for the diabatic pressure drop measurements (friction factor) were obtained using a differential pressure transducer, in the fully developed region of a horizontal circular straight tube. The inlet types considered, once again, were the re-entrant, square-edged and bell-mouth. These experiments were done under isothermal and non-isothermal flow conditions. For these experiments, different heat fluxes (3, 8, and 16 kW/m²) were used, as well as the isothermal heat flux (0 kW/m²). These different heat fluxes showed the effect of the heating on the friction factors (Tam & Ghajar, 1997).

The boundaries for the ranges of Reynolds numbers were between 2 900 and 3 500 for the re-entrant inlet; 3 100 and 3 700 for the square-edged inlet; and 5 100 and 6 100 for the bell-mouth inlet. The exact ranges depending on the heat flux will be given further in this study. The liquid considered for these experiments is ethylene glycol-water mixtures, which have Reynolds numbers which range between 1 000 and 17 000. This range accommodates for laminar, transition and turbulent flow (Tam & Ghajar, 1997).

Generally, it is assumed that temperature does not affect the fluid properties in the flow field. This is just an assumption, and the temperature does in fact affect the friction factor due to a change in the velocity profile of the fluid. Two methods are used to correct the constant property assumptions, the reference-temperature method and the property-ratio method. The property-ratio method is the most common method used and the correlation equation, obtained from Tam and Ghajar, 1997 is:

$$C_f = C_{vp} = C_{cp} \left(\frac{\mu_b}{\mu_w} \right)^m$$

Where:

- μ_b : bulk temperature viscosity
- μ_w : Wall temperature viscosity
- c_p : Constant-property solution (isothermal)
- vp : Variable-property solution (non-isothermal)
- m : Flow parameter

The table below shows the different friction coefficient transition Reynolds number ranges for the isothermal (0 kW/m^2) and three non-isothermal heating rates for the three inlets used in their study (Cengel & Ghajar, 2011).

Heat Flux	Re-entrant	Square-edged	Bell-mouth
0 kW/m² (isothermal)	2870 < Re < 3500	3100 < Re < 3700	5100 < Re < 6100
3 kW/m²	3060 < Re < 3890	3500 < Re < 4180	5930 < Re < 8730
8 kW/m²	3350 < Re < 4960	3860 < Re < 5200	6480 < Re < 9110
16 kW/m²	4090 < Re < 5940	4450 < Re < 6430	7320 < Re < 9560

Table 3: Transition Reynolds numbers for friction coefficient

From Table 3, it follows that that transition occurred much earlier for a re-entrant inlet, and the latest for a bell-mouth inlet. The isothermal results are repeated in this table to show the comparison between the Reynolds number and how it is affected by heating. The table accurately shows how the inlet type affects the transition region between laminar and turbulent flow. The shear stress of the velocity profile increases as the heat flux increases. The density decreases and the friction factor increases. These changes result in the increase in Reynolds number as the heat flux increases.

Diabatic Heat Transfer Measurements

The experiments were done under a uniform wall heat flux condition. The Reynolds number for these experiments ranged from approximately 280 to 49 000, the Grashof number from 1 000 to 2.5×10^5 , and the Prandtl number from 4 to 158. This study was done to create a broad database which could be used to a variety of Reynolds, Grashof and Prandtl numbers for forced and mixed convection heat transfer. This study mainly focused on the type of inlet used and how it affected the region of transition (Ghajar & Tam, 1994).

It was found that the Reynolds number for the transitional regime were 2 000 to 8 500 for a re-entrant inlet; 2 400 to 8 800 for a square-edged inlet; and 3 800 to 10 500 for a bell-mouth inlet (Ghajar & Tam, 1994). This, however, accommodates for both the inlet and outlet regions of the tube. The table below shows the comparison of the Reynolds number transition region for the re-entrant, square-edged and bell-mouth experiments, for the inlet and outlet regions (Ghajar & Tam, 1994).

Inlet type	Reynolds number	
	Inlet	Outlet
Re-entrant	2 000 < Re < 6 700	2 100 < Re < 8 500
Square-edged	2 400 < Re < 7 300	2 500 < Re < 8 800
Bell-mouth	3 400 < Re < 9 400	3 800 < Re < 10 500

Table 4: Transition region for diabatic heat transfer measurements

For the table above, the experiments were done using 3^*D for the inlet and 192^*D for the outlet. The heat transfer transition Reynolds number is not affected by the presence of mixed convection.

An equation was developed for determining the Nusselt number in the transition region. This equation differs slightly for each inlet type at the beginning and end of transition. The equation is defined as:

$$Nu_{tr} = \left\{ Nu_t + e^{\frac{a-Re}{b}} + Nu_t^c \right\}^c$$

The table below gives the values for constants a, b and c, depending on the inlet type.

Inlet type	Conditions	a	b	C
Re-entrant	$3 \leq x/D \leq 192$ $1\,700 \leq Re \leq 9\,100$ $5 \leq Pr \leq 51$ $4\,000 \leq Gr \leq 2.1 \times 10^5$ $1.1 \leq \mu/\mu_w \leq 2.2$	1 766	276	-0.955
Square-edged	$3 \leq x/D \leq 192$ $1\,600 \leq Re \leq 10\,700$ $5 \leq Pr \leq 55$ $4\,000 \leq Gr \leq 2.5 \times 10^5$ $1.2 \leq \mu/\mu_w \leq 2.6$	2 617	207	-0.950
Bell-mouth	$3 \leq x/D \leq 192$ $3\,300 \leq Re \leq 11\,100$ $13 \leq Pr \leq 77$ $6\,000 \leq Gr \leq 1.1 \times 10^5$ $1.2 \leq \mu/\mu_w \leq 3.1$	6 628	237	-0.980

Table 5: Constants for correlation equation of inlet type influence

Effect of heating and inlet geometries on the entrance

In these experiments, the effects of different inlets and heating on the friction factor in the laminar and transition regions of flow were investigated. These experiments were done on horizontal tubes and pressure measurements were made at the entrance and the fully developed regions. The inlets tested were the re-entrant and the square-edged and isothermal and non-isothermal conditions were used. Different mixtures of ethylene glycol and water were used for a Reynolds number range of 800 to 22 000. This Reynolds number range covers all of the flow regimes (Tam et al., 2013).

The transition region, under isothermal conditions, had a Reynolds number range for the different inlets were found to be:

- $2\,222 < Re < 3\,588$ for the square-edged inlet and,
- $2\,032 < Re < 3\,031$ for the re-entrant inlet.

The earlier start for the Reynolds number range for the transition region for the re-entrant inlet shows that this type of inlet causes the greatest disturbance in flow. It is obvious from these experiments, and the preceding ones, that the range of Reynolds numbers can be significantly influenced using inlet types.

The effect of heating on the Reynolds number range in the transition region is shown in Table 6. From this table that with the addition of heat, the Reynolds number range for the transition region

shifts to higher numbers for both inlet type. This is for the fully-developed friction factor (Tam *et al.*, 2013)

Inlet type	Isothermal conditions	With heating
Square-edged	2 222 < Re < 3 588	2 316 < Re < 3 941
Re-entrant	2 032 < Re < 3 031	2 257 < Re < 3 250

Table 6: Effect of heating on Reynolds number range for the transition region

Previous correlations were found by Tam and Ghajar (1997), which were applicable to Reynolds number ranges of 2 700 to 5 500 for re-entrant inlets and 3 500 to 6 900 for square-edged inlets. As can be seen from the ranges above, these ranges are outside of the correlation ranges. The correlation found is:

$$C_{f,tr,iso} = \left(\frac{16}{Re}\right) \{ [1 + (0.0049Re^{0.75})^a]^{1/a} + b \}$$

Inlet type	Reynolds number range	Length-to-diameter ratio	a	B
Re-entrant	2 026 < Re < 3 257	3 < x/D < 200	0.52	-3.47
Square-edged	2 111 < Re < 4 141	3 < x/D < 200	0.50	-4.0

Table 7: Coefficients for correlation equation

$$f_{app,tr,iso} = C_{f,tr,iso} \left[1 + \left(\frac{c}{x/D} \right) \right]$$

This equation is applicable to the following ranges, given in the table below.

Inlet type	Reynolds number range	Length-to-diameter ratio	c
Re-entrant	2 019 < Re < 3 257	3 < x/D < 200	4.8
Square-edged	2 019 < Re < 4 184	3 < x/D < 200	3.0

Table 8: Ranges and constants for corrected correlation equation

To accommodate for heating, further manipulation is necessary and viscosity is taken into account.

$$f_{app,tr,heat} = f_{app,tr,iso} \times \left(\frac{\mu_b}{\mu_w} \right)^m$$

Inlet type	Re-entrant	Square-edged
M	-1.8 + 0.46 Gr ^{-0.13} Pr ^{0.41}	-1.13 + 0.48 Gr ^{-0.15} Pr ^{0.55}
Reynolds range	1 883 < Re < 3 262	2 084 < Re < 3 980
Prandtl range	19.1 < Pr < 46.5	19.6 < Pr < 47.3
Grashof range	4 560 < Gr < 24 339	6 169 < Gr < 35 892
μ_b/μ_w	1.12 < μ_b/μ_w < 1.54	1.10 < μ_b/μ_w < 1.54

Table 9: Correlation equation ranges

This study investigated the effect of the inlet and heating on the entrance and fully developed friction factors in the laminar and transition regions. Isothermal and non-isothermal pressure drops were measured for all flow regimes between a uniform heat flux range of 4.3 to 8.9 kW/m². Heating was found to decrease friction factors. Essentially, the biggest contributor to affecting the transition region Reynolds number range is the inlet type (Tam *et al.*, 2013)

2.5 Work by Meyer

Augmentation experiments (Olivier & Meyer, 2010) have been performed on Reynolds number ranges of 2 000 to 150 000 for turbulent flow, and 15 and 30 000 for laminar flow. This work was performed on water and in some cases, air or glycol-water mixtures. Majority of the time, these experiments were conducted by heating the fluid. Studies by Manglik and Bergles (1993) have been done on the cooling of the fluid for operation in the transitional regime.

Turbulent augmentation of the tubes can be accomplished by the following means: internally finned, single-helix ridging, multi-helix ridging, micro-finned tubes, v-nozzle turbulators and finned inserts. Laminar augmentation can be accomplished by using twisted cap insets. This is for a Reynolds number range of 15 to 30 000. In previous experiments, positive displacement pumps were used. These pumps caused flow pulsations which are unfavourable. Therefore accumulators were introduced to stabilise the flow (Meyer & Olivier, 2010).

Multi-walled carbon nanotubes

This experiment dealt with the “convective heat transfer enhancement of aqueous suspensions of multi-walled carbon nanotubes flowing through a straight horizontal tube” (Meyer *et al.*, 2012). The Reynolds numbers under investigation were in the range of 1 000 to 8 000 (including the transitional flow regime). The aim of this experiment was to measure the heat transfer coefficients and friction factor, from the temperature and pressure drop readings, respectively.

An important aspect to consider with this investigation is the effect of thermal conductivity of the fluid in the heat exchanger. A heat exchanger must be as energy-efficient as possible, and therefore requires fluids with higher thermal conductivities. The thermal conductivities of water, engine oil and ethylene glycol are not high and therefore hinder the performance of the heat exchanger. This is why multi-walled carbon nanotubes (MWCN) have been developed, and are being tested. The MWCN have a thermal conductivity of 3 000 W/m·°C, in comparison to that of water, which is 0.61 W/m·°C.

The concentrations tested of the MWCNT water nanofluids, for convective heat transfer, were of 0.33 vol%, 0.75 vol% and 1.0 vol% in the range of 1 000 to 8 000 for the Reynolds number. When considering laminar flow, the heat transfer is decreased for MWCN at a concentration of 0.33 vol%, and enhanced for concentrations of 0.75 vol% and 1.0 vol%.

From the results on the multi-walled carbon nanotubes, higher concentrations result in an earlier transition region between laminar and turbulent flow. When considering the Nusselt number versus Reynolds number, the curve shifts horizontally to the right for lower concentrations of MWCN.

All concentrations of multi-walled carbon nanotubes show an enhancement on the Reynolds number versus Nusselt number graph. The MWCN have a higher viscosity than water and therefore lower Reynolds numbers were found. Simply, viscosity is how easily a substance can move through a tube, and corresponds to thickness, for liquids. Thus, an increased viscosity decreases the velocity.

Adiabatic pressure drops (enhanced tubes)

Meyer and Olivier (2010) dealt with enhanced tubes which lead to higher process efficiencies when operating in the transition region of flow. Three inlets were tested: re-entrant, square-edged and bell-mouth. Once again, it was found that the transition region differed with the type of inlet used. It was found that the following regions of transition occurred for the different inlets (Meyer & Olivier, 2010):

Inlet type	Range
Re-entrant	1 980 < Re < 2 600
Square-edged	2 070 < Re < 2 840
Bell-mouth	2 125 < Re < 3 200

Table 10: Transition range for different inlets (Meyer & Olivier, 2010)

It was found that transition occurs earlier in a smooth tube than in an enhanced tube. The friction factors have shifted to higher ranges for the enhanced tubes compared to the smooth tubes. The friction factors were found to be more dependent on the relative roughness and helix angle of the enhanced tube, than on the diameter of the tube. For Reynolds numbers in the range of 3 000 to 10 000, it was found that a case of ‘secondary transition’ existed. This is thought to be as a result of the increase in the roughness of the fins. This increases the resistance and therefore the friction (Meyer & Olivier, 2010).

Two different helix angles of the enhanced tubes were investigated; namely 18° and 27°. This was tested using the same inlet type, as not to affect the Reynolds number range further. It was found that the transitional region between laminar and turbulent flow, occurred at Reynolds numbers between 1 900 and 2 100 for both helix angles tested. The larger diameter (19.1 mm), 27° helix angle tube, underwent transition last, at a Reynolds number of 2 070. The other tubes tested, underwent transition at a Reynolds number of approximately 1 870. The fin-pitch ration can also affect the transitional region. The table below summarises the results found for the enhanced tubes, by Meyer and Olivier (2010).

Tube	E1	E2	E3	E4
Diameter (mm)	15.8 (15.806)	15.8 (15.859)	19.1 (19.160)	19.1 (19.089)
Helix angle	18°	27°	18°	27°
Fin-pitch-to-diameter ratio	0.39	0.18	0.39	0.18
Fin-height-to-diameter ratio	0.027	0.027	0.027	0.022
Transition Reynolds number	1870	1870	1870	2070

Table 11: Properties of different enhanced tubes tested

When considering the type of inlet used, only the end of transition seems to be affected by the helix angle. Table 12 summarises the results found for the Reynolds number ranges for the types of inlets and different helix angles (Meyer & Olivier, 2010).

		Re-entrant	Square-edged	Bell-mouth
E1	15.8mm 18°	1 985 < Re < 3 000	Starting at 2 800	3 900 < Re < 4 600
E2	15.8mm 27°	1 985 < Re < 2 500	Starting at 2 500	3 900 < Re < 4 600
E3	19.1mm 18°	2 080 < Re < 3 000	Starting at 2 200	5 500 < Re < 5 800
E4	19.1mm 27°	2 080 < Re < 2 500	Starting at 2 050	5 500 < Re < 5 800

Table 12: Reynolds number ranges for enhanced tubes with different inlet types

From Table 12, it follows that the inlet with the highest Reynolds number range for the transition region occurs for the bell-mouth inlet. The re-entrant inlet has the lowest range of Reynolds numbers.

Friction occurs in the laminar region due to buoyancy. Friction was found to also occur as a result of the helix angle, as this obstructs secondary flow through the tube.

The friction factor in the transitional region of flow is given by the following correlation as shown in Meyer and Olivier, 2011:

$$f_{te} = 4 \left(\frac{16}{Re_{cr}} \right)^{c_1} \exp \left(c_2 \frac{Re}{Re_{cr}} \right) \left(\frac{\beta}{90} \right)^{c_3} \left(\frac{e^2}{p_f D} \right)^{c_4} \times \left(\frac{p_f}{D} \right)^{c_5} \left(\frac{e}{D} \right)^{c_6} Pr^{c_7} Gr^{c_8} \left(\frac{\mu}{\mu_w} \right)^{c_9}$$

The constants were determined using a least-squares optimisation method. These constants were found to be:

- $c_1 = -0.131$
- $c_2 = -0.111$
- $c_3 = 2.363$
- $c_4 = -0.313$
- $c_5 = 0.766$
- $c_6 = 0.786$
- $c_7 = 0.081$
- $c_8 = 0.0268$
- $c_9 = -0.289$

Heat Transfer Measurements (enhanced tubes)

This study on heat transfer measurements was done on helical finned tubes which operate in the transition region between laminar and turbulent flow. This included experimentation for the fully developed, and developing flow, and different inlet types were investigated, once again. The inlets have a significant effect on the Reynolds number ranges found from the experiments, and thus are continually done. This investigation was done alongside the pressure drop investigation, discussed previously in this thesis.

An important note to make is that the diameter used for smooth tubes is the inner diameter whilst for the enhanced tubes, the enveloped diameter is used. The fluid properties were those which correlated with the average temperature of the fluid in the tube.

The j-factors for this experiment were found to range between 1 000 and 12 000. The Colburn j-factor is a representation of the heat transfer as a non-dimensionalised parameter. The j-factor decreases as the Reynolds number increases, except for the Reynolds number region between 3 000 and 8 000. This is due to the fin-height-to-diameter ratios for the enhanced tubes. Any additional changes in the increase were as a result of the helix angle. This angle spins the fluid. At a Reynolds number of 2 600 for the 15.8 mm diameter enhanced tube, the 27° tube deviates from the 18° tube. This can be seen for the 19.1 mm tube, at a Reynolds number of 2 500. At a Reynolds number of 9 000, the deviations dissipate, and the shape of the curves are similar, just shifted, depending on the geometry of the tube (Meyer & Olivier, 2010).

In the laminar flow region, the heat transfer results were lower for the enhanced tubes than for the smooth tubes. Also, the 15.8 mm enhanced tubes had lower heat transfer measurements than the 19.1 mm tubes. The helix angle does not have a significant effect on the heat transfer. The fins are thought to obstruct the flow through the tube (for secondary flows) and thus decrease the heat transfer.

For heat transfer, the following equation exists for the Reynolds number:

$$Nu_{te} = [Nu_{Le}^{c_1} + Nu_{Te_{38}}^{c_1}]^{\frac{1}{c_1}}$$

C1 is a constant and was found to be equal to approximately 7, to correlate with the data. Thus the relationship is:

$$Nu_{te} = [Nu_{Le}^7 + Nu_{Te_{38}}^7]^{\frac{1}{7}}$$

This is for the following ranges:

- $1\,900 \leq Re \leq 4\,000$
- $4.5 \leq Pr \leq 5.4$
- $2.62 \times 10^5 \leq Gr \leq 4.45 \times 10^5$
- $0.686 \leq \mu/\mu_w \leq 0.804$
- $286 \leq L/D \leq 349$
- $18^\circ \leq \beta \leq 27^\circ$
- $0.176 \leq P_f/D \leq 0.387$
- $0.023 \leq e/D \leq 0.027$

It was found that there exists an overall increase in heat transfer of enhanced tubes compared to smooth tubes. The fins, themselves, as well as the helix angle influence the heat transfer and cause it to increase (Meyer & Olivier, 2010).

Smooth tubes

In this investigation, three inlet configurations were used, namely: bell-mouth, square-edged, and re-entrant inlets. Fouling was considered to possibly have an effect when using water (Olivier & Meyer, 2010). Fouling occurs as a result of deposits accumulating on the heat transfer surfaces, which cause an additional resistance, and therefore decrease the heat transfer (Cengel & Ghajar, 2011). Heat transfer rates varied between 1 kW and 15 kW, and was dependent on the flow rate in

the inner tube (Olivier & Meyer, 2010). It was found that transition from laminar to turbulent flow started at a Reynolds number of 2 100 and ended at a Reynolds number of 2 900. When considering the adiabatic friction factors, the smoother the inlet, the later transition occurred. The bell-mouth inlet, the smoothest inlet, showed the latest transition at a Reynolds number of approximately 12 000. When considering heat transfer measurements, transition was found to be independent on inlet configuration. This was also found for diabatic friction factor results (Olivier & Meyer, 2010).

Cooling of Water inside Smooth Tubes

For this experiment, four inlet types were investigated, bell-mouth, square-edged, re-entrant and hydro-dynamically fully developed inlets. Reynolds numbers in the range of 1 000 to 20 000 were tested for the cooling of water. Two tube diameters were tested, 15.88 mm and 19.02 mm, for a tube length of 5 m (Olivier & Meyer, 2010).

Adiabatic friction factors showed that the laminar and turbulent results were in agreement with theories for the fully developed inlet. The transition region range was found to be between Reynolds numbers of 2 100 and 2 900. There was a negligible difference between the Reynolds numbers for the two tube diameters in the transition region. The bell-mouth inlet showed the transition region to begin at a Reynolds number of 12 000 (for the 19.02 mm tube) and 7 000 for the 15.88 mm tube. This difference occurred as a result of manufacturing of the inlet and the contraction ratio. The re-entrant inlet showed similar results to those of the hydro-dynamically fully developed inlet, whilst the transition region for the square-edged inlet occurs after the re-entrant inlet, but before the bell-mouth inlet transition region (Olivier & Meyer, 2010).

Adiabatic heat transfer results showed turbulent results very similar to those in theory. Usually laminar flow results show a constant of 3.66 or 4.36 for the Nusselt number for constant surface temperature and constant surface heat flux respectively. In these experiments, the constants were found to be higher, due to secondary flow in the tubes (Olivier & Meyer, 2010).

Diabatic pressure drop results showed that the laminar flow friction factors increased when the heat flux was increased. Once again, the bell-mouth showed the latest transition region (when considering the Reynolds number range), and the fully developed inlet and re-entrant inlets showed the earliest transition from laminar to turbulent flow (Olivier & Meyer, 2010).

2.6 Conclusion

In conclusion, the effects of tube augmentation and inlet configuration have been investigated and a database drawn up. It is now necessary to create a database to show the effect of surface roughness on the transitional flow regime. Much work has been done by Meyer and Ghajar on the transitional flow regime, and this study will contribute to the existing databases which they have created. Tube augmentation and inlet type have significant effects on the transitional flow region. Information is now known on the previous work which has been performed as well as the important factors and numbers to consider. The next chapter deals with the calculations and the experimental design and setup for the investigation into the effect of surface roughness on the transitional flow regime.

Chapter 3

Design

3.1 Introduction

A simulation was performed in order to determine the necessary length and diameter of the tube heat exchanger. The equations which were used to determine whether a diameter and length were sufficient are given in the calculations section of this chapter. Different equations exist for laminar and turbulent flow, and thus it is important to differentiate between these when performing the simulation.

3.2 Calculations

The calculations necessary in the design of this experiment, were to determine the diameter and length of the pipe which will allow for transitional flow to occur, so that this region can be investigated with respect to the effect of surface roughness.

Some important factors in these calculations and for the design of the experiment include:

- A uniform heat flux exists as the heating method for this experiment.
- The Nusselt number is constant in the laminar flow regime.
- Assuming the properties at the average temperature will give a negligible error.
- The roughness value for the rough tubes is equal to the filter size.
- For smooth tubes, the relative roughness ϵ is 0.
- The diameter and length of the tubes need to be found for the experimental setup.

Laminar flow

The friction factor is:

$$f = \frac{64}{Re}$$

In the entry region for laminar flow (Cengel & Ghajar, 2011),

$$Nu = 3.66 + \frac{0.065(D/L)RePr}{1 + 0.04[(D/L)RePr]^{2/3}}$$

For fully developed laminar flow in circular tubes, the following factors exist (Cengel & Ghajar, 2011):

- For a constant surface heat flux:

$$\begin{aligned}\dot{q}_s &= \text{constant} \\ Nu &= 4.36\end{aligned}$$

- For a constant surface temperature:

$$T_s = \text{constant}$$

$$Nu = 3.66$$

Turbulent Flow

For turbulent flow in tubes,

For smooth tubes:

$$f = (0.790 \ln Re - 1.64)^{-2} \quad 3\,000 < Re < 5 \times 10^6$$

$$Nu = 0.125 f Re Pr^{1/3}$$

$$Nu = 0.023 Re^{0.8} Pr^n$$

Where 'n' is equal to 0.4 for heating and 0.3 for cooling.

When a large temperature difference occurs:

$$Nu = 0.027 Re^{0.8} Pr^{1/3} \left(\frac{\mu_b}{\mu_s} \right)^{0.14}$$

For this equation: $0.7 \leq Pr \leq 16\,700$ and $Re \geq 10\,000$

These equations are suitable to Reynolds numbers above 10 000 and thus an equation developed by Meyer and Bateman (2013), shows:

$$Nu = \frac{\pi}{70} f Re^{1.11} Pr^{1/3}$$

To determine the friction factor for turbulent flow, the Colebrook equation can be used. This equation requires iterations to determine the friction factor and is thus not preferred.

$$\frac{1}{\sqrt{f}} = -2 \log \left(\frac{\epsilon/D}{3.7} + \frac{2.51}{Re \sqrt{f}} \right)$$

The Haaland equation is within two percent of the Colebrook equation, and is defined as:

$$\frac{1}{\sqrt{f}} \cong -1.8 \log \left(\frac{6.9}{Re} + \left(\frac{\epsilon/D}{3.7} \right)^{1.11} \right)$$

The Nusselt number determined by these equations, for fully developed turbulent flow, can be used for developing flow, as the developing region is short in comparison to the total tube length, usually ten tube diameters (Cengel & Ghajar, 2011).

Laminar and Turbulent Flow

The pressure drop can then be calculated as:

$$\Delta P = f \frac{L \rho V^2}{D 2}$$

And the head loss can be calculated as:

$$h_f = \Delta z + \frac{\Delta P}{\rho g}$$

Since this is a horizontal tube application, there is no change in height, and the head loss can be defined as:

$$h_f = \frac{\Delta P}{\rho g} = f \frac{L V^2}{D 2g} \quad [m]$$

3.3 Simulation

An Excel spreadsheet was used to determine the correct diameter and length for the tube which will be used for this experiment. The equations used in the previous section (Calculations) were used, as well as various others given below. It was decided to keep the length constant at 1.8 m because this is the maximum distance for which sand can correctly be used to roughen the tube. Examples of the simulation are given in Appendix E. These spreadsheets show the formulae used in Excel.

Area:

$$A = \pi r^2 = \pi \frac{D^2}{4}$$

Reynolds number:

$$Re = \frac{\rho V D}{\mu} = \frac{V D}{\nu} = \frac{4 \dot{m}}{\pi \mu D}$$

Heat transfer:

$$\dot{Q} = \dot{m} C_p \Delta T = VI$$

$$\dot{Q} = h A_s (T_s - T_\infty)$$

Exit temperature:

$$T_e = T_i + \frac{q_s \left(\frac{A_s}{2} \right)}{\dot{m} C_p}$$

It was found that the inner diameter of the tube (for a tube length of 1.8 m) should be 14.46 mm. Sample calculations are given in Appendix D of this report. The available tube from Copper Tubing Africa is a 15.88 mm outer diameter tube with a wall thickness of 0.71 mm (Copper Tubing Africa, 2012).

3.4 Experimental Design

The design of this experiment is very important and is discussed in this section. An important consideration is that standard components should be used because this prevents the necessity for the manufacturing and therefore the waiting time to continue with the build.

Since a constant heat flux occurs as a result of the thermocouples used as heating wires, the temperature along the length of the tube is a linear graph, and thus by knowing the inlet and outlet temperatures of the water, it is simple to determine the temperature at any point along the tube.

It is important to note the following:

- A calming section is necessary in order to ensure that any disturbances in the flow are removed. Essentially the calming section is a metal honeycomb which ensures that the flow is modular. This calming section can usually be used to house different inlet types. For this experiment, only the square-edged inlet is used.
- Thermocouples are used to create the constant surface heat flux. These need to be calibrated.
- The pressure drop will be measured using a differential pressure transducer. The pressure diaphragms also need to be calibrated.
- A mixing well is used at the exit of the test section to ensure that the bulk exit temperature can be measured.

The pump which is being used is:

- Model Number: SP3EPDM
- Serial Number: 10747

This pump can handle a maximum temperature of 60°C before it will fail.

The thermocouple which is being used is:

- Part number: TT-T-30-SLE (ROHS)

This thermocouple is supplied by Omega. This thermocouple wire consists of two wires, a constantan wire and a copper wire. For this thermocouple, the diameter is 0.25 mm and the resistance is 3.043 Ω /ft. The necessary length of the thermocouple can be determined.

$$\begin{aligned}H &= ND_{t-c} \\2 &= N \times 0.00025 \\N &= 8000 \text{ turns}\end{aligned}$$

$$\begin{aligned}L &= \pi ND_{o(\text{tube})} \\&= \pi \times 8000 \times 0.022 \\&= 553 \text{ m}\end{aligned}$$

Adding a safety factor to the length of the thermocouple wire, of 7 m, the total length of the wire needed is 560 m. Since four thermocouple wires will be used in parallel, the length of each will be

140 m. When converting this value to feet, the length of each of the four thermocouple wires is found to be 460 feet. The resistance per wire will therefore be equal to 1 398 Ω .

The total resistance of the thermocouple wires is 349.43 Ω . The current in each wire is assumed to be 0.43 A (a total current of 1.7 A). This means that the heat transfer is equal to 1 000 W. The voltage across the entire system is 588 V.

3.5 Experimental Setup

The experimental setup for this research project was similar to those which have been used before, for transitional flow regime experiments. The test section was inserted into the experimental test facility. The test section consisted of a 14.46 mm inner diameter, 15.88 mm outer diameter, half-hard copper tube which was a standard tube from Copper Tubing Africa. This test section was subject to a constant surface heat flux, caused by thermocouples surrounding the entire tube. The total length of the tube was 1.835 m, with a maximum length-to-diameter ration (L/D) of 126.2. This total length accommodated for the space requirements of the compression fitting at the inlet, as well as the coupling connection at the outlet. Four thermocouple wires were used in parallel, and were wound around the tube. Different heat fluxes were tested.

A smooth tube and a rough tube, of equal diameter, were used for this experiment in order to determine the effect of surface roughness on the heat transfer and pressure drop in the transitional flow region. This experiment used one test fluid, water.

The rough tube was manufactured by the use of a copper tube, with sand glued to its inner walls. This was not necessarily the best way to roughen a tube, however, through past experiments it was determined that it was a satisfactory means to roughen a tube. One side of the tube was taped closed, and the glue was poured into the tube. Once the taped side was wet, the other end was taped closed. The tube was then turned in all directions to ensure an even layer. Excess glue was allowed to drip out of the tube, whilst it was being turned. The sand was then poured into the tube until it flowed out the other side. The tube was then knocked on the floor to remove any excess sand. Many test pieces of tube were tried and cut open with the band-saw before the actual test section was glued and sanded. The test pieces were acceptable. The problem with this method was that it was difficult to ensure an equal glue thickness, and equal distribution of the sand. The glue adds an additional surface roughness to the tube, but this will be assumed to be negligible.

The test section was insulated from the environmental conditions using Armaflex insulation. This insulation has a thermal conductivity of 0.038 W/m²·K (PipeLagging, 2013). The approximate required thickness of the insulation was 55 mm. Three layers of insulation were used in order to achieve this thickness.

A positive displacement pump was used in order to pump the test fluid through the entire flow loop. This pump was electronically controlled and could be used to select the flow rate of the test fluid. Positive displacement pumps cause pulsations in the fluid and thus the stability of flow is not as required. An accumulator was used to decrease these pulsations. In this experimental setup, a Hydac, 2.7 bar accumulator was used. The flow rate was controlled by a frequency drive which was

attached to the pump. A data-acquisition system was used to determine the frequencies of the drive and therefore the flow rate.

The water used in this experiment existed at ambient conditions, but it could be cooled using a chiller to the desired temperature. Water entered the system between temperatures of 15°C and 18°C and was pumped through the system using the positive displacement pump.

The water flowed through the coriolis flow meters which were used to measure the flow rate of the test fluid, before it entered the test section. Two coriolis flow meters were used for this experiment, depending on the flow rates. The first coriolis flow meter was used for flow rates between 4.11 l/hr and 100 l/hr and the second was used for flow rates between 54.1 l/hr and 1 090 l/hr.

A feedback line existed from the pump back into the tank. This was used when the pump was first switched on and the flow rate needed to be set. The ball valves on the feedback line and by the coriolis flow meters were used to control the pump setting, so that it operated in the best range of approximately 800 to 1 200 rpm.

A calming section existed prior to the flow of the water into the test section. This calming section removed disturbances in the flow and allowed for uniform velocity distribution of the test fluid before it entered the test section. It was in this section that the inlet bulk temperature was measured.

The calming section consisted of a perspex tube containing a honeycomb and a mesh. These were used to remove the disturbances in the flow. Air bleed valves existed in the calming section at the top of the tube. This allowed for the removal of air from the fluid. If air was to exist in the water as it moves through the test section, pressure drop results would not be accurate. This is because water is incompressible and air is compressible. Thus the air bleed valves were necessary. The calming section could accommodate different test section diameters, as the end cap of the calming section can be replaced. Directly after the calming section, the flow moved into the test section through a square-edged inlet ('a' in the figure below). This was the only inlet type considered for this experiment, and was used for both the smooth and rough tube. Figure 5 depicts an example of a calming section (Meyer & Olivier, 2010):

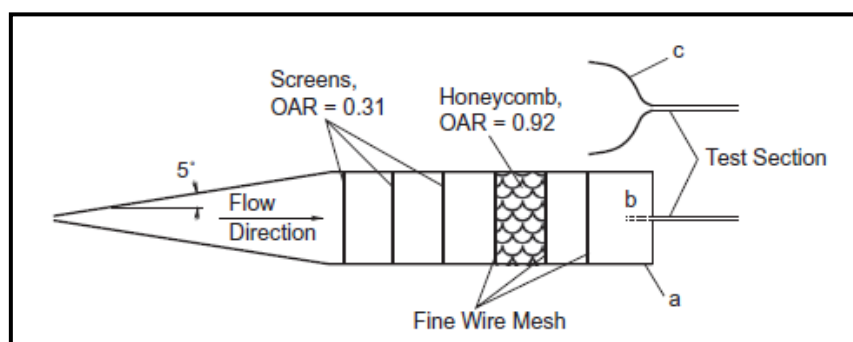


Figure 5: Schematic of calming section

The thermocouples were placed in close proximity of one another, whereby four thermocouple wires, in parallel, were wound about the entire tube length. Omega TT-T-30 Copper Constantan wires were used. Constantan was used for these thermocouple wires as it has a constant resistivity over a wide range of temperatures. These thermocouple wires were insulated T-Type. These

thermocouples created the constant surface heat flux when a current travelled through them, and a voltage drop existed across them. Thermocouples were also used to measure the inlet and outlet fluid temperatures, as well as the temperature along the tube. Calibration of these thermocouples was necessary in order to ensure an acceptable accuracy. Calibration was performed using two Pt-100 temperature probes.

A calculation was done in the previous section, showing the required length of thermocouple (heating) wire necessary to wrap the tube. Through an experiment, the resistivity and actual thickness of the thermocouple wire was found. The resistivity was found using a multimeter. It must be noted that the diameter of the wire was 1.2 mm due to both thermocouple wires being used (copper and constantan), and the surrounding insulation.

$$H = ND_{t-c}$$

$$1.8 = N \times 0.0012$$

$$N = 1\,500 \text{ turns}$$

$$L = \pi ND_{o(\text{tube})}$$

$$= \pi \times 1\,500 \times 0.01588$$

$$= 74.83 \text{ m}$$

Calculations were performed for three thermocouple wires in parallel and for four thermocouples in parallel. It was found that the voltage drop across the system was significantly less for the four thermocouples in parallel.

A safety factor of 5.17 m was added to the calculated length. The total length of heating wire used was 80 m and the length for each of the four thermocouple wires is 20 m. The resistance per wire was 188.4 Ω , and the total resistance for the four wires was 47.1 Ω . When considering three different heat fluxes, the following results were found using the equation:

$$Q = IV = I^2R$$

Heat transfer (W)	500	1 000	1 500
Total resistance (Ω)	47.1	47.1	47.1
Total current (A)	3.3	4.6	5.6
Current per wire (A)	0.82	1.2	1.4
Voltage drop (V)	153	868	266
Heat flux (W/m^2)	5 600	11 200	16 700

Table 13: Electrical calculations for different heat fluxes

The current in each wire was less than 1.8 A for each heat flux, and the voltage drop was less than 300 V over the system. Thus, one power supply could be used, and the system would not burn.

The thermocouples measured the temperature of the fluid at eleven stations along the tube. At each station, four temperature measurements were taken: 0°, 90°, 180° and 270°. The stations were placed at different intervals, depicted in Figure 6. The intervals were closer together at the inlet because this region was most likely to contain developing flow as opposed to fully developed flow. Small grooves were made in the outer diameter of the tube at these stations using a hand drill, and the thermocouples were soldered into these grooves. Solder was first placed into the drilled grooves by the use of a blow torch in order to heat the copper tube. The solder was then ‘dabbed’ into the

grooves. The ends of the thermocouple were stripped approximately 1 mm and the constantan and copper wire were soldered together. This end was then attached to the copper tube by heating the copper tube once again. The other ends of the thermocouple wires were attached to the data cards. The thermocouples were calibrated to ensure maximum accuracy.

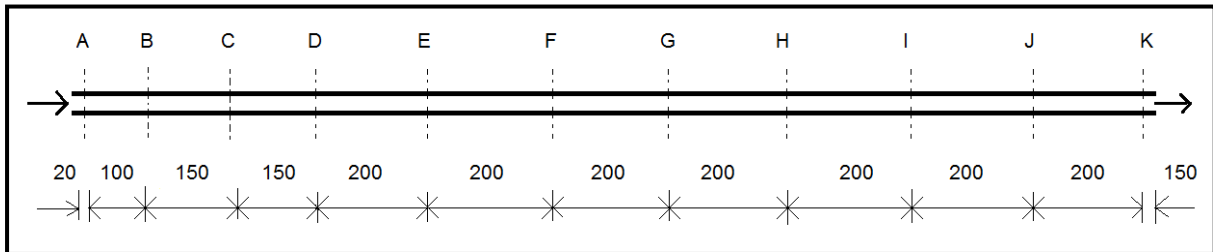


Figure 6: Thermocouple placement along the tube

The voltage drop across the test section was measured using a voltmeter, and the current through the thermocouple wires was measured using an ammeter.

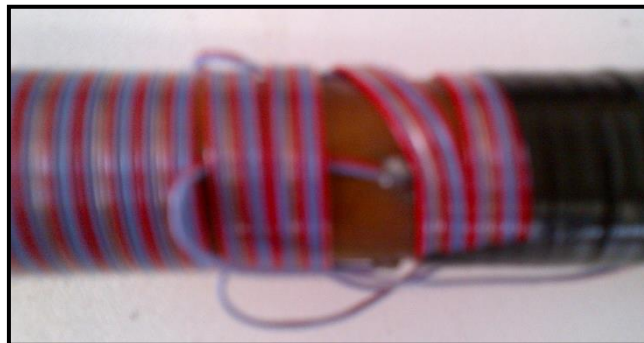


Figure 7: Wrapping of the test section showing how crossing over of the thermocouple stations was performed

Heat transfer measurements were taken by measuring the local outside wall temperatures at a number of different stations, along the tube. The inlet and outlet bulk temperatures, flow rate, voltage drop and current readings also assisted in the calculation of the heat transfer measurements. The local heat transfer coefficient and Nusselt number were then calculated for each station along the tube. The average heat transfer coefficient and Nusselt number could then be calculated by using the bulk temperature and the average surface temperature. The mean fluid temperature was assumed to increase linearly across the test section (due to the constant surface heat flux).

Pressure drop measurements could be taken by measuring the pressure drop between two pressure taps on the test section, one at the inlet and one at the outlet. The pressure taps were positioned along the top of the outer wall of the tube surface. The friction factor, along the length of the tube, could then be calculated for different flow rates. Pressure drop measurements were made with a DP15 variable reluctance differential pressure transducer.



Figure 8: Pressure tap

Figure 8 shows the pressure tap. Hydraulic tubing is inserted into the top of the tap, which is attached to the pressure transducer on the other end.

Diaphragms were used in the pressure transducers depending on the maximum pressure seen by the experimental setup. The smooth tube test section was expected to be subject to a maximum pressure drop of approximately 0.5 kPa. Thus a Dash Number 20 diaphragm was used for the smooth tube test section. The rough tube test section was expected to be subject to a maximum pressure drop of approximately 1.1 kPa and thus a Dash Number 22 diaphragm was used for this test section. These pressure diaphragms were calibrated using a manometer and a water column. Calibration factors were found for each diaphragm which were then applied to all for the pressure drop readings throughout the experimental phase of this project.

The pressure taps were positioned 1.7 m apart (50 mm from either end of the first and last thermocouple on the tube). The pressure taps were at the top of the tube and were approximately 20 mm long. This was so that the drill bit could fit through the entire tap to make an incision in the tube. This is shown in Figure 9.

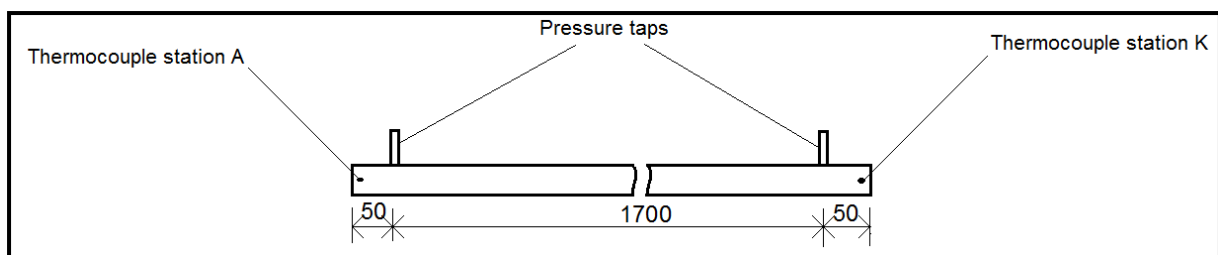


Figure 9: Location of pressure taps

Once the water had passed through the test section, it entered a mixing well. The bulk exit temperature was measured in this region. The mixing well comprised of a tube with the same diameter as the test section, which contained baffles. The ratio L/D was important when considering the length of the mixing well.

$$\frac{L}{D} = 1.5$$

Where L is the length each baffle and D is the inner diameter of the tube. The required length of each baffle was found to be 21.7 mm. It was decided to use five 22 mm baffles per mixing well and the total length of the mixing well was thus 110 mm. An additional length of tube was attached to the exit of the mixing well, with a coupling, in order to attach the mixing well thermocouples. The mixing well was attached to the end of the test section with a coupling, by means of solder. Silver solder would have created a better joint, however, the temperature would have increased too high and would have burnt out the sand at the outlet of the test section.

Once the water had flowed through the mixing well, it flowed through the filter. The filter was used in the flow loop in order to remove any dirt which existed in the test fluid as well as any sand particles which may have become loose as high temperatures and high flow rates occurred. This ensured that the components did not become damaged, and fouling did not occur. Filters were readily available in the laboratories and therefore needed not be specified.

The water then flowed through a non-return valve, which prevented the backflow of water into the test section. This allowed for accurate results. The water then flowed back into the storage tank.

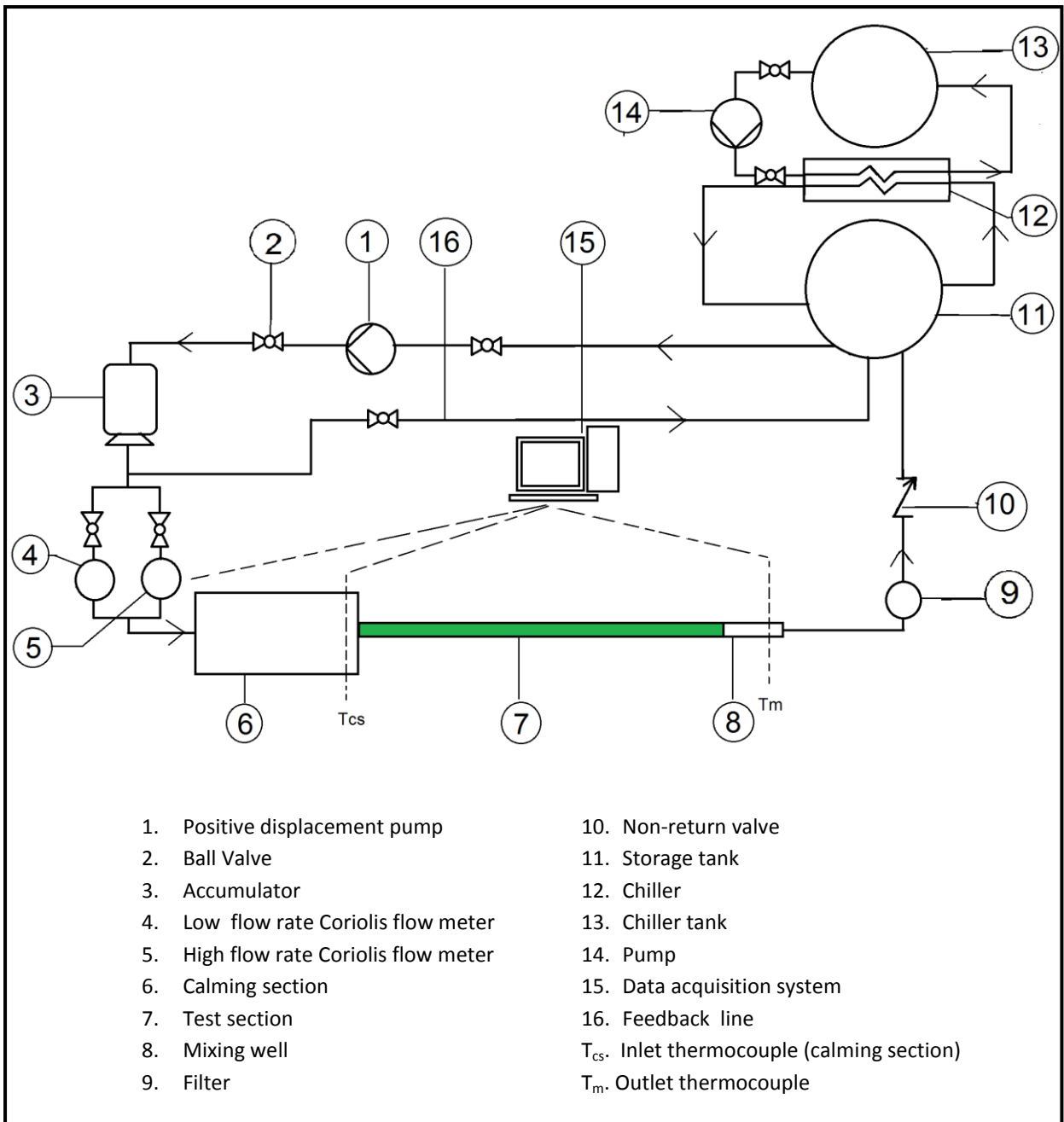


Figure 10: Schematic of the experimental setup

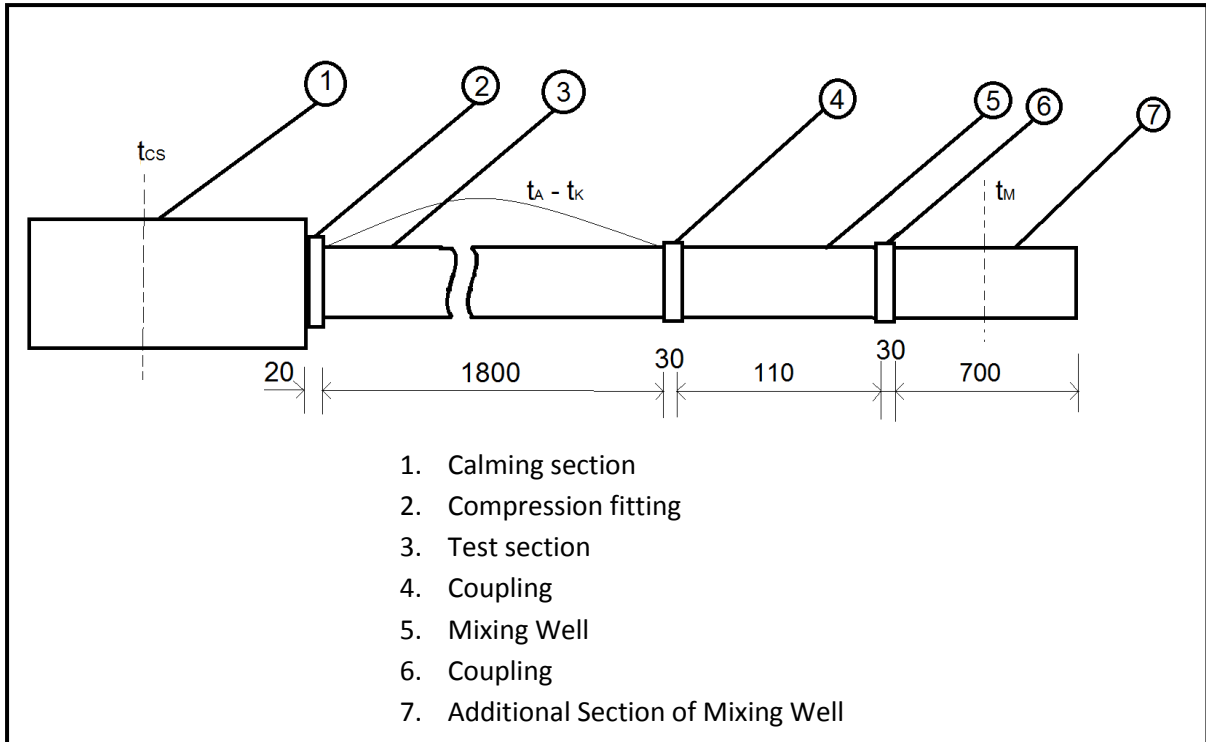


Figure 11: Test section

Where t_{cs} contained one thermocouple probe, and t_A to t_k , as well as t_M contained four thermocouples, attached at 0° , 90° , 180° , and 270° . Figure 10 depicts the cross-section of the test section, through one of the thermocouple stations.

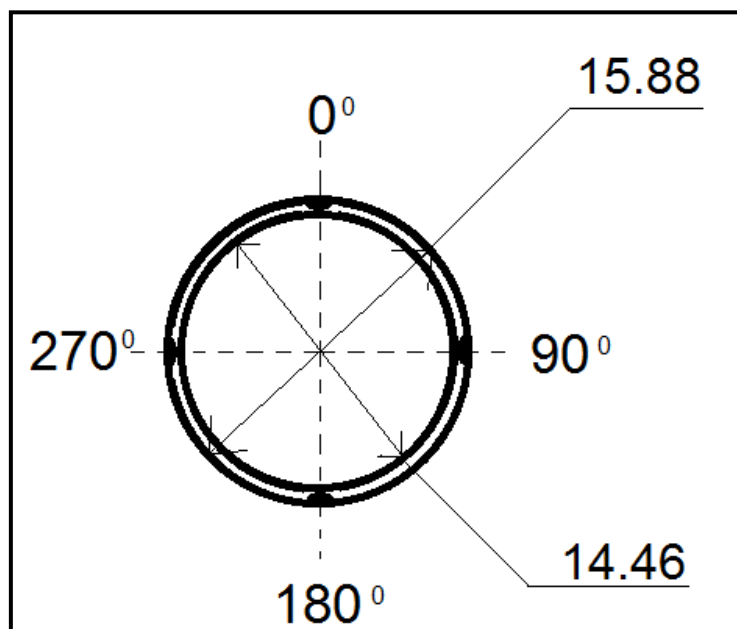


Figure 12: Thermocouple placement (A to M)

The assembly method is summarised below:

1. Drill grooves into both tubes

2. Solder the grooves in both pipes so that a slight ridge exists
3. Cut the thermocouple wires to length (leaving an excess of 0.75 m)
4. Strip the ends of the thermocouples
5. Solder one end of the stripped sides of each thermocouple (and cut to 1mm)
6. Silver solder the pressure tap copper tube to the pressure tap locations on both tubes
7. Attach the thermocouple ends (which were soldered) to the drilled and soldered holes, by the soldering method
8. Glue and sand the tube which is to be roughened
9. Drill through the pressure tap copper tubes
10. Attach pressure tap fittings
11. Wrap the tubes with the heating wires
12. Attach compression fittings to the inlets of both tubes
13. Solder the coupling to the outlets of both tubes as well as to the mixing well
14. Attach a filter to the mixing well of the tube which has been roughened
15. Attach the thermocouples to the cards
16. Add the insulation
17. Place the test section on the bench
18. Attach the inlet to the calming section
19. Attach mixing well to the tank

3.8 Conclusion

The experimental setup for the heat transfer and pressure drop measurements were discussed, including the thermocouples, pressure transducer, test section and the flow loop (path of flow travel). This experimental setup was designed and built to determine the effect of surface roughness on the transitional flow regime. Any deviations from this setup, are discussed further on in the report. Changes needed to be made in order to accommodate for any problems encountered.

Chapter 4

Data Analysis and Validation

4.1 Introduction

This chapter discusses the methods used to determine the heat transfer coefficient as well as the friction factors found for different Reynolds numbers. The heat transfer coefficient calculations require the temperatures along the length of the copper tube, and the friction factor calculations require the pressure drop across the length of the tube.

Adiabatic tests were done in order to validate the experiment. The experimental results for the adiabatic investigation were compared to existing models for the heat transfer coefficients, and to existing laminar and turbulent flow equations for the pressure drop. Once the adiabatic results were similar to those in literature, it was possible to continue with the experiment and obtain diabatic results.

4.2 Data Reduction

The results found in the experiments needed to be analysed in order to determine the quantities required: the Nusselt number and friction factor. The two quantities which were found during the experimental phase were the temperatures along the tube as well as the pressure drop. These were then transformed into the required quantities by the use of various equations and correlations. It must be noted that the properties found at various temperatures were obtained from correlations for liquid water for heat transfer calculations (Popiel & Wojtkowiak, 2007).

4.2.1 Heat Transfer

The local heat transfer coefficients are found in order to determine the Nusselt number. The local heat transfer coefficient was found using:

$$\dot{Q} = h_{local}(x) \times A_s \times (T_{si}(x) - T_m(x))$$

Where x denotes the position along the tube, and T_m is the temperature in the centre of the tube (y direction). T_m was found using the gradient of the line joining the calming section temperature, and the mixing well temperature. This mean temperature increased linearly along the length of the tube. T_s is the surface temperature measured by the thermocouples.

$$\begin{aligned} h_{local}(x) &= \frac{\dot{Q}}{A_s \times (T_{si}(x) - T_m(x))} \\ &= \frac{\dot{q}}{T_{si}(x) - T_m(x)} \end{aligned}$$

Where q is the heat flux [W/m^2].

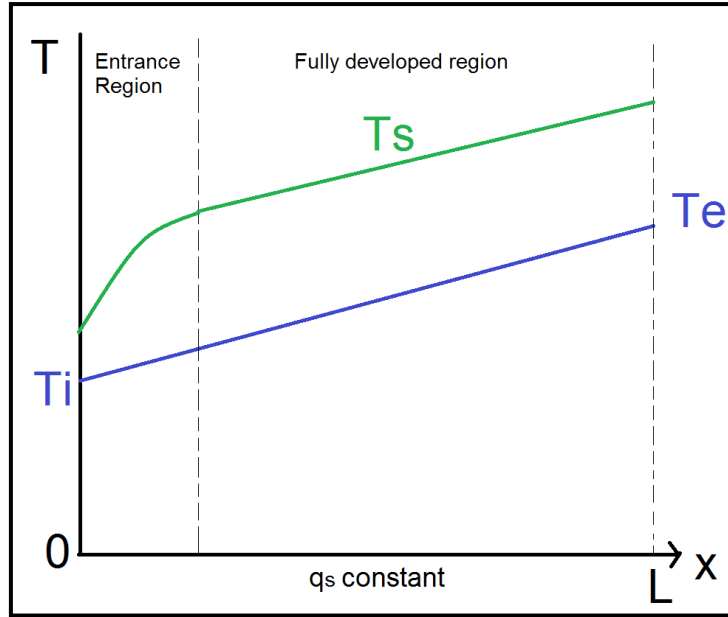


Figure 13: Mean fluid temperatures and surface temperatures along a tube for the case of a constant surface heat flux

To determine T_m from Figure 13 (Cengel & Ghajar, 2011), the following equation was used:

$$T_m(x) = \left(\frac{T_e - T_i}{L} \right) x + T_i$$

Where T_e is the outlet bulk temperature (of the mixing well) and T_i is the inlet temperature measured in the calming section. In order to determine the average heat transfer coefficient, the following equation was used:

$$\dot{Q} = h_{average} \times A_s \times (T_{s,average} - T_b)$$

Where $T_{s,average}$ is the average surface temperature of the tube (average temperature of thermocouple stations A to K) and T_b is the bulk temperature, which is the average temperature of the inlet and outlet. The surface area of the tube is:

$$A_s = \pi \times D_o \times L$$

Where D_o is the outer diameter of the tube and L is the length of the test section. The equation used to determine the actual heat transferred to the system was:

$$\dot{Q} = \dot{m}c_p(T_e - T_i)$$

Where \dot{m} is the mass flow rate measured by the coriolis flow meters and c_p is the specific heat for the water. The specific heat is measured at the bulk temperature for the average heat transfer coefficient, and at the mean temperature for the local heat transfer coefficient. These values are determined using thermophysical correlations for liquid water (Popiel & Wojtkowiak, 2007). These values were entered into the following equations in order to determine the local heat transfer coefficient h_{local} and the average heat transfer coefficient $h_{average}$:

$$h_{local}(x) = \frac{\dot{m}c_p(T_e - T_i)}{\pi \times D_o \times L \times (T_s(x) - T_m(x))}$$

$$h_{average} = \frac{\dot{m}c_p(T_e - T_i)}{\pi \times D_o \times L \times (T_{s,average} - T_b)}$$

The Nusselt Number was determined using the following equation:

$$Nu = \frac{hD_i}{k}$$

Where k is the thermal conductivity of the water, determined from the thermophysical formula (Popiel & Wojtkowiak, 2007) and D_i is the inner diameter of the tube. The heat added was also found using the equation:

$$\dot{Q} = V \times I$$

Where V denotes voltage and I denotes current. These quantities were entered into the power supply and were at the discretion of the user. The heat flux for the tube was:

$$\dot{q} = \frac{V \times I}{\pi \times D_o \times L}$$

Three different heat fluxes were investigated in this experiment. The energy balance of the system was very important and is defined below.

$$Energy\ Balance = \frac{\dot{Q}_{in} - \dot{Q}_{water}}{(\dot{Q}_{in} + \dot{Q}_{water})/2} \times 100$$

Where:

$$\dot{Q}_{in} = V \times I$$

$$\dot{Q}_{water} = \dot{m}c_p(T_e - T_i)$$

4.2.2 Friction Factor

In order to determine the friction factor, the following equation was used:

$$\Delta P = f \frac{L}{D_i} \frac{\rho V^2}{2}$$

$$V = \frac{\dot{m}}{\rho A_c}$$

$$A_c = \frac{\pi}{4} D_i^2$$

Where L was the distance between the two pressure taps. The velocity V was determined from the mass flow rate (\dot{m}), which was obtained experimentally, the cross sectional area and the density at the bulk temperature. The density ρ was determined at the bulk temperature using an existing formula (Popiel & Wojtkowiak, 2007). The pressure drop ΔP was determined experimentally. This equation was manipulated in order to make the friction factor the subject.

$$f = \frac{2 \times \Delta P \times D_i}{L \times \rho V^2}$$

This equation was compared to the existing correlations for friction factor as a function of Reynolds number in both the laminar and turbulent regions. For the laminar region, the existing correlation is Poiseuille's Law (Cengel & Ghajar, 2011):

$$f = \frac{64}{Re}$$

The correlation which was used for the turbulent region is the Blasius correlation which is defined as (Meyer, McKrell, & Grote, 2012):

$$f = 0.3164Re^{0.25}$$

This correlation could be used for data validation as it is an existing correlation for smooth tubes.

4.3 Data Acquisition

Data acquisition was done by calibration of both the thermocouples and the pressure transducer diaphragms. Calibration of these was very important as it ensured that the experimental results were as correct as possible.

Calibration of the pressure transducer diaphragms was done using a 200 kPa manometer and a water column. A Labview programme named "Skripsie" gave values in terms of milli-amps (mA) which were converted to kilopascals (kPa). This was done by zeroing the Skripsie values to 4 mA at the minimum pressure (0 kPa), and changing the span to 20 mA at the maximum pressure for each diaphragm. The maximum pressure for the diaphragm being used for the smooth tube was 0.86 kPa, which was greater than the maximum expected pressure of 0.466 kPa. This diaphragm was a Dash-20 diaphragm. The diaphragm used for the rough tube could withstand a maximum pressure of 1.4 kPa. The maximum expected pressure for the rough tube was 1.057 kPa. Thus the Dash-22 diaphragm could be used.

The calibration factors were found using an existing MATLAB programme which applied the 'Polyfit' function and returned a polynomial for the pressure calibration factors.

The method for calibration of the thermocouples was In-Situ Calibration. This method of calibration was done once the tube was built completely. This meant that re-attaching thermocouples during the building phase was not a problem. The zero was set to 0 L/hr at 4 mA, and the span was set to 600 L/hr at 20 mA.

Calibration of the thermocouples was done using Pt-100's, a geyser, a chiller and the Skripsie programme. The Pt-100's were placed at the entrance to the calming section and at the exit of the mixing well. These were used as the correct temperature readings, which the thermocouples were calibrated to. The geyser was used to increase the temperature of the water flowing through the test section and readings were taken at two to three degree increments. The chiller was then used to decrease the temperature of the water in two to three degree increments down to 15°C. These

values were then compared to the values of the Pt-100's and the calibration factors were found for each individual thermocouple.

An existing MATLAB programme was used to determine the calibration factors of each individual thermocouple. A third order polynomial was determined by the use of the 'Polyfit' function, for each thermocouple.

4.4 Validation

4.4.1 Pressure Drop

Validation of the experiment needed to be completed before results could be found. Validation was done on an adiabatic system, to find the pressure drops. The pressure drops were then converted into friction factors. These results are then compared to the moody chart in order to determine whether the system performs as required and expected, in both the laminar and turbulent regions.

The results obtained for the smooth tube during this adiabatic test were unacceptable, as displayed in Figure 14. The results varied too much from what is expected in theory. The results in the turbulent flow regime (Reynolds numbers greater than 5 000) were similar to the Blasius correlation. However, the results for the laminar flow regime were too different to Poiseuille's Law. This was possibly due to the fact that a 200 kPa manometer was used during calibration, which had previously been used on an active test, where as the manometer should only be used on a static test (for example, with the water column). Also, the manometer was not sensitive to very low pressures which were expected in this application. Thus the calibration factors found using the equipment were unacceptable and due to time constraints, calibration could not be re done. A new manometer was ordered but would not arrive in time. It was therefore decided, along with the supervisor, that pressure drop and friction factor experiments could be neglected from this point forward.

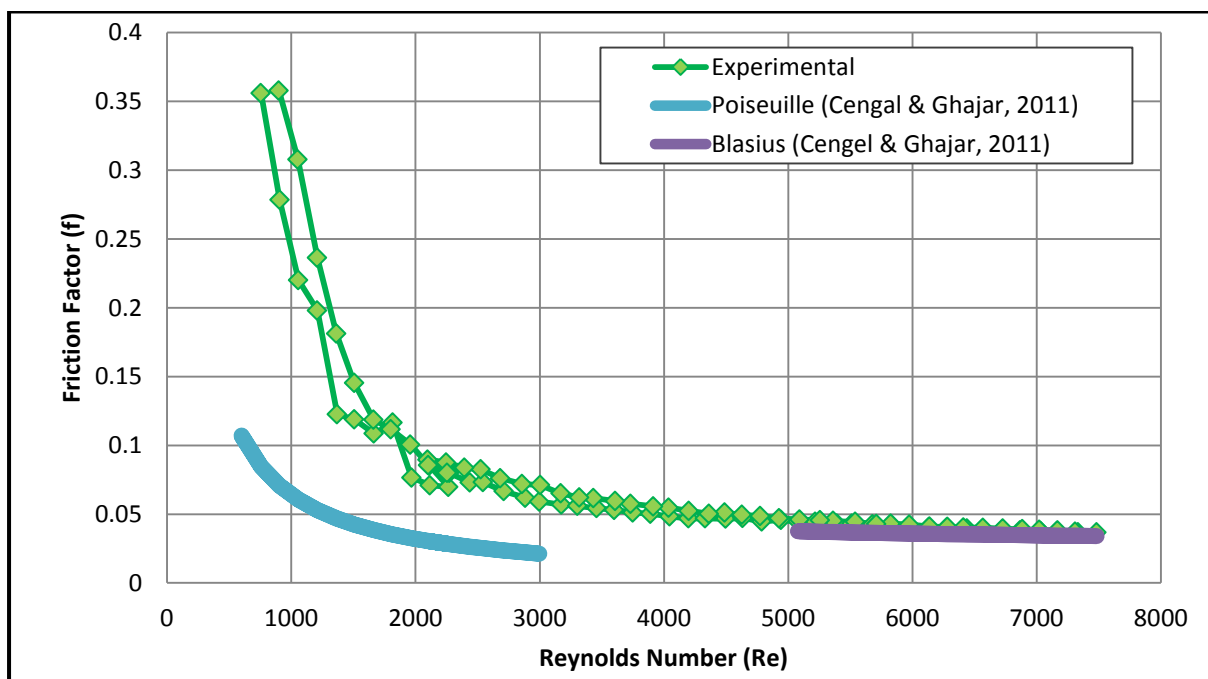


Figure 14: Comparison between adiabatic experimental results and existing correlations

4.4.2 Heat Transfer

A validation test was then done on a diabatic system in order to find the heat transfer coefficients for both the laminar and turbulent regions. Existing Nusselt number and Reynolds number correlations were used to determine whether the experimental results are applicable to the laminar and turbulent regions. This allowed for the determination of the relationship between the Nusselt number and the Reynolds number in the transition region. This validation is given in Chapter 5 of this report.

4.5 Uncertainties

Various uncertainties existed with regard to the thermal properties and the equipment used. The thermal property correlations that were used have uncertainties given in Table 14 (Popiel & Wojtkowiak, 2007).

Property	Uncertainty (%)
Density	± 0.004
Thermal conductivity	± 0.6
Dynamic viscosity	± 1.0
Prandtl number	± 2.3
Specific heat	± 0.04
Volumetric thermal expansion coefficient	± 0.5

Table 14: Property uncertainties

Uncertainties also exist with respect to the measuring equipment used.

Equipment	Measuring	Uncertainty
Validyne pressure transducer	Pressure drop	$\pm 0.25\%$
Pt-100	Temperature	$0.1\text{ }^{\circ}\text{C}$
Station thermocouples	Temperature	$0.1\text{ }^{\circ}\text{C}$

Table 15: Equipment uncertainties

4.6 Conclusion

In conclusion, this chapter has shown how the final results were found from the raw data obtained during the experimental testing process. The uncertainties were known, however, they would have little effect on the final results of the project, as similar overall correlations were found. For the remainder of the project, pressure drop and friction factor will be ignored, as it was seen in the validation section, that the calibration was incorrect. Because calibration could not be redone as a manometer was not available, friction factor results could not be used.

Chapter 5

Results

5.1 Introduction

This chapter discusses the results found during the testing stage of this research project. This chapter is divided into five main sections, including the smooth tube results, heat transfer validation, rough tube results, a comparison between the smooth and rough tubes and a conclusion. Any changes to the experimental setup will be discussed where they are valid.

5.2 Smooth Tube Results

Three heat fluxes were tested once calibration was complete. Table 16 summarises the voltage, current and heat added for the smooth tube.

Test	Current (A)	Voltage (V)	Heat added (W)	Heat flux (W/m ²)
1	2.55	194.8	497	5 600
2	2.53	290.5	735	8 300
3	3.62	276.9	1002	11 300

Table 16: Smooth tube electrical input quantities

The heat fluxes used are rounded off to the nearest hundred. These heat fluxes are dependent on the heat added (W) and the outer surface area of the tube. Table 17 summarises a sample of the energy balance values for the experiments, for certain Reynolds numbers, based on the bulk temperature. Averages for the 14 tabulated values, as well as for the total 34 readings are given.

Approximate Reynolds number	Energy balance (%)		
	5 600 W/m ²	8 300 W/m ²	11 300 W/m ²
1 125	7.6	34	1.1
1 675	11	33	0.8
1 930	2.9	36	8.7
2 840	3.2	27	1.8
3 750	1.8	17	1.9
4 710	0.0	12	1.3
5 680	0.3	7.5	3.0
6 660	4.0	0.5	0.4
7 640	1.3	1.0	1.1
8 645	0.7	8.1	1.3
9 550	0.4	12	2.3
10 550	5.4	15	1.4
11 445	5.4	20	0.2
11 730	3.5	1.2	1.2
Table average	3.4	16	1.9
Total average	3.1	14	1.9

Table 17: Smooth tube energy balances

From Table 17, it follows that the energy balance for the 8 300 W/m² run is completely off. This is because two of the wires burnt out when a 16 900 W/m² run was tried. This resulted in the loss of a constant surface heat flux and thus the results are inaccurate. It was decided to attempt a surface heat flux of 8 400 W/m², however, this heat flux was not possible due to limitations on the voltage drop and current through each of the two wires. A heat flux of 8 300 W/m² was possible, and thus the final test for the smooth tube was performed at this heat flux.

The energy balances for the smooth tube are not good at the lower Reynolds numbers. This could be due to the fact that steady state was not yet reached. At lower Reynolds numbers, the time necessary to reach steady state is longer because each fluid particle has more time at a specific point to heat up. It also takes longer for a particular particle to move through the system.

The table averages and total averages for both the 5 600 and 11 300 W/m² runs conclude that the overall energy balances of the test runs are satisfactory and acceptable. Thus these results can be used. The maximum error for the 5 600 W/m² run is 11 % and the maximum error for the 11 300 W/m² run is 8.7 %. These values are quite high and the results would therefore be inaccurate. These results are thus neglected when further data analysis is performed. The overall energy balances for these two heat fluxes have a maximum error of 3.4%. This is an acceptable value and thus the results are valid.

Graphs of the local Nusselt number versus the ratio of x/D (ratio of the distance along the tube to the outer diameter of the tube) are given in Figure 15, 16 and 17. Each graph shows five different Reynolds numbers per heat flux.

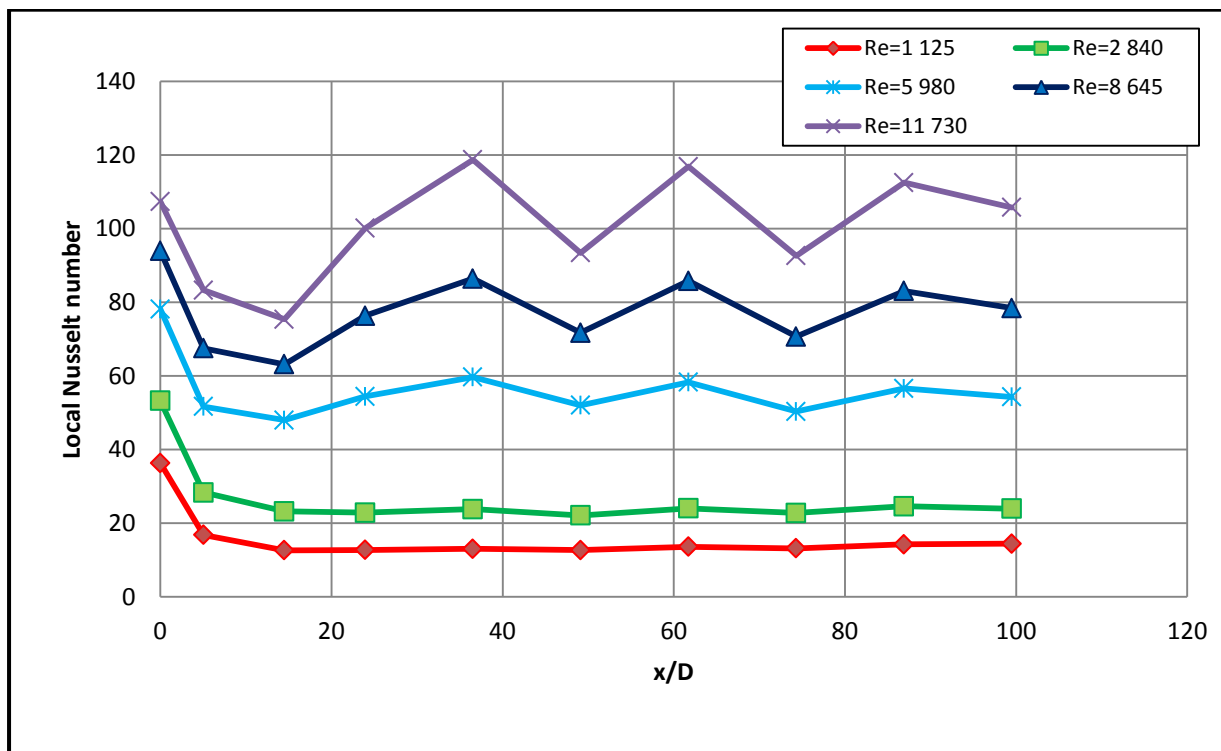


Figure 15: Graph of local Nusselt number versus position along the smooth tube for various Reynolds number. This graph shows the results of the 5 600 W/m² surface heat flux test.

In theory, fully developed flow occurs at a distance of '10D' (ten diameters) along the tube, for the turbulent flow regime. From Figure 15 it follows that the curves perform as expected for a distance of approximately 17 diameters. The local Nusselt number then begins to increase. The local Nusselt number fluctuates in a band for each of the different Reynolds numbers of 5 980, 8 645 and 11 730. These are the higher Reynolds numbers where turbulent flow is more likely to exist. The idea that fully developed turbulent flow exists at a distance of ten diameters is not valid for a square-edged inlet, and thus it is possible that the flow was not yet fully developed. Even though the results fluctuate, they fluctuate within an acceptable band. The results for the lower Reynolds number of 1 125 and 2 840 are as expected. Negligible fluctuations occur for these Reynolds numbers and the results are accurate.

Once the 11 300 W/m² test was performed on the smooth tube, a 16 900 W/m² test was started, but two of the heating wires burnt out. It was found that the length of wire from the pipe to the power supply was too long, and these wires got too hot (they were not being cooled by the water in the pipe). It was then decided to rather use heat fluxes of 5 600, 8 400 and 11 300 W/m² for the experiments. It was not possible to reach a heat flux of 8 400 W/m² once two of the heating wires were burnt out, and thus the influence of the maximum possible heat flux of 8 300 W/m² was tested.

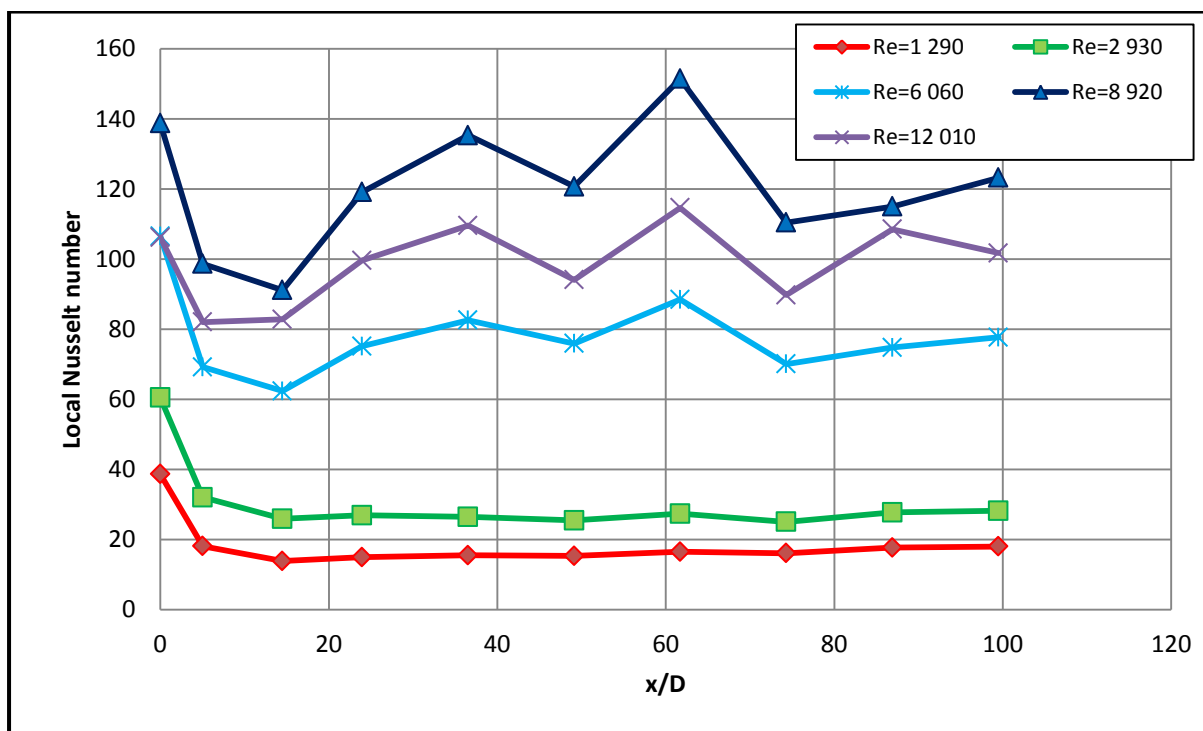


Figure 16: Graph of local Nusselt number versus position along the smooth tube for various Reynolds number. This graph shows the results of the 8 300 W/m² surface heat flux test.

Although the data for the 8 300 W/m² run is assumed to be incorrect due to the burning out of two of the heating wires, the local Nusselt number versus position along the tube graph is similar to those for the two test runs done whilst all of the heating wires were still in use. The values for the local Nusselt number are higher than they should be; however, the curves for the different Reynolds numbers are comparable to those of the other two heat flux tests. The curves for the lower Reynolds numbers show that the flow appears to be fully developed, and variations in the local Nusselt number do not exist.

Figure 16 concludes that the results for this heat flux are incorrect. This is because a higher Reynolds number results in higher local Nusselt numbers. For this heat flux, a Reynolds number of 8 920 had higher Nusselt numbers than a Reynolds number of 12 010. This is incorrect. The results for the 8 300 W/m² test are thus neglected in further discussions.

Once again, it can be concluded that for lower Reynolds numbers (1 290 and 2 930), the curves behave as expected. Although the values are high, the shape is comparable to other heat fluxes. The results for the higher Reynolds numbers tend to follow a similar pattern. These results fluctuate in a band of approximately 30 after a distance of 20 diameters.

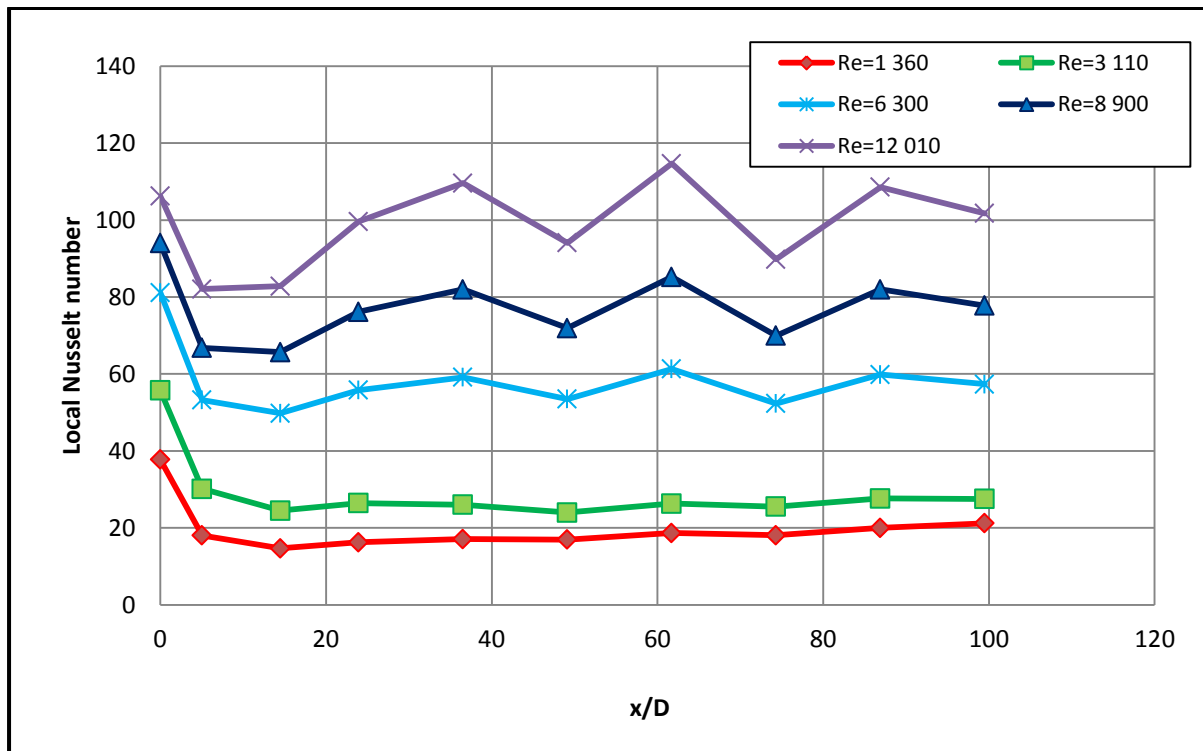


Figure 17: Graph of local Nusselt number versus position along the smooth tube for various Reynolds number. This graph shows the results of the 11 300 W/m² surface heat flux test.

From Figure 17 it can be concluded that for all heat fluxes, higher Reynolds numbers result in fluctuations for the local Nusselt number as a function of distance along a pipe. For the heat flux of 11 300 W/m², the fluctuations occur in a band of approximately 10 for the higher Reynolds numbers. The fluctuation band for this heat flux is lower than those for the previous two heat fluxes. Low Reynolds numbers perform as expected in theory, for a smooth tube. The curves for Reynolds numbers of 6 300, 8 900 and 12 010 are very similar. Essentially it appears as though the 6 300 curve has been translated in the positive local Nusselt number direction. It can therefore be concluded, that these fluctuations are likely to occur for any Reynolds number in the range of 6 300 and 12 010. These fluctuations are minimal. The curves are constant, however, they are not linear.

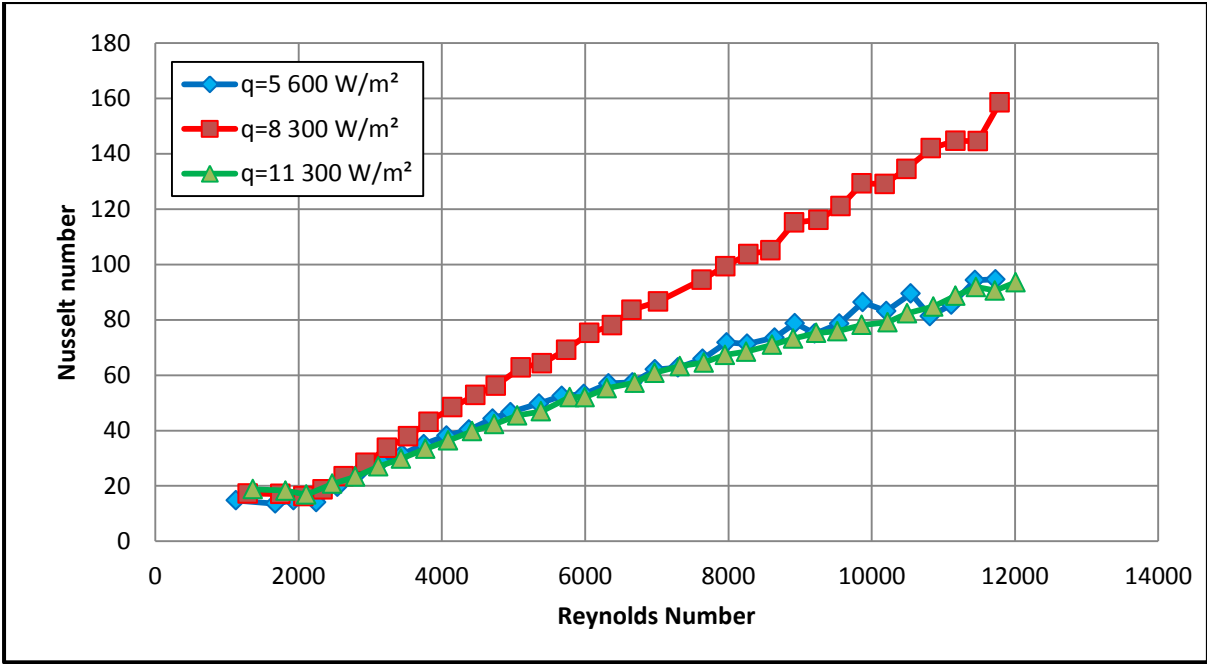


Figure 18: Graph of average Nusselt number versus Reynolds number for the smooth tube for three different heat fluxes: 5 600, 8 300 and 11 300 W/m².

Figure 18 above shows that the Nusselt number for the 5 600 and 11 300 W/m² heat fluxes are similar. The 8 300 W/m² results conclude that this test run was not acceptable, and thus is omitted from further discussion. If one were to omit the incorrect 8 300 W/m² measurements, the graph would be:

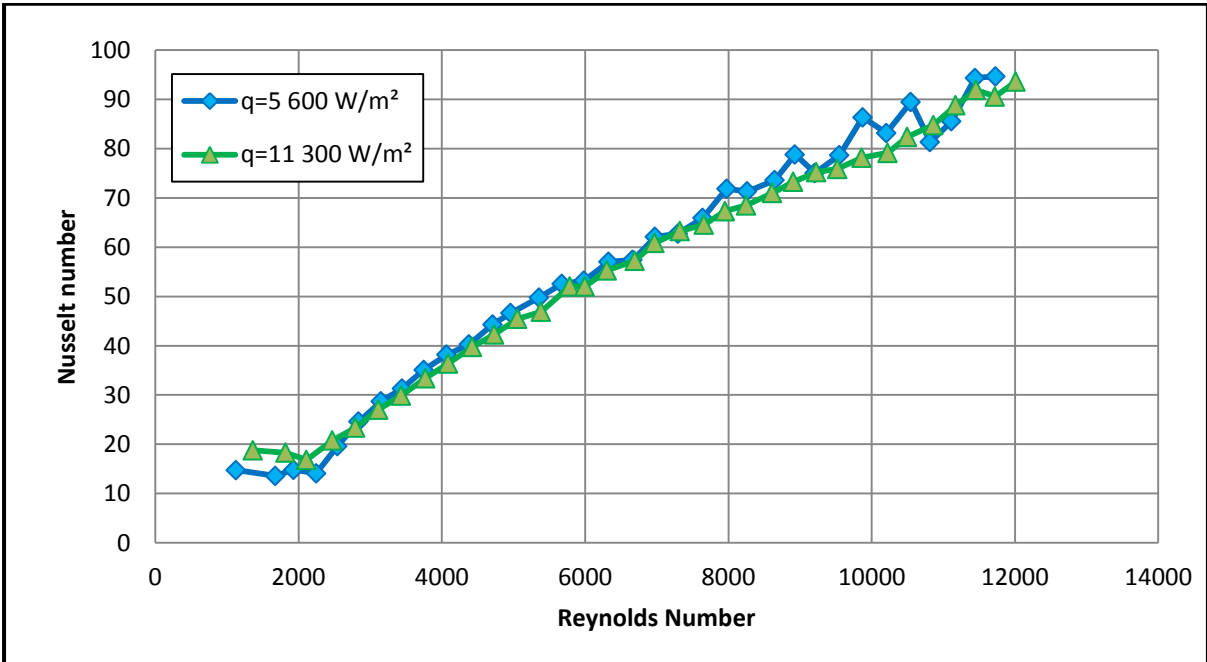


Figure 19: Graph of average Nusselt number versus Reynolds number for the smooth tube for two different heat fluxes: 5 600 and 11 300 W/m².

Figure 19 concludes that the heat flux does not have a significant effect on the Nusselt number. Both of the curves follow the same pattern and are almost superimposed on one another. The laminar region (Reynolds numbers up to approximately 2 300) shows that the Nusselt number was constant,

which was expected by theory. However, this constant value is higher than the expected value of 4.36 (Cengel & Ghajar, 2011). Using the results from the graph above, validation can be performed. Some fluctuations occur between Reynolds numbers of 8 000 and 11 500. These fluctuations are less than a Nusselt number difference of 10, and thus are minimal. For higher Reynolds numbers, a gradual increase in Nusselt number occurs for an increasing Reynolds number. Heat flux does not have an effect in this region because the Nusselt number is only dependent on the Reynolds number and Prandtl number.

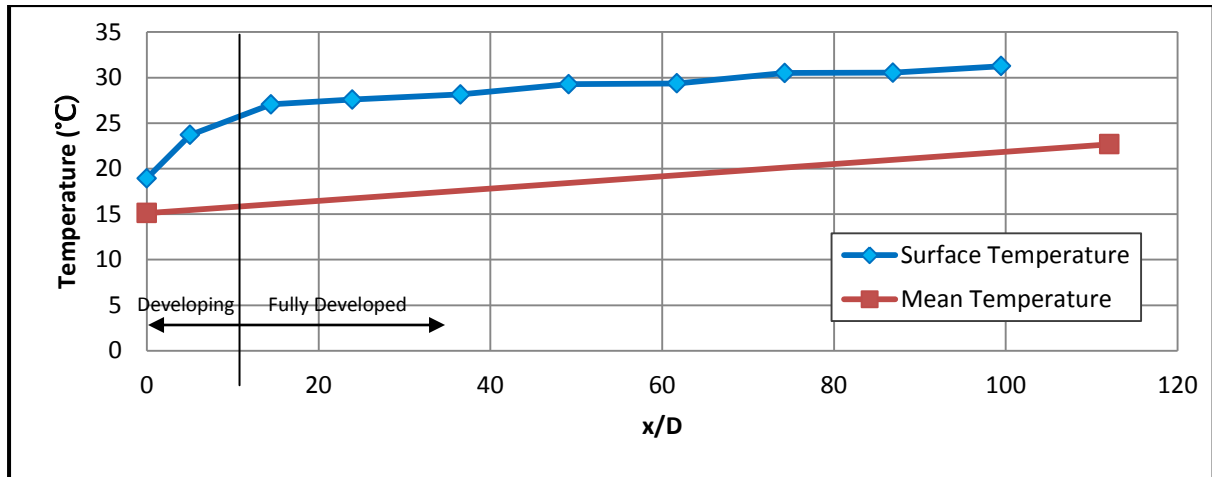


Figure 20: Temperature distributions for 5 600 W/m² smooth tube test, at a Reynolds number of 1 125.

From Figure 20, it follows that the increase in surface temperature is gradual and forms a smooth curve. This explains why the graph of the local Nusselt number versus position along the tube is smooth for this low Reynolds number. The curve of surface temperature is as expected in theory (Figure 13). The developing flow region is approximately 17 diameters, rather than the theoretical distance of 10 diameters. This is possibly because the theoretical entrance length of 10 diameters is not valid for a square-edged inlet. Figure 21 below is a graph of the surface temperature and mean temperature for the 5 600 W/m² run, at a Reynolds number of 8 650.

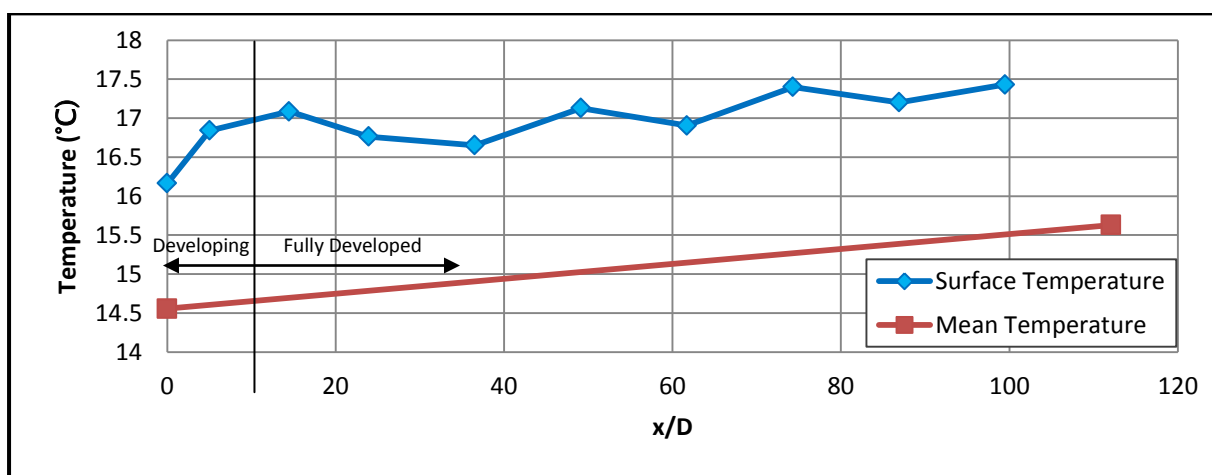


Figure 21: Temperature distributions for the 5 600 W/m² smooth tube test, at a Reynolds number of 8 650.

From Figure 21, it follows that the surface temperature does increase as distance along the tube increases. However, this is not a linear graph but the range in which the surface temperature

fluctuates is only a maximum of a 1°C band. This is because the difference in temperature of the inlet and outlet is minor at high Reynolds numbers and thus a minor variation in temperature appears to be major. This shows why the local Nusselt number versus position along the tube graph is not a smooth one. The local Nusselt number is directly affected by the surface temperature curve. A graph can be drawn showing the entire temperature scale. The fluctuations then tend to become less evident, as shown in Figure 22.

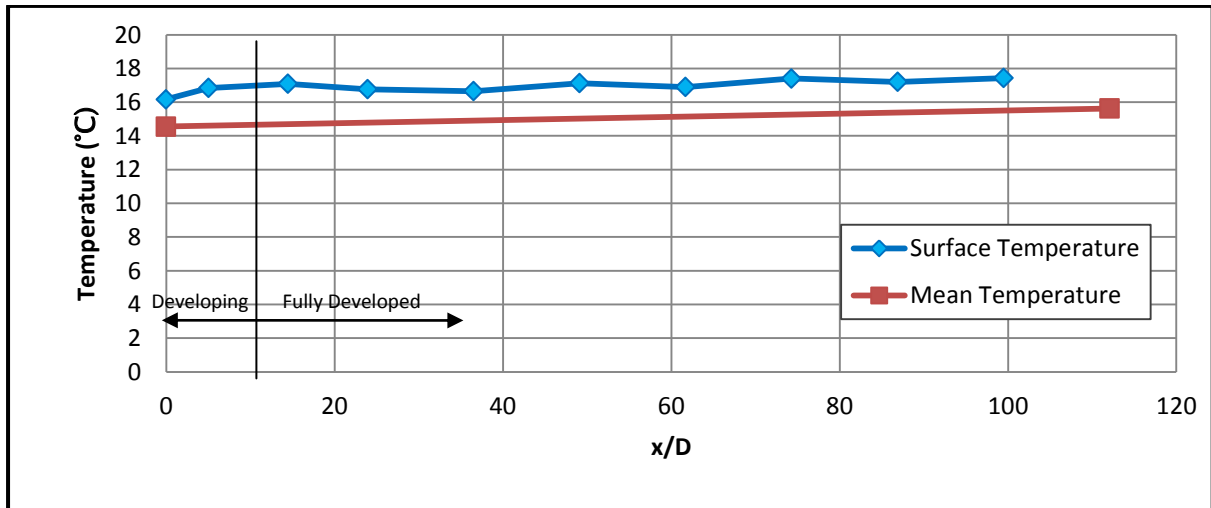


Figure 22: Temperature distributions for the entire temperature scale, for the 5 600 W/m² smooth tube test, at a Reynolds number of 8 650.

Figure 22 concludes that although fluctuations in the average surface temperature occur, they are minor. The figure shows that the difference in temperature between the inlet and outlet, approximately 2°C, is much lower than that for a low Reynolds number (Figure 20), which is approximately 8°C. This concludes that the increase in surface temperature will have a lower gradient. This explains why the temperature fluctuation band is a maximum of 1°C.

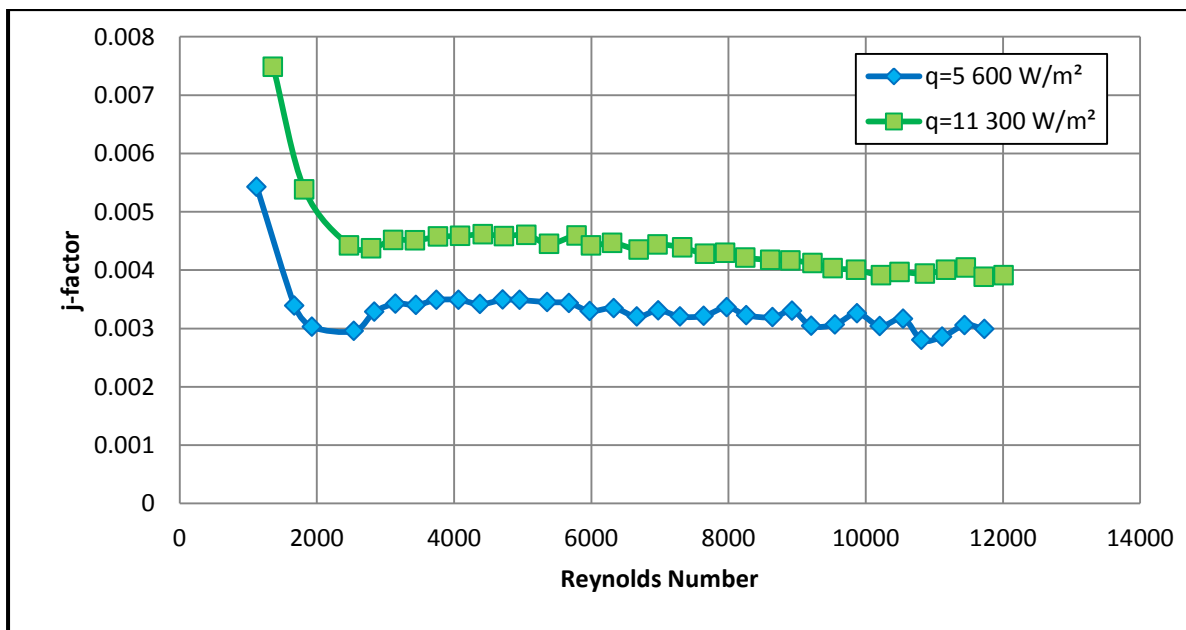


Figure 23: Graph of Colburn j-factor as a function of Reynolds number for the smooth tube. The heat fluxes depicted on the graph are 5 600 and 11 300 W/m².

The final correlation found is that which exists between the Colburn j-factor and Reynolds number. From Figure 23 it follows that the j-factor gradually decreases as Reynolds number increases. In the laminar flow regime (up to a Reynolds number of 2 100) the j-factor decreases at a faster rate than in the turbulent flow regime. In the turbulent flow regime, the graphs should become very similar, in that they should converge at high Reynolds numbers. This does not occur for these results, however, the two curves do tend to converge towards one another. The results vary by less than 0.001 and thus it is assumed that the results are acceptable. The curves of the graphs are similar to that in theory and thus the results are valid.

5.3 Validation

Validation of the test results is performed on the smooth tube data. This validation was executed on the 5 600 W/m² data as this was the first test performed. The experimental results were compared to existing correlations between the average Nusselt number and Reynolds number. The correlations used are the Dittus-Boelter equation, and the correlation determined by Olivier (2009). The correlations are tabulated below:

Author	Correlation	Restrictions
Dittus and Boelter (1930)	$Nu = 0.023Re^{0.8}Pr^{1/3}$	$0.7 \leq Pr \leq 160$ $Re > 10\ 000$
Olivier (2009)	$Nu = 2.686 \left[Re^{0.105} Pr^{1.133} \left(\frac{D}{L} \right)^{0.483} + 1.082 \left(Gr^{0.362} Pr^{-2.987} \left(\frac{L}{D} \right)^{0.202} \right)^{0.277} \right]^{2.226} \left(\frac{\mu_b}{\mu_w} \right)^{0.152}$	$940 \leq Re \leq 2\ 522$ $4.43 \leq Pr \leq 5.72$ $0.695 \leq \frac{\mu_b}{\mu_w} \leq 0.85$

Table 18: Correlations used for heat transfer validation

Where the Grashof number is determined by the equation:

$$Gr = \frac{\beta \Delta T g L^3 \rho^2}{\mu^2}$$

The volumetric expansion coefficient (β), density (ρ) and viscosity (μ) are determined from Popiel and Wojtkowiak (2007) at the bulk temperature. In this case, the length is the inner diameter of the tube and 'g' is gravitational acceleration (9.81 m/s²). The temperature difference is that which exists between the average surface temperature and the bulk temperature. Olivier's equation uses the bulk temperature and the wall (or surface) temperatures. This means that the heat flux plays a role for this equation, and thus the heat flux has an effect in the laminar flow regime.

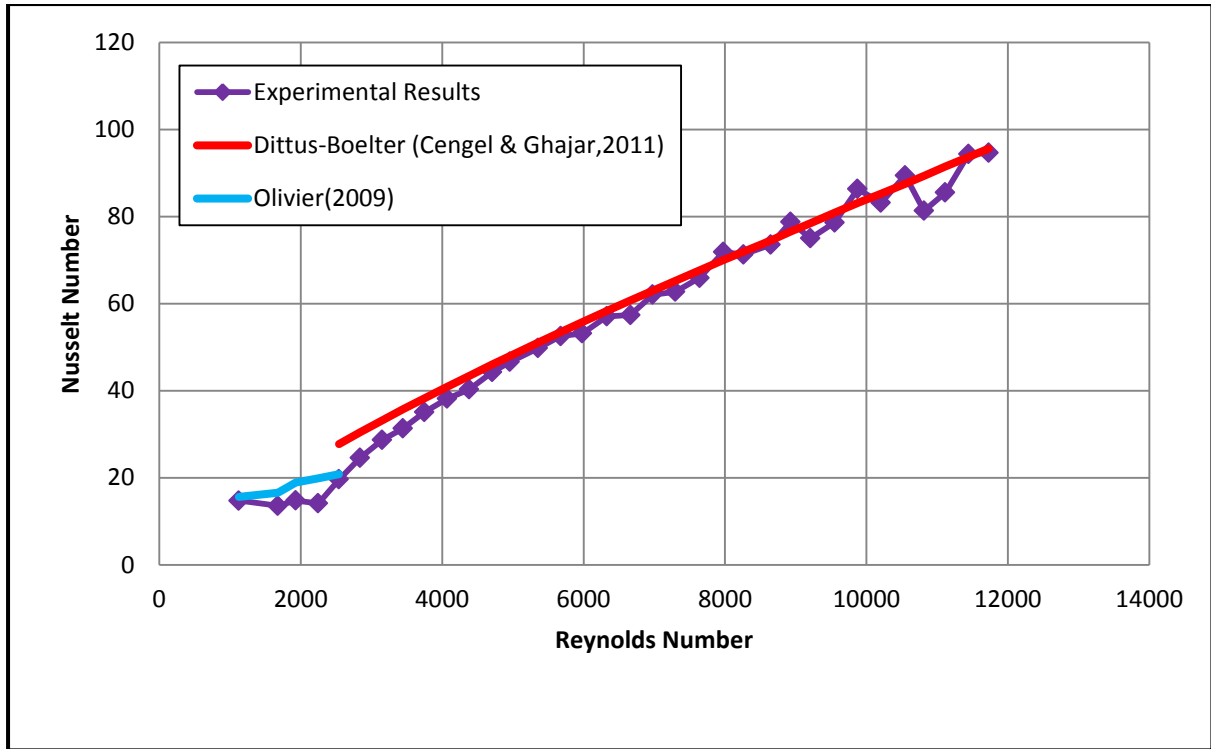


Figure 24: Heat transfer validation for the smooth tube for a heat flux of 5 600 W/m².

Figure 24 concludes that the smooth tube data closely resembles that of theory. Although some deviations occur, these are minimal and thus can be neglected. It can thus be assumed that the test results are valid. The Olivier equation is used for laminar flow up to Reynolds numbers of 2 522. This region is the region in which the most error in energy balances occurred. This could possibly be the cause in the deviation from the theoretical correlation. At Reynolds numbers between approximately 2 300 and 4 200, the data does not resemble either of the correlations. This is the transitional flow regime, and thus it is not expected that the data will agree completely with either of the correlations used.

5.4 Rough Tube Results

The calming section was removed for the rough tube experiments because one of the bolts used for the bleeding holes was tightened too much and cracked the perspex of the calming section. An attempt to seal the crack was made by using perspex glue, however, at high flow rates, water started leaking once again, due to the pressure. It was then decided, along with the supervisor, to remove the calming section for the rough tube experiment. Time constraints meant that a new calming section could not be built in time. Three heat fluxes were tested once calibration was complete. Table 19 summarises the voltage, current and heat added for the smooth tube.

Test	Current (A)	Voltage (V)	Heat added (W)	Heat flux (W/m ²)
1	2.96	169	500	5 600
2	3.63	208	755	8 400
3	4.19	239.4	1003	11 200

Table 19: Rough tube electrical input quantities

These values are then used to determine the energy balance of the system.

Approximate Reynolds number	Energy balance (%)		
	5 600 W/m ²	8 400 W/m ²	11 200 W/m ²
1 280	4.3	2.4	2.9
1 730	1.8	1.8	2.5
2 060	1.2	1.4	2.0
3 010	0.3	1.2	1.4
4 000	0.5	1.5	1.7
5 040	2.1	2.0	1.8
6 030	3.2	1.6	1.5
7 030	0.7	2.1	1.9
8 090	1.6	2.6	2.2
9 090	1.8	0.5	0.1
10 150	3.0	2.8	2.0
11 210	2.8	1.4	1.1
12 270	3.8	0.8	3.7
12 590	3.3	1.8	3.8
Table Average	1.9	1.5	1.9
Total Average	2.2	1.7	2.0

Table 20: Rough tube energy balances

A sample of 14 Reynolds numbers were used in Table 20 to give an indication as to the energy balances of the system. It can be concluded from Table 20 that the energy balances for the rough tube were good. The maximum error was 3.8% across all three heat fluxes which was acceptable. The average energy balance values conclude that a maximum error of 2.2% occurred over the entire data set. This is a good indication that the results are acceptable.

Figure 25, 26 and 27 show the variation in local Nusselt number versus position along the rough tube. Where x is the distance along the tube, and D is the outer diameter of the tube. This allows for the graph to show non-dimensionalised values for the experimental results.

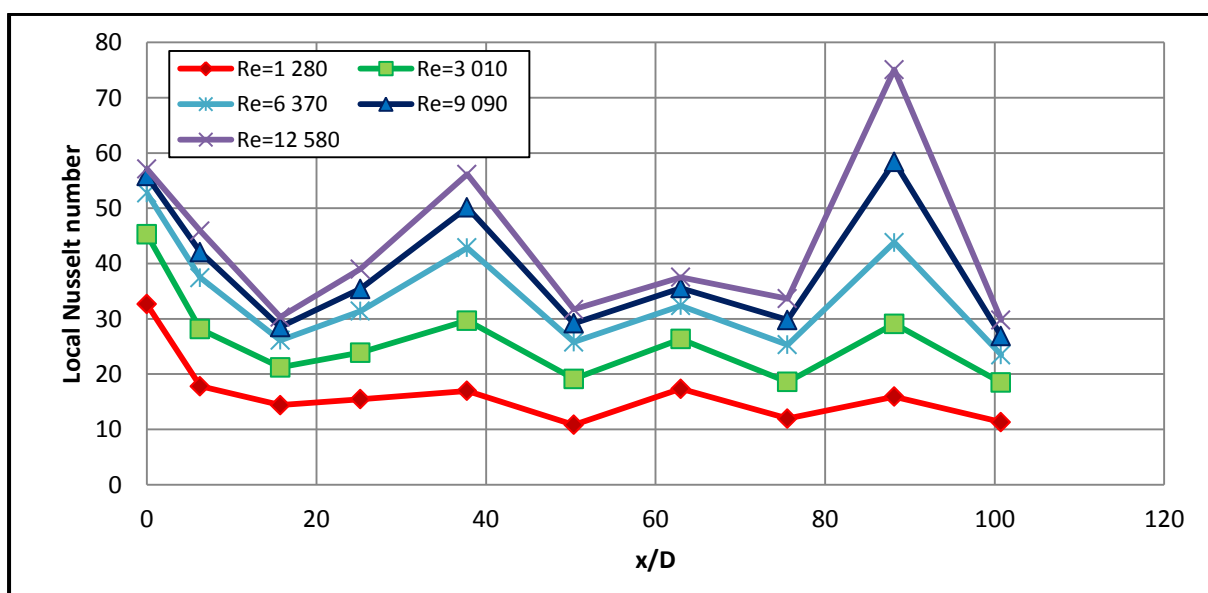


Figure 25: Graph of local Nusselt number versus position along the rough tube for various Reynolds number. This graph shows the results of the 5 600 W/m² surface heat flux test.

From Figure 25 it follows that fluctuations in the local Nusselt number occur as the position along the tube increases. The results for the first three thermocouple stations are as expected for all of the Reynolds numbers. At approximately 20 diameters, the Nusselt numbers begin to fluctuate at the higher Reynolds numbers. The lower Reynolds numbers show variations, however, these are within a 10 Nusselt number band. This is acceptable. The local Nusselt numbers tend to follow a similar pattern for the higher Reynolds numbers. The sudden increase in local Nusselt number at distances of 17 diameters and 77 diameters could be caused by disturbances in the flow due to the lack of a calming section.

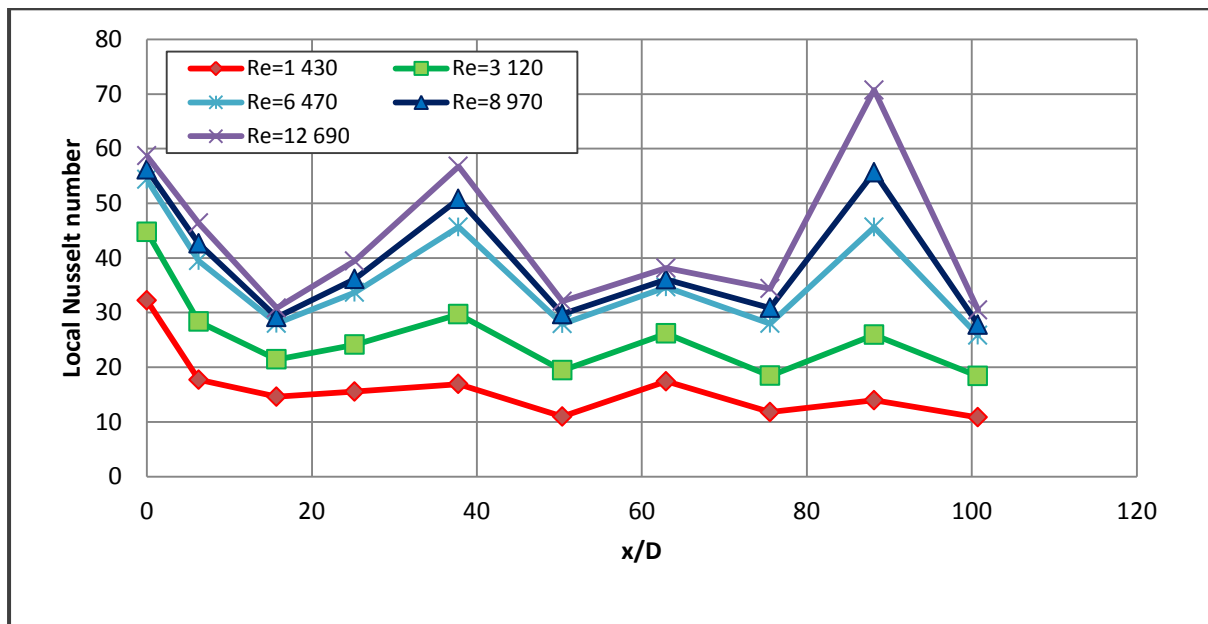


Figure 26: Graph of local Nusselt number versus position along the rough tube for various Reynolds number. This graph shows the results of the $8\,400\text{ W/m}^2$ surface heat flux test.

Similar conclusions can be made from Figure 26. This figure depicts fluctuations beginning at approximately 17 diameters along the tube. The graph once again proves to be as expected prior to this position. The fluctuations are lower for the lower Reynolds numbers and greater for the higher Reynolds numbers. The temperature difference at high Reynolds numbers is minor, in comparison to the difference at low Reynolds numbers, and thus a small temperature change along the tube will prove to have a big affect on the Nusselt number. This is the reason for the fluctuations in the Nusselt number to be more visible for the higher flow rates. The curves for the local Nusselt number follow a similar pattern at high Reynolds numbers.

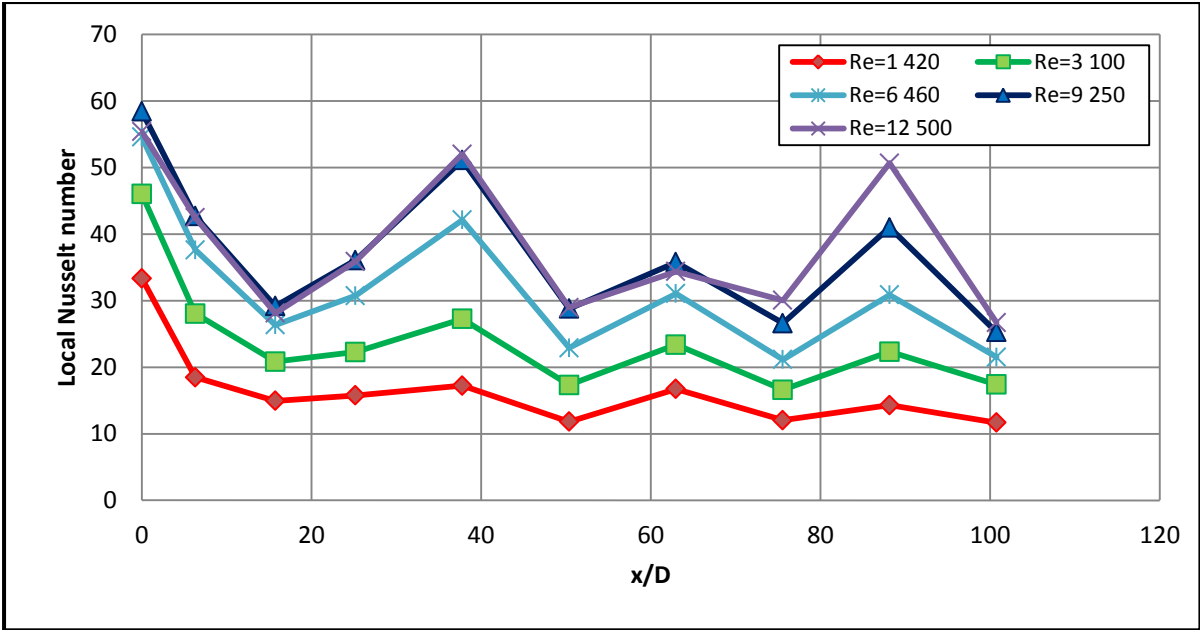


Figure 27: Graph of local Nusselt number versus position along the rough tube for various Reynolds number. This graph shows the results of the $11\ 200\ \text{W/m}^2$ surface heat flux test.

Figure 27 shows similar results to Figure 25 and Figure 26. Once again, the curves perform as expected for approximately 17 diameters along the tube. Fluctuations exist for all of the Reynolds numbers shown. Fluctuations are higher for higher Reynolds numbers, however, these fluctuations occur within a band. Reynolds numbers of 9 250 and 12 500 tend to show curves which are very similar, in fact they are the same for the majority of the points. This concludes that the Reynolds number begins to have negligible effect on the local Nusselt number when a high surface heat flux is applied. This is applicable to Reynolds numbers in the turbulent flow regime. Increases occur at 17 and 77 diameters along the tube, once again.

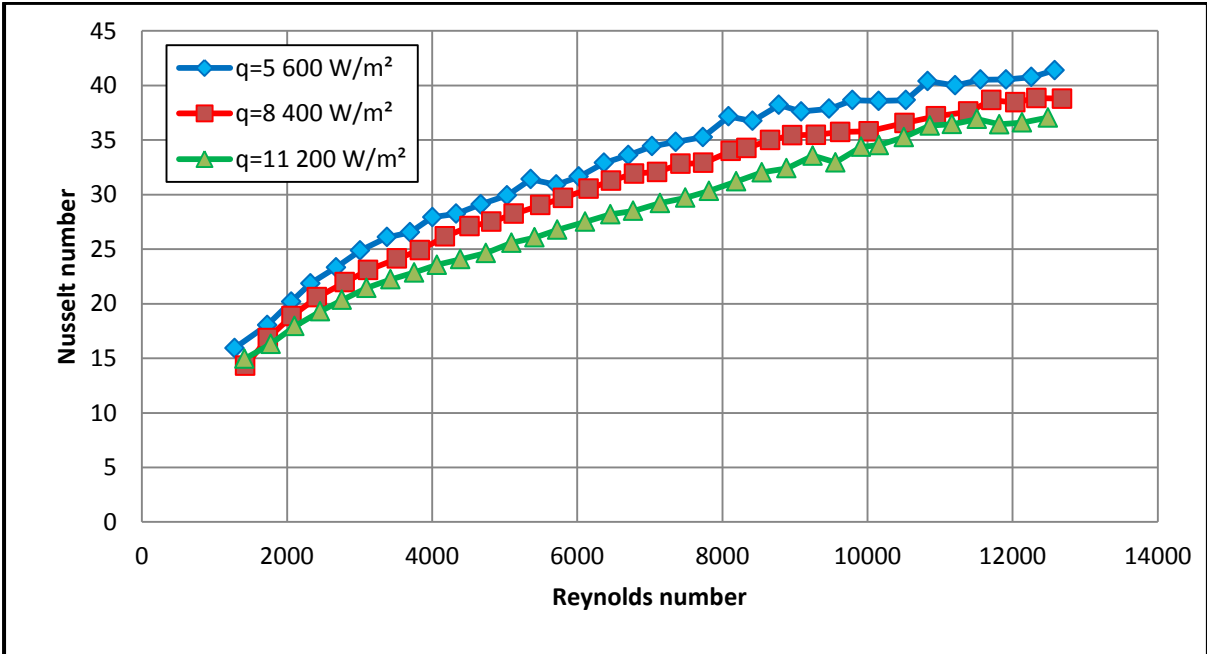


Figure 28: Graph of average Nusselt number versus Reynolds number for the rough tube for three different heat fluxes: 5 600, 8 400 and $11\ 200\ \text{W/m}^2$.

Figure 28 depicts the relationship between Nusselt number and Reynolds number for three different constant surface heat fluxes. The curves for the three heat fluxes are similar, and at any specific point, the difference in Nusselt number from the highest heat flux ($11\,200\text{ W/m}^2$) to the lowest heat flux ($5\,600\text{ W/m}^2$) is less than 10. This shows that the heat flux tends to have a negligible effect on the Reynolds number. This is because the Nusselt number is a function of the Reynolds number and the Prandtl number, which do not consider heat flux, in the turbulent region. It appears as though the laminar flow regime is not depicted in Figure 28. This means that transition occurs very early for the relative roughness of 0.04.

For comparison, the same Reynolds number and heat flux temperature distributions are shown. Figure 29 and 30 are temperature distributions for the $5\,600\text{ W/m}^2$ tests.

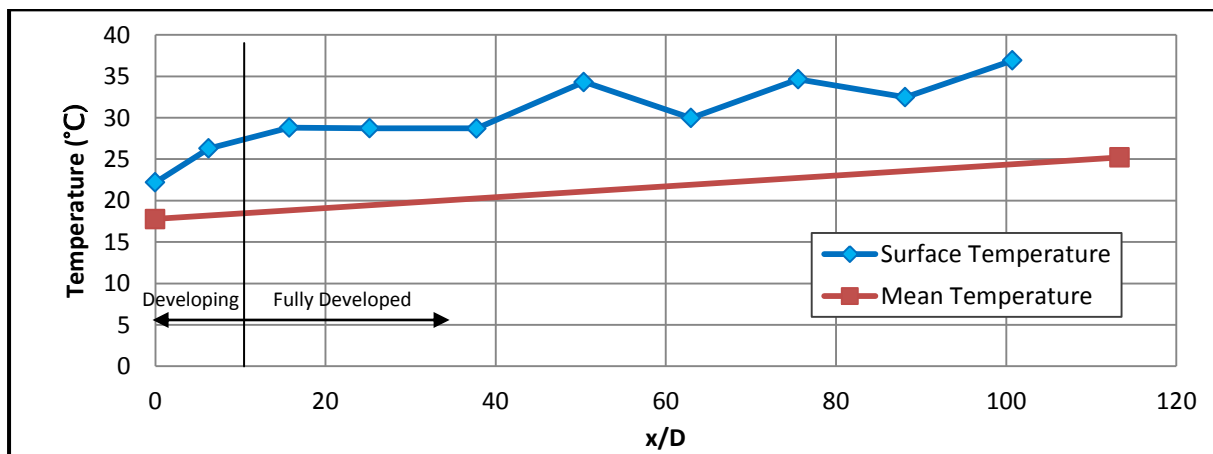


Figure 29: Temperature distribution for $5\,600\text{ W/m}^2$ rough tube test, for a Reynolds number of 1 280.

From Figure 29 it follows that the average surface temperature does increase as position increases. This is as expected in theory. Minimal fluctuations occur in the surface temperature along the tube instead of the expected linear curve for fully developed flow. The curve performs as expected for approximately 40 diameters. The fluctuations which occur are within an acceptable range, lying in a band of approximately 5°C .

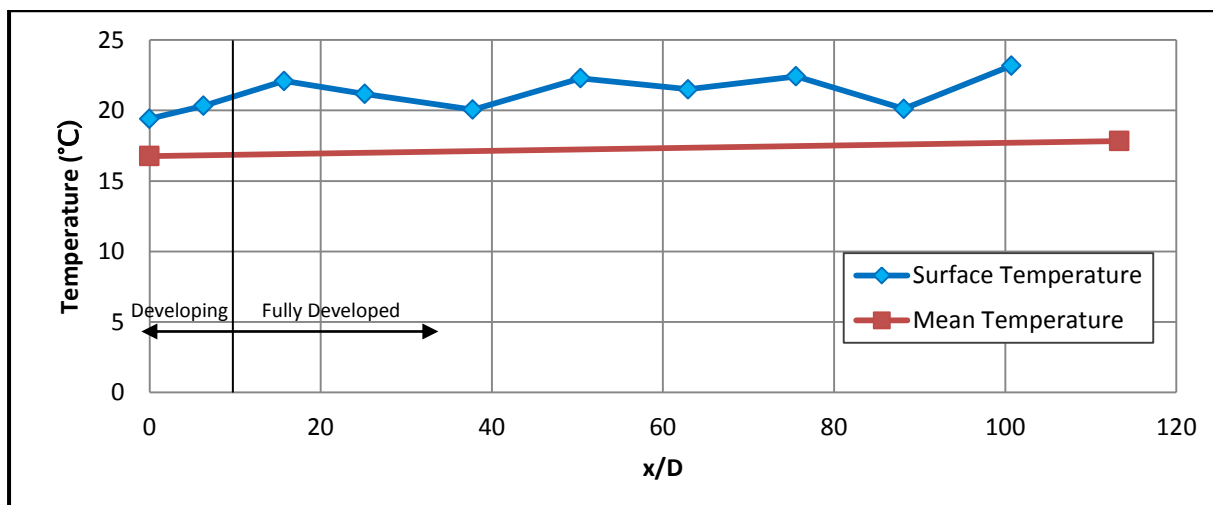


Figure 30: Temperature distribution for $5\,600\text{ W/m}^2$ rough tube test, for a Reynolds number of 9 090.

Figure 30 concludes that surface temperature fluctuations do occur along the tube, rather than the expected linear graph. The fluctuations for the Reynolds number of 9 090 tend to be minimalised in comparison to that of the 1 280 Reynolds number. These temperature fluctuations occur within a 2°C band of the expected curve. Thus, it can be assumed that the local Nusselt number results are valid. The fluctuations in temperature have a direct influence on the local Nusselt numbers and thus the graphs of local Nusselt number versus position along the tube are not completely smooth. The fluctuations in surface temperature for the rough tube tend to be more deviant (the band is larger) at similar Reynolds numbers. This could possibly be due to the effect of surface roughness and the lack of the calming section.

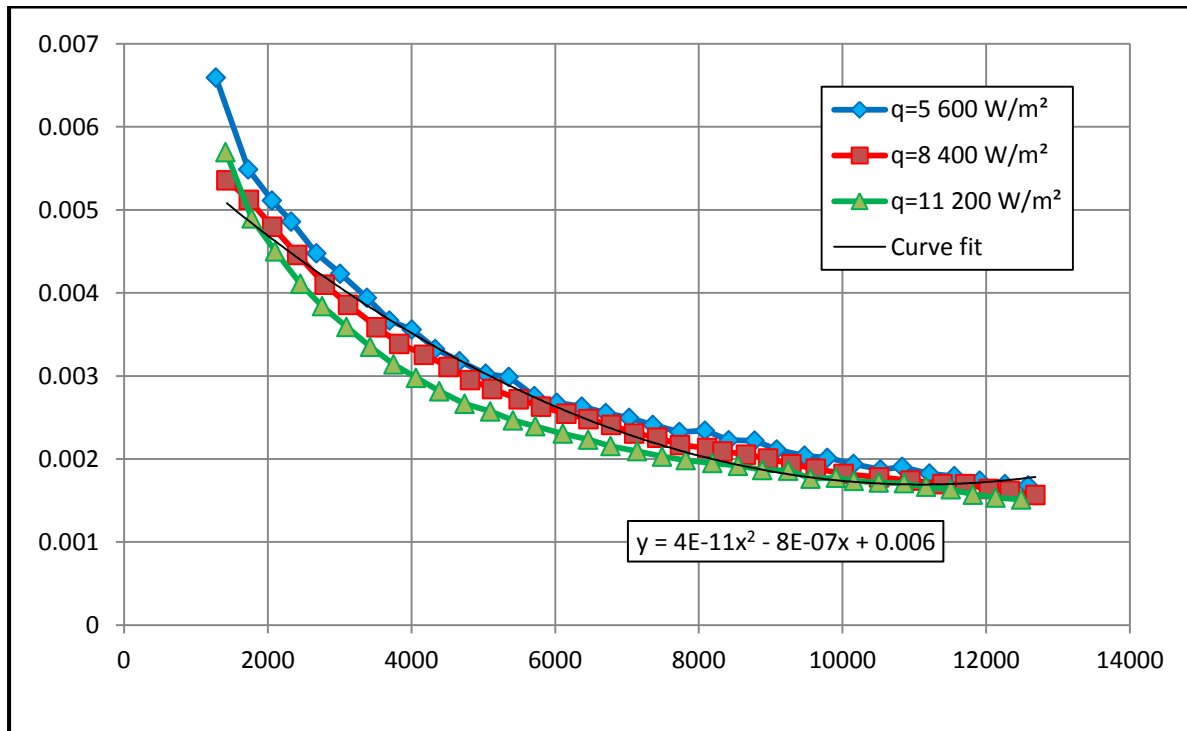


Figure 31: Graph of Colburn j-factor as a function of Reynolds number for the rough tube. The heat fluxes depicted on the graph of 5 600, 8 400 and 11 200 W/m².

From Figure 31 it follows that the Colburn j-factor gradually decreases as Reynolds number increases. The three heat fluxes give very similar results and essentially follow the same pattern. It appears as though only the turbulent flow regime is depicted on the graph. It was decided that the lowest Reynolds number tested would be approximately 1 200. This is to prevent the damage of equipment and possible burn out of the tube. This data can be plotted on a logarithmic scale as depicted in Figure 32.

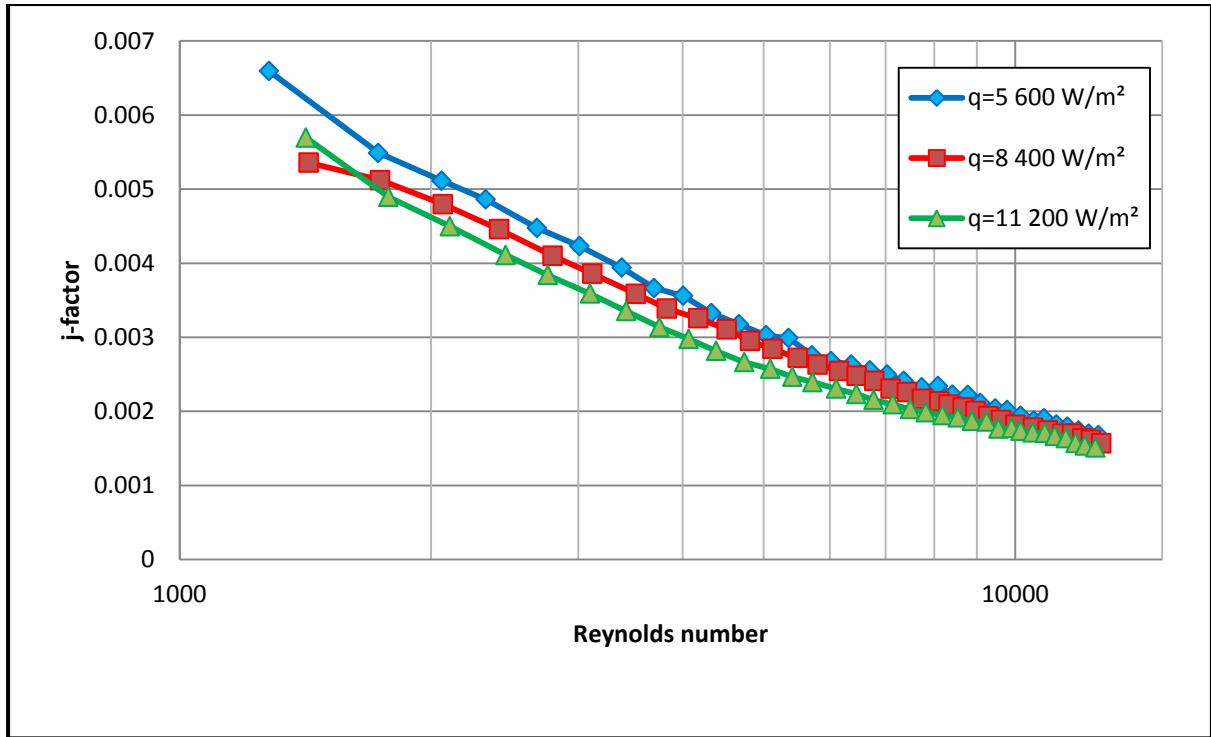


Figure 32: Graph of Colburn j-factor versus Reynolds number for three heat fluxes, on a logarithmic scale. The heat fluxes depicted on the graph of 5 600, 8 400 and 11 200 W/m².

The equation of the trend line for all three heat fluxes together test is:

$$j = (4 \times 10^{-11})Re^2 - (8 \times 10^{-7})Re + 0.006$$

This equation is a second order polynomial and describes the relationship between the Reynolds number and the Colburn j-factor for a constant surface heat flux of 5 600, 8 400 and 11 200 W/m² on a tube with a relative roughness of approximately 0.0415. The equation shows that the maximum value for this tube at this heat flux is 0.006 (at a zero flow rate) and this decreases as the Reynolds number increases. The Reynolds number has a significant effect on the j-factor of the system.

This equation can be written in terms of the Nusselt number, Prandtl number and Reynolds number. This gives a theoretical equation, to determine the Nusselt number, which can be compared to the measured Nusselt numbers.

$$j = \frac{Nu}{RePr^{1/3}}$$

$$Nu = RePr^{1/3}[(4 \times 10^{-11})Re^2 - (8 \times 10^{-7})Re + 0.006]$$

This equation ensures that the Nusselt number is no longer dependent on heat flux, but only the Prandtl number and the Reynolds number. This relation is applicable to a circular tube with a relative roughness of 0.04.

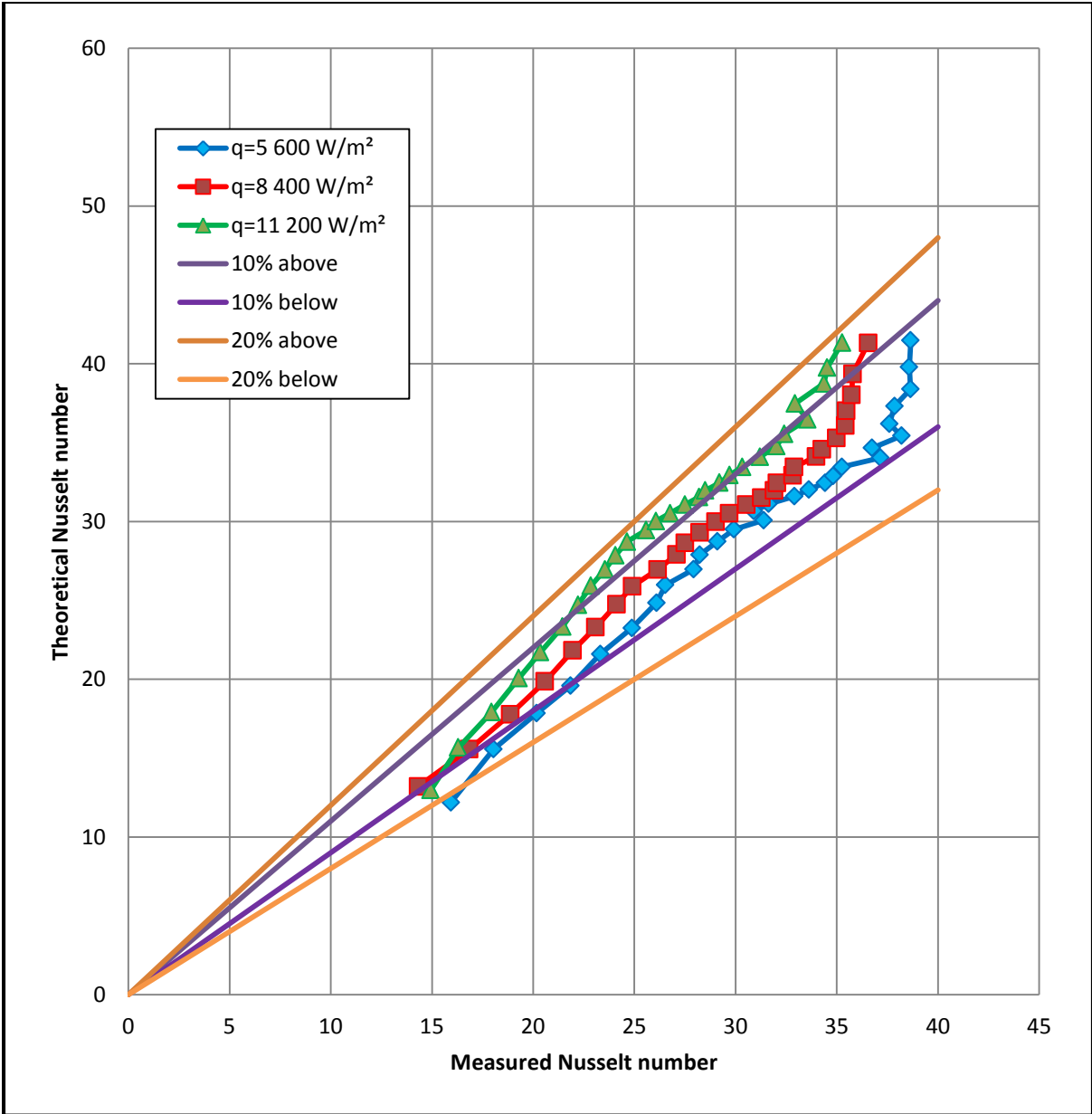


Figure 33: Graph depicting the relationship between the measured Nusselt number and the theoretical Nusselt number for three heat fluxes. The heat fluxes on the graph are: 5 600, 8 400 and 11 200 W/m².

Figure 33 depicts the relationship between the measured Nusselt number and the theoretical Nusselt number obtained from the curve fit in Figure 31. This graph gives the relationship when the theoretical Nusselt number is not dependent on the heat flux. It can be concluded that the correlation lies within a 20% error margin which is acceptable when considering heat transfer. The majority of the values obtained for the heat fluxes of 5 600 and 8 400 W/m² lie within a 10% error of the expected values. The relationship for the heat flux of 11 200 W/m² depicts that the values lie within a 20% error margin. The lower and higher Nusselt numbers are the regions in which the highest deviation from the expected relationship occurs.

5.5 Comparison between smooth and rough tube

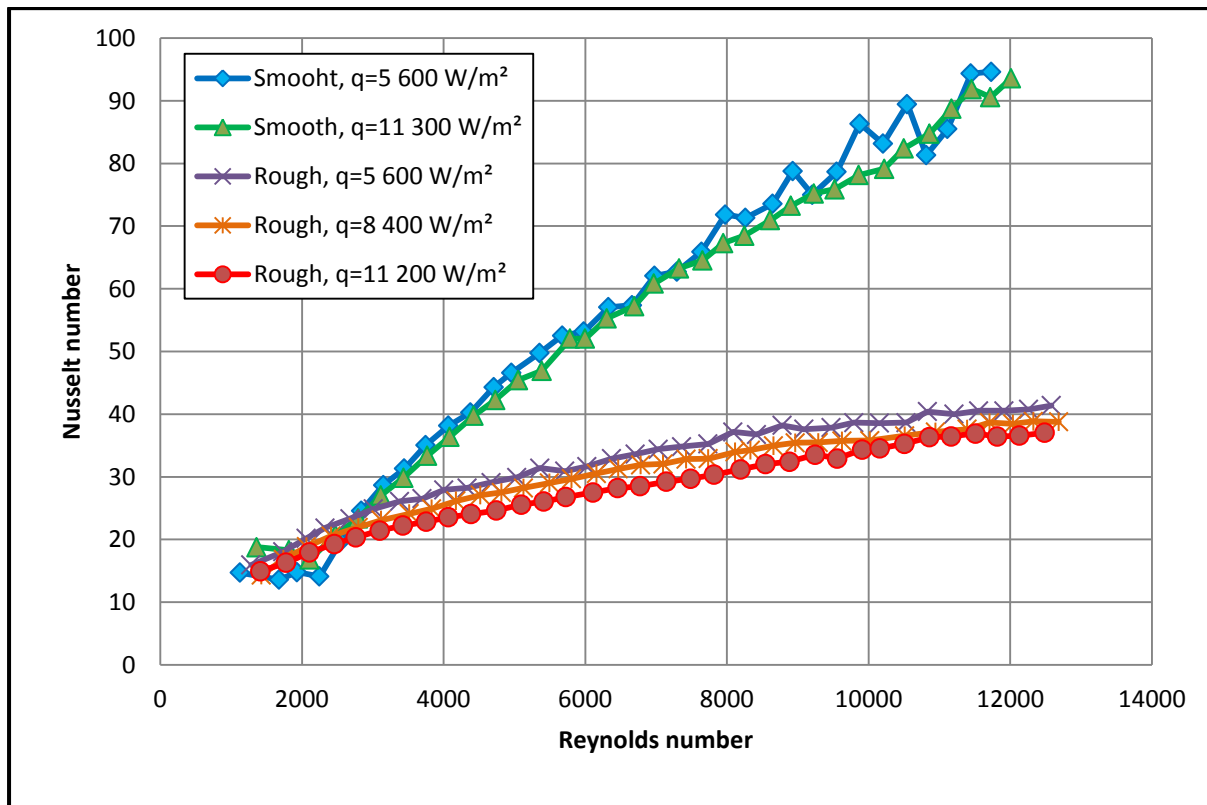


Figure 34: Graph of average Nusselt number versus Reynolds number for the smooth and rough tubes

Conclusions can be drawn from Figure 34. The Nusselt number decreases slightly as the surface heat flux increases. The smooth tube results are much higher than the rough tube results. This is possibly due to the increase in thermal resistance in the rough tube. The thermal resistance in the rough tube is higher than that of the smooth tube because the glue and sand have a lower thermal conductivity than the copper. Thus they tend to act as a form of insulation.

In the turbulent flow regime, the change in surface heat flux has very little effect on the Nusselt number. This is because the Nusselt number is a function of Reynolds number and Prandtl number, and thus the change in heat flux has very little effect on the heat transfer coefficient.

The results for the smooth tube are very similar for the two heat fluxes shown in Figure 34. The rough tube results are very similar to each other for the three heat fluxes. This is because the majority of the points plotted are in the turbulent region.

When considering the smooth tube results in the laminar region, the Nusselt number is a function of the Reynolds number, Prandtl number and the Grashof number. The Grashof number is affected by the heat flux, as the difference in surface temperature and bulk temperature is considered. This explains why variations between the two smooth tube heat fluxes occur in the laminar flow regime.

It appears as though the laminar region is not visible in Figure 34 for the rough tube. A calming section was not used for this tube, and thus disturbances in the flow could possibly exist. Also, it was decided to test from a Reynolds number of approximately 1100, as this would cause an exit

temperature of less than 60°C, which is the maximum temperature that the pump can handle. Also, it was important that the sand in the tube would not burn out. At a very low Reynolds number, the temperature increase would be very high, and thus the glue could start to melt. For these reasons, the starting value for the experiment was a Reynolds number of 1 100.

Transition occurs earlier in a roughened tube, and a square-edged inlet no longer existed, due to the removal of the calming section. This has affected the results for the rough tube.

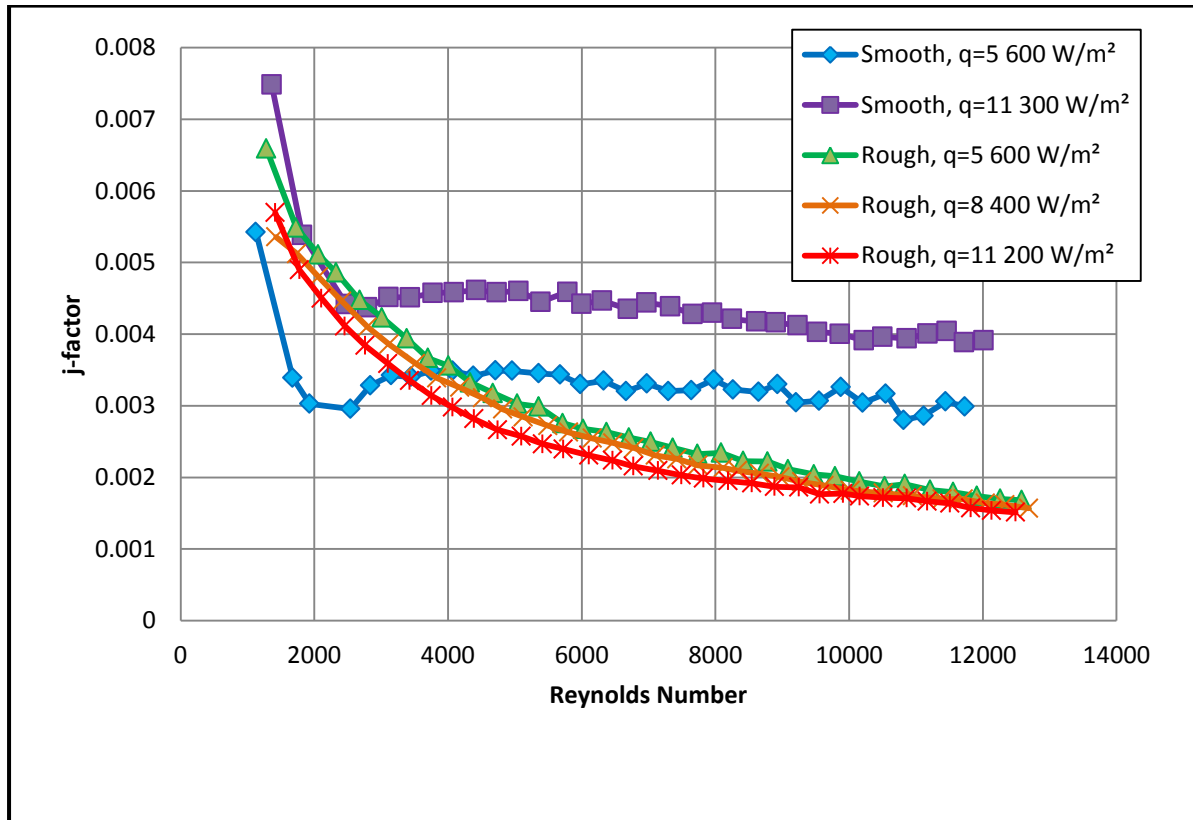


Figure 35: Graph of Colburn j-factor as a function of Reynolds number for the smooth and rough tube. The heat fluxes depicted on the graph of 5 600 and 11 300 W/m² for the smooth tube, and 5 600, 8 400 and 11 200 W/m² for the rough tube.

From Figure 35 it can be concluded that the Colburn j-factors are lower for the rough tube than for the smooth tube, particularly in the turbulent flow regime at Reynolds numbers greater than 4 000. The results for the smooth tube depict a curve which is similar to that in theory for the laminar and turbulent flow regimes, however, the two smooth tube curves do not converge as quickly as they should. The rough tube results depict what is expected for the turbulent flow regime. The graphs are similar and converge at a Reynolds number of approximately 9 000.

5.6 Summary, Discussion and Conclusions

The results were proven to be valid when comparing the experimental results of the smooth tube, to the Olivier (2009) and Dittus-Boelter (1930) equations. The correlation between the experimental data and theory was acceptable (Figure 24). Minor fluctuations occurred towards the end of the turbulent flow regime, but even at these points, the variations were minimal. When comparing the

measured Nusselt number to the theoretical Nusselt number, depicted in Figure 33, the data correlates well error margin of 20% exists, which is acceptable when considering heat transfer.

The average energy balances for the results are good, when excluding the $8\ 300\ \text{W/m}^2$ heat flux on the smooth tube. These results are unacceptable due to the burn out of two of the heating wires. This occurred as a result of the length of heating wire between the tube and the power supply being too long. This caused a high temperature in the wires, and these wires were not being cooled down by the water in the tube. This problem did not occur on the rough tube, as the length of heating wire between the tube and the power supply was shortened.

The removal of the calming section had a big effect on the overall rough tube results. Flow disturbances could not be removed, and thus, at low Reynolds numbers, laminar flow was not present. This also caused some fluctuations in the results. Transition occurred much earlier in the roughened tube.

When considering the graphs of local Nusselt number versus position along the tube, it can be seen that as the Reynolds number increases, the local Nusselt number increases, for both the smooth and rough tubes. Fluctuations occur in both tubes, for the higher Reynolds numbers (greater than 6 000), however, these fluctuations occur within an acceptable band.

The change in surface heat flux has very little effect on both the smooth and roughened tubes average Nusselt number results. This is due to the fact that the Nusselt number is a function of only the Reynolds number and Prandtl number in the turbulent flow regime. It is not dependent on heat flux and thus the graphs tend to follow the same pattern over the same range of Reynolds numbers.

When comparing the smooth tube results and the rough tube results for the average Nusselt number as a function of Reynolds number, it is obvious that the average Nusselt number for the rough tube is much lower than that for the smooth tube. This is unexpected and it can be concluded that thermal resistance plays an important role, causing lower Nusselt numbers. The thermal resistance of the rough tube was increased by the addition of a glue layer and a sand layer. Neglecting insulation from the system, the following is found for the thermal resistance:

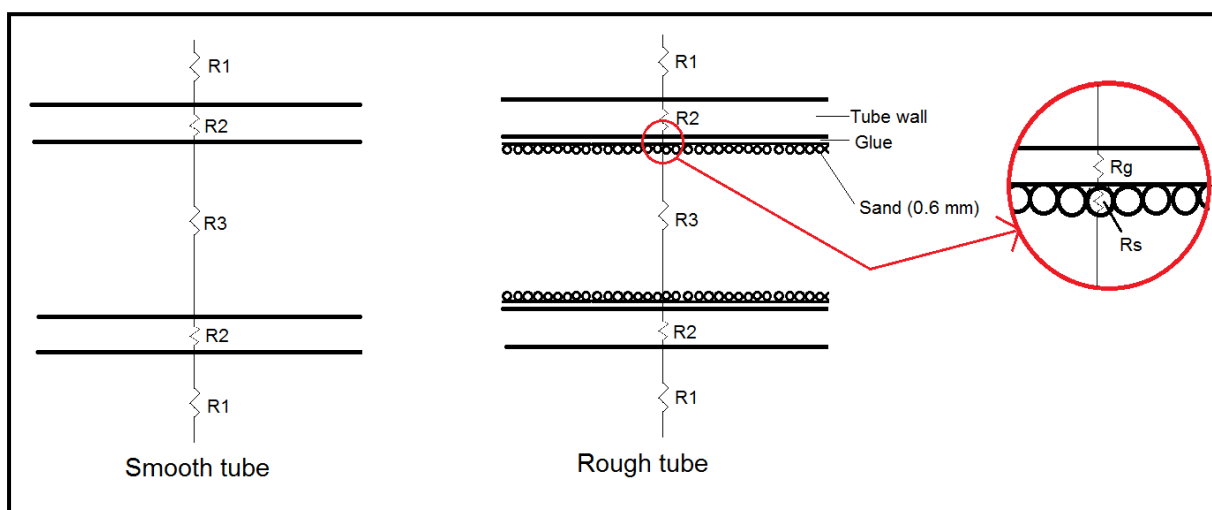


Figure 36: Thermal resistance of the smooth and rough tubes

For the smooth tube, the thermal resistance is determined by the following equations.

$$R_{total} = R_1 + R_2 + R_3$$

$$= \frac{1}{h_o A_o} + \frac{\ln\left(\frac{D_o}{D_i}\right)}{2\pi k L} + \frac{1}{h_i A_i}$$

Where h_o is the heat transfer coefficient to the surroundings and h_i is the heat transfer coefficient of the water. A_o and A_i are the outer surface areas and the inner surface areas respectively. L is the length of the tube and k is the thermal conductivity of the copper tube. D_o and D_i are the outer diameters and inner diameters respectively. The thermal resistance for the rough tube is given by:

$$R_{total} = R_1 + R_2 + R_g + R_s + R_3$$

$$= \frac{1}{h_o A_o} + \left(\frac{\ln\left(\frac{D_o}{D_i}\right)}{2\pi k L}\right)_{tube} + \left(\frac{\ln\left(\frac{D_o}{D_i}\right)}{2\pi k L}\right)_{glue} + \left(\frac{\ln\left(\frac{D_o}{D_i}\right)}{2\pi k L}\right)_{sand} + \frac{1}{h_i A_i}$$

Where the thermal conductivities k , inner, and outer diameters are those stipulated by the subscripts. The equations above prove that for the addition of glue and sand, the thermal resistance will increase. However, it is recommended that in follow up work, these resistances be measured. The Nusselt number of rough tubes can then be determined accordingly. A thinner layer of glue should be used with a higher thermal conductivity. Sand with a higher thermal conductivity should also be used. This will ensure that the resistance of the glue and sand is negligible. The heat transferred through the tube is given by the equation:

$$\dot{Q} = \frac{\Delta T}{R_{total}}$$

Where ΔT is the change in temperature between the mean and ambient temperatures. This proves that the heat transfer for the rough tube will be less than that for the smooth tube. The heat transfer coefficients will be lower resulting in lower Nusselt numbers.

The relationship between the Colburn j-factor and Reynolds number is a good representation of the results. The rough tube correlation is good, because the results converge. The correlation for the smooth tube depicts laminar, transition and turbulent flow regimes, however, the curves for the different heat fluxes don't converge as fast as they should.

Transition occurred very quickly in the rough tube. In order to reduce the possibility of damaging equipment and possibly burn out of the tube, it was decided to start testing at Reynolds numbers of approximately 1 100. Burn out could occur as a result of very high outlet temperatures at low Reynolds numbers. Therefore it appears as though laminar results do not exist.

Chapter 6

Summary, Conclusions, Recommendations and Limitations

6.1 Summary

The purpose of this project was to determine the effect of surface roughness on heat transfer and pressure drop in the transition region. It has not been possible to determine the pressure drop due to a faulty manometer. The heat transfer results were found and conclusions have been drawn. Further conclusions are given in this chapter as well as recommendations for further work. Limitations with regard to this project are also discussed in this chapter.

The test section, including the mixing well was essentially inserted into an existing system which has been used for similar projects. The test section consisted of a 15.88 mm outer diameter copper tube with a wall thickness of 0.71 mm. Thermocouples were attached along the outer surface in order to record the temperature. Two pressure taps were silver soldered on to the tube in order to measure the pressure drop across the system, and therefore obtain the friction factor. This was not possible as the calibration of the pressure diaphragms was ineffective due to faulty equipment. The mixing well was attached to the exit of the test section. This test section was then attached to a calming section (at the entrance) and to the storage tank.

Reynolds numbers of 1 125 to 12 700 were tested in order to determine the effect of surface roughness. The Prandtl numbers ranged from 6.3 to 8.1. Three heat fluxes were tested for each tube. The smooth tube was subject to heat fluxes of 5 600, 8 300 and 11 300 W/m², and the rough tube was subject to heat fluxes of 5 600, 8 400 and 11 200 W/m².

6.2 Conclusions

The Nusselt number is higher at higher Reynolds numbers and thus the heat transfer coefficient is higher. At higher Reynolds numbers (typically in the turbulent flow regime), the change in heat flux seems to have little effect on the Nusselt number.

The local Nusselt number for the smooth tube shows good results at low Reynolds numbers, with a smooth graph, however, at higher Reynolds numbers the curve seems to fluctuate within a band. This is because the overall increase in the average surface temperature is less for higher Reynolds numbers, and thus any minor deviation from the expected appears to be major deviation. Local Nusselt numbers, for Reynolds numbers in the transition region, tend to behave as the local Nusselt numbers, for Reynolds numbers in the turbulent flow regime, do. These also fluctuate in certain, acceptable bands.

The results from the rough tube experiment are not completely comparable with the smooth tube results because a calming section was not used for the rough tube. A square-edged inlet was no longer used as the calming section housed this.

The results for the average Nusselt number as a function of Reynolds number depict that the Nusselt numbers for the roughened tubes are much lower than the Nusselt numbers for the smooth tube. This is because the layer of sand and the layer of glue add additional thermal resistance to the test section. This thermal resistance essentially acts as insulation, and thus the heat transfer coefficient is less. This results in a lower Nusselt number.

Surface temperature distributions have a direct and large effect on the local Nusselt number. The surface temperature distributions are varying for the higher Reynolds numbers. This explains the irregular pattern of the local Nusselt numbers. Although fluctuations occur, they occur within acceptable bands for each Reynolds number and heat flux. For the rough tube, irregular curves can be seen at low flow Reynolds numbers as well. This is possibly due to transition occurring earlier in a roughened tube. It could also be due to the removal of the calming section. Friction could cause these fluctuations as well. Flow disturbances and inconsistent velocity profiles could have affected these results. The graphs are constant, but they are not linear.

The friction in this rough tube test section is expected to be very high in comparison to the smooth tube. The relative roughness of the tube is 0.04. This caused a very early transition period and thus the results do not cover all flow regimes for the rough tube. It was decided to limit the starting Reynolds number to approximately 1 100 in order to prevent burn out of the tube and the damage of the equipment such as the pump.

The coriolis flow meters are adjusted by volume flow rate in L/hr. Thus higher Reynolds numbers are visible in the rough tube than the smooth tube for the same volume flow rate. This is because the cross-sectional area of the roughened tube is less than that of the smooth tube. Thus the graphs given are not for the exact same Reynolds numbers, but the same volume flow rate. The change would be minor when comparing the two tubes.

The Colburn j-factor versus Reynolds number correlation shows that the rough tube results are valid. The curve is not affected by the heat flux, because the properties with which the j-factor is determined, are the Nusselt number, Prandtl number and Reynolds number. None of these quantities are dependent on the surface heat flux.

In conclusion, the heat transfer coefficient and the Nusselt number are lower for a roughened tube than for a smooth tube. If changes can be made as recommended, these quantities could increase. In terms of a roughened tube being a better option for increasing energy demands and the possibility of operation in the transitional flow regime, the results prove differently, when considering the turbulent flow regime. The thermal resistance is much higher for a roughened tube and this plays a major role in heat transfer. The roughened tube has a decreased surface area over which heat can be transferred. Transition occurs much earlier for a roughened tube than for a smooth tube, and thus to operate in this region will require low Reynolds numbers, for the roughened tube.

6.3 Recommendations

With any experiment, better methods are only found when one is busy completing the project. With regards to this project, the build could have been made simpler by re-ordering some of the assembly steps.

Human error is a concern with a project such as this one. The indentations drilled into the tubes may not necessary all be the same size, as well as the size of the solder and the depth of the thermocouples in the tube walls. Thus temperatures may not be exact. A possible recommendation would be to have additional thermocouple stations. The flow is thermally developing for the entire distance when considering laminar flow. It would be helpful to see the increase in surface temperature at more points.

A recommendation would be to attempt this research on longer tubes. The sanding of the tube is a problem, but sections of tube can be joined together using couplings.

When wrapping the tube with the heating wires, the thermocouple stations have to be skipped. For a certain distance before the station (approximately 10 mm), heating wire is not used. This should not make a major difference to the results because copper has a high thermal conductivity, but the heat flux is not applied directly to the area in which the surface temperature is being measured. The space between the heating wire and the thermocouple station could be lessened in order to remove this effect.

When calibration of the pressure transducer was being done, a manometer which is meant for larger pressure ranges was used. This causes errors at low pressures and thus the pressure values may not be very precise. Due to time constraints, calibration could not be re-done as a new manometer would not be available in time. It is recommended that once a manometer is available, pressure calibration is done and an adiabatic test performed so that the influence of surface roughness on pressure drop can be determined.

The sanding technique was practised many times, however, the layer of sand in the test section is not known, and it is therefore difficult to predict whether or not it was done perfectly. This could further have influenced the results. More practise could result in a more even glue and sand layer which could result in better experimental data. A possibility is to research types of glues and sands that will have a higher thermal conductivity. This will reduce the thermal resistance and increase the heat transfer. Thus the heat transfer coefficients and Nusselt numbers will be higher.

If time constraints were not an issue, a new calming section could be built which would allow for a more accurate inlet temperature reading for the rough tube. This is because the Pt-100 at the inlet had to be read off a screen rather than from the mean of 100 data files. Because a calming section was used for the rough tube and not for the smooth tube, the bulk temperatures and mean temperatures are not on the same scale. Thus, a new calming section could resolve this problem.

When considering the smooth tube, two of the heating wires burnt out. If time constraints were not an issue, the tube could be re-wrapped with heating wire, and the $8\ 400\ \text{W/m}^2$ heat flux test could be performed again. This would ensure better results.

A major recommendation for this project would be to perform all of the tests more than once in order to get the most accurate results by using the average from various tests. Time constraints have prevented this from happening. Calibration of the thermocouples should be repeated in order to determine the best calibration factors. Calibration could possibly be performed in 1°C temperature increments to obtain better factors for the temperatures.

A recommendation would be to test the rough tube again, at lower Reynolds numbers in order to see the effect of surface roughness on the laminar flow regime. This was not possible for the experiment because it was decided that the lowest and highest Reynolds numbers tested, should be the same in order to compare results successfully. Also, in order to prevent the possibility of burn out of the tube and the damage of the equipment (such as the pumps), a high enough Reynolds number was necessary for the starting value.

6.4 Limitations

The limitations with respect to this project are time, skills and knowledge.

When considering time, this project was very lengthy and required many hours of work for the building and testing phases. This meant that when problems occurred such as the leak in the calming section and the faulty manometer, there was not enough time to rectify or solve the problems. Thus changes to the project were made which have affected the results.

Skills are a limitation to this project because all of the tasks were performed by the student, who is not a professional with respect to the tasks at hand. This means that the drilling and soldering are not necessarily perfect or equal. This could further affect the quality of the results. Although the techniques and methods used were new, it was a valuable learning experience in that I understand the difficulty of the tasks, and I am able to perform them. I gained confidence through this project and I have learnt that I am able to do more than I thought I could.

When this project was started, the time it would take was unexpected. Even though the build was started in the June holidays, the amount of work which needed to be performed was unknown. A lot of independent study was done during the theoretical phase as well as the experimental phase. Decisions were made based on independent research and investigation.

At the beginning of this project, a lot of the concepts were new, and time was spent understanding them. Skills had to be learnt and practised before they could be performed on the actual test section. If the theory and practical sides of this project were known beforehand, further, more in-depth research could be done, as well as a more uniform execution of the test section. A lot of research has been done and the knowledge gained is invaluable.

References

- Armacell. (2010, November). *AP Armaflex Technical Information*. Retrieved May 17, 2013, from Armacell Engineered Foams: [www.armacell.com/www/armacell/ACwwwAttach.nsf/ansFiles/003-003-004-NA\(NA\).pdf/\\$File/003-003-004-NA\(NA\).pdf](http://www.armacell.com/www/armacell/ACwwwAttach.nsf/ansFiles/003-003-004-NA(NA).pdf/$File/003-003-004-NA(NA).pdf)
- Borgnakke, C., & Sonntag, R. E. (2009). *Fundamentals of Thermodynamics Seventh Edition*. Asia: John Wiley & Sons, Inc.
- Cengel, Y. A., & Ghajar, A. J. (2011). *Heat and Mass Transfer Fundamentals and Applications, Fourth Edition*. Singapore: McGraw-Hill .
- Copper Tubing Africa. (2012, November). Plumbing Code of Practice. Johannesburg, South Africa.
- Everts, M. (2012).
- Ghajar, A. J., & Madon, K. F. (1992). Pressure Drop Measurements in the Transition Region for a Circular Tube with Three Different Inlet Configurations. *Experimental Thermal and Fluid Science* , 129-135.
- Ghajar, A. J., & Tam, L.-M. (1994). Heat Transfer Measurements and Correlations in the Transition Region for a Circular Tube with Three Different Inlet Configurations. *Experimental Thermal and Fluid Science* , 79-90.
- Grote, K. (2012). *The influence of multi-walled carbon nanotubes on single-phase heat transfer and pressure drop characteristics in the transitional flow regime of smooth tubes*. Not yet published.
- Manglik, R., & Bergles, A. (1993). Heat transfer and pressure drop correlations for twisted-tape inserts in isothermal tubes: Part 1 - Laminar flows. *Journal of Heat Transfer* 115 , 881-889.
- Meyer, J., & Bateman. (2013). Article in progress.
- Meyer, J., & Olivier, J. (2010). Transitional flow inside enhanced tubes for fully developed and developing flow with different types of inlet disturbances: Part I - Adiabatic pressure drops. *International Journal of Heat and Mass Transfer* , 1587-1597.
- Meyer, J., & Olivier, J. (2010). Transitional flow inside enhanced tubes for fully developed and developing flow with different types of inlet disturbances: Part II - heat transfer. *International Journal of Heat and Mass Transfer* , 1598-1607.
- Meyer, J., McKrell, T., & Grote, K. (2012). The influence of multi-walled carbon nanotubes on single-phase heat transfer and pressure drop characteristics in the transitional flow regime of smooth tubes. *International Journal of Heat and Mass Transfer* 58 , 597-609.
- Olivier, J., & Meyer, J. (2010). Single-Phase Heat Transfer and Pressure Drop of the Cooling of Water inside Smooth Tubes for Transitional Flow with Different Inlet Geometries (RP-1280). *HVAC&R Research*, 16:4 , 471-496.

Olivier, J., & Meyer, J. (2010). Single-Phase Heat Transfer and Pressure Drop of the Cooling of Water inside Smooth Tubes for Transitional Flow with Different Inlet Geometries (RP-1280). *HVAC&Research* 16(4) , 471-496.

PipeLagging. (2013). *Armaflex Pipe Insulation* . Retrieved May 22, 2013, from PipeLagging: www.pipelagging.com/armaflex-pipe-insulation-lagging-tape-50mmx3mmx15m-class-p-71.html

Popiel, C., & Wojtkowiak, J. (2007). Simple Formulas for Thermophysical Properties of Liquid Water for Heat Transfer Calculations (from 0°C to 150°C). *Heat Transfer Engineering* , 87-101.

Tam, H. K., Tam, L. M., & Ghajar, A. J. (2013). Effect of inlet geometries and heating on the entrance and fully-developed friction factors in the laminar and transition regions of a horizontal tube. *Experimental Thermal and Fluid Science* , 680-696.

Tam, L.-M., & Ghajar, A. J. (1997). Effect of Inlet Geometry and Heating on the Fully Developed Friction Factor in the Transition Region of a Horizontal Tube. *Experimental Thermal and Fluid Science* , 52-64.

White, F. M. (2011). *Fluid Mechanics, Seventh Edition*. Mc-Graw Hill: Singapore.

Appendix

Appendix A: Protocol

Project Protocol

MSC 412/422

Determine the influence of surface roughness in the transitional flow regime

Samantha Ayres
1026172

1. Purpose

Research is being done into the transitional flow regime (the region where the Reynolds number changes from laminar to turbulent flow). This region is subject to uncertainties and instabilities. There is also a deficit of information regarding the relationship between heat transfer and mass flow rate. The purpose of this project is to investigate the influence of tube roughness when considering the Reynolds number as a function of the friction factor, and the Nusselt number as a function of mass flow rate (Reynolds number).

2. Objective

The influence of tube roughness will be investigated by measuring the heat transfer and pressure drop at different heat fluxes for water. This will be done using a smooth and rough tube and making comparisons. One set diameter will be used. A constant heat flux and square edge inlet will be used.

3. Goal and Importance

The goal of this project is to determine relationships of the transitional flow regime for a smooth and rough tube, of the same diameter. The relationships to be determined are that of the friction factor and the Reynolds number, as well as that of the Nusselt number and the mass flow rate (Reynolds number).

This project is important because very little information exists for this transitional flow regime, and therefore it is not really used. If relationships can be drawn up for this region, systems could operate here.

4. Scope

The scope of this project involves theoretical research into work that has already been completed with respect to the transitional flow regime. An experiment will be built and setup, where testing of will be completed to determine the pressure drop measurements and the different heat fluxes for water (in a smooth and rough tube). Conclusions will be drawn from the results found.

A graph of friction as a function of the Reynolds number will be drawn up, for both the smooth and rough tubes, as well as a graph of the Nusselt number as a function of the Reynolds number. The beginning and end of the transitional region will be determined. The relationship between the pressure drop (f) and the heat transfer (j) will be calculated.

5. Chapters

5.1 Introduction	17 May
5.2 Literature Study	17 May
5.3 Design	17 May
5.3.1 Experimental Setup	
5.3.2 Calculations	
5.3.3 Methodology	
5.4 Building of the experimental setup	19 July
5.5 Experimental Measurements and Testing	1 August (if second test is required – 15 August)
5.6 Results	27 September
5.7 Conclusions	27 September
5.8 Recommendations	5 October

6. Experimental Setup

- 6.1 Design setup
- 6.2 Make use of a simulation model (Excel or Programme)
- 6.3 Determine means of roughening the tube (eg. Sand)
- 6.4 Do relevant calculations
 - 6.4.1 Pressure drop
 - 6.4.2 Pump specifications
 - 6.4.3 Pressure increase

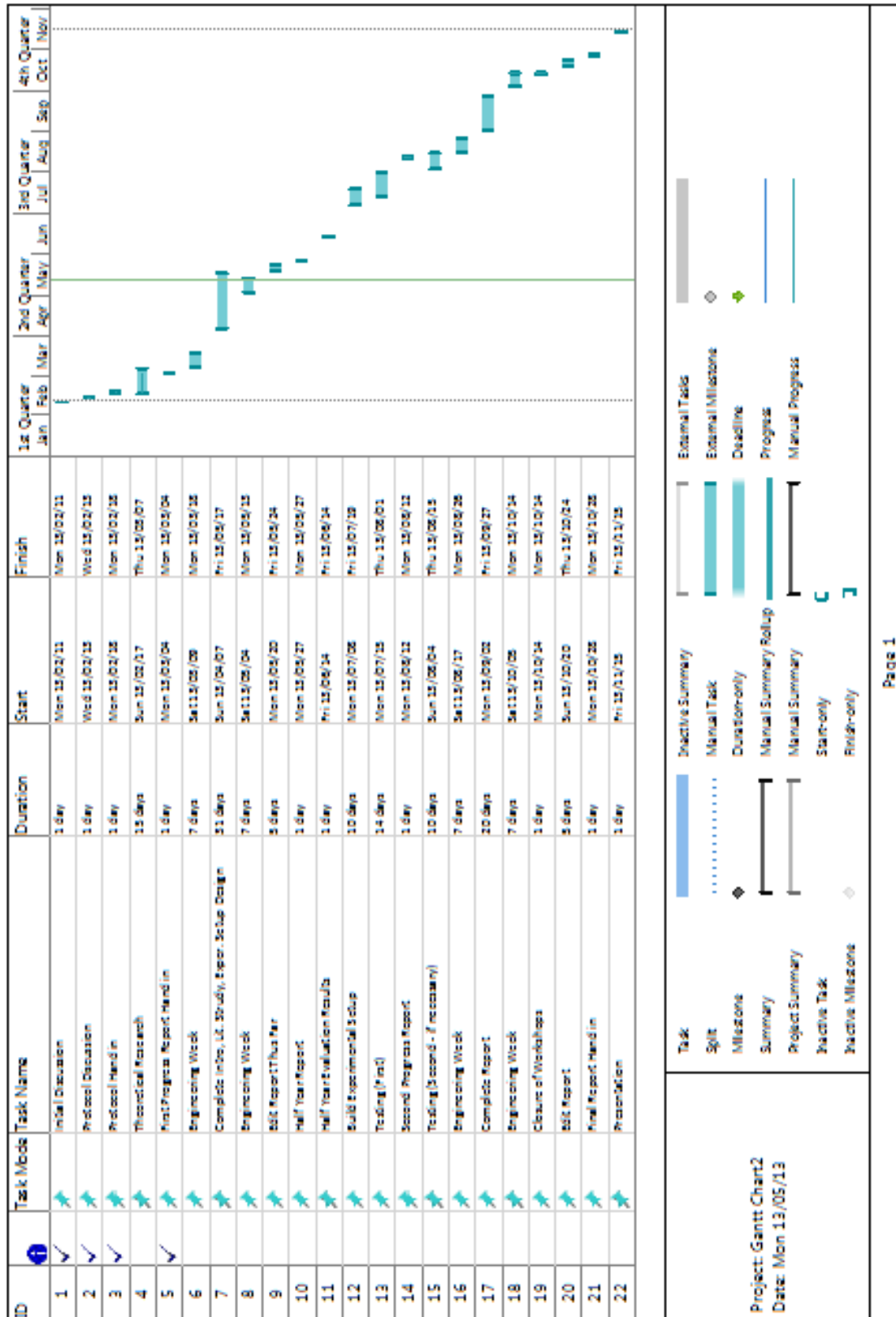
7. Testing

- 7.1 Verification will be completed using the smooth tube
- 7.2 Determine the pressure drop for smooth and rough tube
- 7.3 Determine the heat flux for smooth and rough tube

8. Deliverables

A report will be written to reflect the project and the results obtained, as well as conclusions drawn and possible recommendations. A presentation will be given at the end of the course which will convey the important aspects of the project, and give the results and conclusions.

9. Project Plan



Appendix B: Protocol/Research Project Compliance Matrix

Requirement	Protocol		Project Report	
	Section	Page	Sections	Page
Determine purpose of project	1	1	1.3	2
Determine objectives and requirements for project	2	1	1.4	3
Determine goal and importance of project	3	1	1.5	3
Determine scope of work	4	2	1.5	2
Set out the report in terms of chapters and what needs to be done	5	2	1.6	3
Do theoretical research with respect to work performed on the transitional flow regime	5.2	2	2	4
Design the experimental setup	6	2	3	19
Build the test section	5.4	2	3.5	23
Measure the heat transfer across the test section (temperature increase)	7.3	2	5.2 5.4	38 46
Measure the pressure drop across the test section	7.2	2	4.4	36
Compare Results to other experiments and theoretical information	5.6	2	4.4 5.3	36 45
Draw conclusions with respect to results obtained	5.7	2	5.6 6.2	55 58
Make recommendations for further improvements	5.8	2	6.3	60

Appendix C: Progress Reports

First Progress Report

The aim of this progress report is to show the progress which has been made and the work started so far, with regards to the research project. The supervisor can monitor progress made and determine whether it is sufficient, or if the work needs to be done at a quicker pace.

Thus far, I had planned to do theoretical research into the history of the work done on the transitional flow regime between laminar and turbulent flow. I have done the majority of my research and have started my literature study. I am a bit ahead of schedule, but I prefer to work in this manner. I aim to continue working at this pace on my project, and possibly finish other topics earlier. This will allow for any problems encountered, in the future of the project, to be dealt with in due course. I have set out my report, with the headings I will be using and the lists of figures and tables, as well as the table of contents.

I have researched the work done by Ghajar and his co-workers and I'm currently investigating the work done by Meyer and his team. I have found results for different experiments and will compare these at the end of my literature study. So far I have found correlations between Meyer and Ghajar with the respect to the type of inlet used.

My aim for the next few weeks is to complete my literature study and introduction, so that I can begin with my simulations and calculations as soon as possible. I aim to be finished with the first semesters work before May, so that I can compile my half-year report and not be pushed for time. Once the literature study, simulation and experimental design are complete, I will begin with the building and testing of my experiment. This will give me the results I require to complete this project and report.

I have also started my introduction to the project. Essentially, the work completed up to now will change quite a lot, as further investigation is done. This is a basic introduction which will be added to.

Second Progress Report

The aim of this progress report is to show the progress which has been made and the work started so far, with regards to the research project. The supervisor can monitor progress made and determine whether it is sufficient, or if the work needs to be done at a quicker pace.

Much work has been done on my research project since the handing in of the half year report. Thus far, the majority of the build for my research project has been completed. It has been a lengthy process and has involved intricate tasks that have required much practise before the actual tube lengths could be worked on. It has taken longer than expected to complete the build up to now because more steps were involved in the building process than originally planned for.

The tubes have been drilled and soldered and the thermocouple ends were stripped, soldered and labeled. The pressure taps have been silver soldered onto the tubes and the thermocouples attached. The thermocouples were then attached to the tube at the specific locations.

The build still requires the sanding of the rough tube, wrapping of the tube (with heating wires) and the build of a mixing well in order to have a feasible outlet temperature. The connections will then be put on the tube.

Calibration will then be done for the thermocouples and then an adiabatic test can be done. The formal testing can then be completed by changing the mass flow rates and recording the temperatures and pressure drops.

With respect to the report, both the experimental setup and data reduction sections have been started. It is still necessary to complete these sections before testing can be started, however, the experimental setup section can only be completed once the build is complete. All that remains after these sections, are the results and conclusion parts. A spreadsheet will be created in order to allow for a quick analysis of the results.

Testing can only be done once the laboratory has been fixed to remove the interference, and thus the project is on schedule, as time can be spent finishing off the experimental setup and data reduction sections, whilst waiting for the laboratory to be in order.

I am on schedule in terms of when I can test my project and thus I believe that I will be able to complete this project in time for the hand in date.

Appendix D: Meeting Log

REPORT CARD FOR THESIS MSC 412 and 422

20.13.....

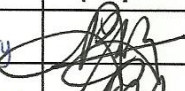




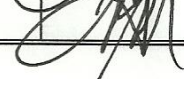
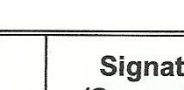
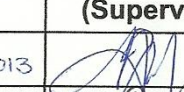

Name Samantha Ayres Reg. no. 10261720





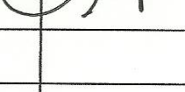

Topic Determine the influence of surface roughness in the transitional flow regime

Supervisor Professor J.P. Meyer

Commencement date:

11 February 2013

Date	Signature (Supervisor)	Signature (Student)	Comments
11 February		S Ayres	Scoping
13 February		S Ayres	Protocol Discussion
15 February		S Ayres	Lab setup
26 February		S Ayres	General Progress Meeting
5 March		S Ayres	Progress Meeting
19 March		S Ayres	Progress Meeting
9 April		S Ayres	
23 April		S Ayres	
14 May		S Ayres	

Date	Signature (Supervisor)	Signature (Student)	Comments
22/05/2013		S Ayres	MSC 412 Report Discussion
3/07/2013		S Ayres	
26/07/2013		S Ayres	Lab work.
28/08/2013		S Ayres	
16/10/2013		S Ayres	
21/10/2013		S Ayres	

Appendix E: Sample Calculations

The following constants were used for these calculations:

Properties at 40°C		
c_p	4179	J/kg·K
μ	0.000653	kg/m·s
k	0.631	W/m·K
ρ	992.1	kg/m ³
Pr	4.32	

Smooth Tube

Laminar Region

$$Re = \frac{\rho V D}{\mu}$$

$$\begin{aligned} V &= \frac{Re \mu}{\rho D} \\ &= \frac{1000 \times 0.000653}{992.1 \times 0.02} \\ &= 0.033 \text{ m/s} \end{aligned}$$

$$\begin{aligned} \dot{m} &= \rho A V \\ &= 992.1 \times \frac{\pi}{4} (0.02^2) \times 0.033 \\ &= 0.0103 \text{ kg/s} \end{aligned}$$

$$\begin{aligned} f &= \frac{64}{Re} \\ &= 0.064 \end{aligned}$$

$$\begin{aligned} h_f &= f \frac{L V^2}{D 2g} \\ &= 0.064 \times \frac{2}{0.02} \times \frac{0.033^2}{2 \times 9.81} \\ &= 3.55 \times 10^{-4} \text{ m} \end{aligned}$$

$$\begin{aligned} \Delta P &= h_f \rho g \\ &= 3.55 \times 10^{-4} \times 992.1 \times 9.81 \\ &= 3.457 \text{ Pa} \end{aligned}$$

$$\dot{Q} = \dot{m} c_p \Delta T$$

$$\begin{aligned}\Delta T &= \frac{\dot{Q}}{\dot{m}c_p} \\ &= \frac{800}{0.0103 \times 4\,179} \\ &= 18.56 \text{ }^\circ\text{C}\end{aligned}$$

$$\begin{aligned}\Delta T &= \frac{\dot{Q}}{\dot{m}c_p} \\ &= \frac{1000}{0.0103 \times 4\,179} \\ &= 23.23 \text{ }^\circ\text{C}\end{aligned}$$

$$\begin{aligned}\Delta T &= \frac{\dot{Q}}{\dot{m}c_p} \\ &= \frac{1200}{0.0103 \times 4\,179} \\ &= 27.88 \text{ }^\circ\text{C}\end{aligned}$$

Turbulent Region

$$\begin{aligned}V &= \frac{Re\mu}{\rho D} \\ &= \frac{9\,000 \times 0.000653}{992.1 \times 0.02} \\ &= 0.2962 \text{ m/s}\end{aligned}$$

$$\begin{aligned}\dot{m} &= \rho AV \\ &= 992.1 \times \frac{\pi}{4} (0.02^2) \times 0.2962 \\ &= 0.0923 \text{ kg/s}\end{aligned}$$

$$\frac{1}{\sqrt{f}} \cong -1.8 \log \left(\frac{6.9}{Re} + \left(\frac{\epsilon/D}{3.7} \right)^{1.11} \right)$$

$$f = 0.0318$$

$$\begin{aligned}h_f &= f \frac{L V^2}{D 2g} \\ &= 0.0318 \times \frac{2}{0.02} \times \frac{0.2962^2}{2 \times 9.81} \\ &= 0.014 \text{ m}\end{aligned}$$

$$\begin{aligned}\Delta P &= h_f \rho g \\ &= 0.014 \times 992.1 \times 9.81 \\ &= 136.26 \text{ Pa}\end{aligned}$$

$$\dot{Q} = \dot{m}c_p \Delta T$$

$$\begin{aligned}\Delta T &= \frac{\dot{Q}}{\dot{m}c_p} \\ &= \frac{800}{0.0923 \times 4\,179} \\ &= 2.074 \text{ }^\circ\text{C}\end{aligned}$$

$$\begin{aligned}\Delta T &= \frac{\dot{Q}}{\dot{m}c_p} \\ &= \frac{1000}{0.0923 \times 4\,179} \\ &= 2.59 \text{ }^\circ\text{C}\end{aligned}$$

$$\begin{aligned}\Delta T &= \frac{\dot{Q}}{\dot{m}c_p} \\ &= \frac{1200}{0.0923 \times 4\,179} \\ &= 3.11 \text{ }^\circ\text{C}\end{aligned}$$

Rough Tube

Laminar Region

$$\begin{aligned} V &= \frac{Re\mu}{\rho D} \\ &= \frac{1000 \times 0.000653}{992.1 \times 0.02} \\ &= 0.033 \text{ m/s} \end{aligned}$$

$$\begin{aligned} \dot{m} &= \rho AV \\ &= 992.1 \times \frac{\pi}{4} (0.02^2) \times 0.033 \\ &= 0.0103 \text{ kg/s} \end{aligned}$$

$$\begin{aligned} f &= \frac{64}{Re} \\ &= 0.064 \end{aligned}$$

$$\begin{aligned} h_f &= f \frac{L V^2}{D 2g} \\ &= 0.064 \times \frac{2}{0.02} \times \frac{0.033^2}{2 \times 9.81} \\ &= 3.55 \times 10^{-4} \text{ m} \end{aligned}$$

$$\begin{aligned} \Delta P &= h_f \rho g \\ &= 3.55 \times 10^{-4} \times 992.1 \times 9.81 \\ &= 3.457 \text{ Pa} \end{aligned}$$

$$\dot{Q} = \dot{m} c_p \Delta T$$

$$\begin{aligned} \Delta T &= \frac{\dot{Q}}{\dot{m} c_p} \\ &= \frac{800}{0.0103 \times 4179} \\ &= 18.56 \text{ }^\circ\text{C} \end{aligned}$$

$$\begin{aligned} \Delta T &= \frac{\dot{Q}}{\dot{m} c_p} \\ &= \frac{1000}{0.0103 \times 4179} \\ &= 23.23 \text{ }^\circ\text{C} \end{aligned}$$

$$\begin{aligned} \Delta T &= \frac{\dot{Q}}{\dot{m} c_p} \\ &= \frac{1200}{0.0103 \times 4179} \\ &= 27.88 \text{ }^\circ\text{C} \end{aligned}$$

Turbulent Region

$$\begin{aligned} V &= \frac{Re\mu}{\rho D} \\ &= \frac{9000 \times 0.000653}{992.1 \times 0.02} \\ &= 0.2962 \text{ m/s} \end{aligned}$$

$$\begin{aligned}
\dot{m} &= \rho AV \\
&= 992.1 \times \frac{\pi}{4} (0.02^2) \times 0.2962 \\
&= 0.0923 \text{ kg/s}
\end{aligned}$$

$$\frac{1}{\sqrt{f}} \cong -1.8 \log \left(\frac{6.9}{\text{Re}} + \left(\frac{\epsilon/D}{3.7} \right)^{1.11} \right)$$

$$f = 0.0435$$

$$\begin{aligned}
h_f &= f \frac{L V^2}{D 2g} \\
&= 0.0435 \times \frac{2}{0.02} \times \frac{0.2962^2}{2 \times 9.81} \\
&= 0.0195 \text{ m}
\end{aligned}$$

$$\begin{aligned}
\Delta P &= h_f \rho g \\
&= 0.0195 \times 992.1 \times 9.81 \\
&= 189.78 \text{ Pa}
\end{aligned}$$

$$\dot{Q} = \dot{m} c_p \Delta T$$

$$\begin{aligned}
\Delta T &= \frac{\dot{Q}}{\dot{m} c_p} \\
&= \frac{800}{0.0923 \times 4179} \\
&= 2.074 \text{ }^\circ\text{C}
\end{aligned}$$

$$\begin{aligned}
\Delta T &= \frac{\dot{Q}}{\dot{m} c_p} \\
&= \frac{1000}{0.0923 \times 4179} \\
&= 2.59 \text{ }^\circ\text{C}
\end{aligned}$$

$$\begin{aligned}
\Delta T &= \frac{\dot{Q}}{\dot{m} c_p} \\
&= \frac{1200}{0.0923 \times 4179} \\
&= 3.11 \text{ }^\circ\text{C}
\end{aligned}$$

Insulation

Assuming a heat transfer coefficient of $10 \text{ W/m}^2 \cdot \text{K}$, an ambient temperature of 20°C and an average fluid temperature of 40°C :

$$\begin{aligned}
\dot{Q}_{\text{without insulation}} &= h A_s (T_{\text{avg}} - T_\infty) \\
&= 10 \times \pi \times 0.022 \times 2 \times (40 - 20) \\
&= 27.65 \text{ W}
\end{aligned}$$

Assuming that the insulation prevents 90% heat loss:

$$\begin{aligned}
\dot{Q}_{\text{with insulation}} &= 0.15 \dot{Q}_{\text{without insulation}} \\
&= 4.1475 \text{ W}
\end{aligned}$$

$$\dot{Q}_{\text{with insulation}} = \frac{(T_{\text{avg}} - T_\infty)}{R_{\text{total}}}$$

$$\begin{aligned}
 R_{total} &= \frac{(T_{avg} - T_{\infty})}{\dot{Q}_{with\ insulation}} \\
 &= \frac{40 - 20}{4.1475} \\
 &= 4.822 \text{ }^{\circ}\text{C/W}
 \end{aligned}$$

$$R_{total} = R_{cyl} + R_{insulation} + R_i + R_o$$

$$\begin{aligned}
 R_{cyl} &= \frac{\ln\left(\frac{r_2}{r_1}\right)}{2\pi kL} \\
 &= \frac{\ln\left(\frac{11}{10}\right)}{4\pi(401)} \\
 &= 1.8914 \times 10^{-5} \text{ }^{\circ}\text{C/W}
 \end{aligned}$$

$$\begin{aligned}
 R_i &= \frac{1}{h_i A_i} \\
 &= \frac{1}{11.04 \times \pi \times 0.02 \times 2} \\
 &= 0.7208 \text{ }^{\circ}\text{C/W}
 \end{aligned}$$

$$\begin{aligned}
 R_o &= \frac{1}{h_o A_o} \\
 &= \frac{1}{10 \times \pi \times 0.022 \times 2} \\
 &= 0.723 \text{ }^{\circ}\text{C/W}
 \end{aligned}$$

$$\therefore R_{insulation} = 3.378 \text{ }^{\circ}\text{C/W}$$

The thermal conductivity of Armaflex insulation is 0.038 W/m·K at 40°C (PipeLagging, 2013).

$$\begin{aligned}
 R_{insulation} &= \frac{\ln\left(\frac{r_2}{r_1}\right)}{2\pi kL} \\
 r_2 &= r_1 e^{R_{insulation} 2\pi kL} \\
 &= 0.011 \times e^{4\pi \times 0.038 \times 3.378} \\
 &= 0.0552 \text{ m}
 \end{aligned}$$

Therefore the required thickness of the insulation is 55.2 mm.

When assuming that the insulation prevents 90% of the heat transfer, the thickness of the insulation is found to be 174 mm which is large. Therefore an assumption that 99% of the heat can be resisted by the insulation is not feasible.

Appendix F: Spreadsheet Examples

	A	B	C	D	E	F	G
1	Properties at 40°C						
2	cp	4179	J/kgK				
3	μ	0.000653	kg/ms				
4	k	0.631	W/mK				
5	ρ	992.1	kg/m3				
6	Pr	4.32					
7	ftam	64/Re	=P11*(E9^2)/4				
8							
9	Smooth				0.0208		assume L=2m
10	Re	500	600	700	800	900	1000
11	D	0.02	0.02	0.02	0.02	0.02	0.02
12	A	=B11^1/2*P11/4	=C11^1/2*P11/4	=D11^1/2*P11/4	=E11^1/2*P11/4	=F11^1/2*P11/4	=G11^1/2*P11/4
13	V	=B10^3*(0.000653/(992.1*B11))	=C10^3*(0.000653/(992.1*C11))	=D10^3*(0.000653/(992.1*D11))	=E10^3*(0.000653/(992.1*E11))	=F10^3*(0.000653/(992.1*F11))	=G10^3*(0.000653/(992.1*G11))
14	A	=P11*(E9^2)/4	=P11*(E9^2)/4	=P11*(E9^2)/4	=P11*(E9^2)/4	=P11*(E9^2)/4	=P11*(E9^2)/4
15	f	=64/B10	=64/C10	=64/D10	=64/E10	=64/F10	=64/G10
16	hf	=B15^1/2/B11*(B13^3/2)/(2*9.81)	=C15^1/2/C11*(C13^3/2)/(2*9.81)	=D15^1/2/D11*(D13^3/2)/(2*9.81)	=E15^1/2/E11*(E13^3/2)/(2*9.81)	=F15^1/2/F11*(F13^3/2)/(2*9.81)	=G15^1/2/G11*(G13^3/2)/(2*9.81)
17	P	=B16^9.81*992.1	=C16^9.81*992.1	=D16^9.81*992.1	=E16^9.81*992.1	=F16^9.81*992.1	=G16^9.81*992.1
18	Nu=h/k	4.36	4.36	4.36	4.36	4.36	4.36
19	h	=B18^0.631/2	=C18^0.631/2	=D18^0.631/2	=E18^0.631/2	=F18^0.631/2	=G18^0.631/2
20	m	=B19^1.813*P11*(B11^1/2)/4	=C19^1.813*P11*(C11^1/2)/4	=D19^1.813*P11*(D11^1/2)/4	=E19^1.813*P11*(E11^1/2)/4	=F19^1.813*P11*(F11^1/2)/4	=G19^1.813*P11*(G11^1/2)/4
21	dT	=B22/(B20^4179)	=C22/(C20^4179)	=D22/(D20^4179)	=E22/(E20^4179)	=F22/(F20^4179)	=G22/(G20^4179)
22	Q=V	800	800	800	800	800	800
23	m=Q/CT	=B22/(4179*40)	=C22/(4179*40)	=D22/(4179*40)	=E22/(4179*40)	=F22/(4179*40)	=G22/(4179*40)
24	V=mm/AP	=B23/(B14^992.1)	=C23/(C14^992.1)	=D23/(D14^992.1)	=E23/(E14^992.1)	=F23/(F14^992.1)	=G23/(G14^992.1)
25	f	=64/B10	=64/C10	=64/D10	=64/E10	=64/F10	=64/G10
26	hf	=B25^1/2/(0.02*(B24^2)/(2*9.81))	=C25^1/2/(0.02*(C24^2)/(2*9.81))	=D25^1/2/(0.02*(D24^2)/(2*9.81))	=E25^1/2/(0.02*(E24^2)/(2*9.81))	=F25^1/2/(0.02*(F24^2)/(2*9.81))	=G25^1/2/(0.02*(G24^2)/(2*9.81))
27	P	=B26^9.81*9.81	=C26^9.81*9.81	=D26^9.81*9.81	=E26^9.81*9.81	=F26^9.81*9.81	=G26^9.81*9.81
28							

	A	CO	CP	CQ	CR
1	Properties at 40°C				
2	cp				
3	μ				
4	k				
5	p				
6	Pr				
7	flam				
8					
9	Smooth				
10	Re	9600	9700	9800	9900
11	D	0.02	0.02	0.02	0.02
12	A	$\frac{-(CO11^2)P}{4}$	$\frac{-(CP11^2)P}{4}$	$\frac{-(CQ11^2)P}{4}$	$\frac{-(CR11^2)P}{4}$
13	V	$-CO10^0.000653/(992.1^*CO11)$	$-CP10^0.000653/(992.1^*CP11)$	$-CQ10^0.000653/(992.1^*CQ11)$	$-CR10^0.000653/(992.1^*CR11)$
14	A	$-P/(0.02^2)/4$	$-P/(0.02^2)/4$	$-P/(0.02^2)/4$	$-P/(0.02^2)/4$
15	f	$\frac{-(1/(-1.8^*LOG((6.9/(CO10).10)))^2}{CO15^2/(CO11^*(CO13^2)/(2^*9.81))}$	$\frac{-(1/(-1.8^*LOG((6.9/(CP10).10)))^2}{CP15^2/(CP11^*(CP13^2)/(2^*9.81))}$	$\frac{-(1/(-1.8^*LOG((6.9/(CQ10).10)))^2}{CQ15^2/(CQ11^*(CQ13^2)/(2^*9.81))}$	$\frac{-(1/(-1.8^*LOG((6.9/(CR10).10)))^2}{CR15^2/(CR11^*(CR13^2)/(2^*9.81))}$
16	hf	$-CO16^*9.81^*992.1$	$-CP16^*9.81^*992.1$	$-CQ16^*9.81^*992.1$	$-CR16^*9.81^*992.1$
17	P	$\frac{-(P/(70^*CO15^*(CO10)^{(1.11)^*(4.32^*(1/3))})}{CO18^*0.631/2}$	$\frac{-(P/(70^*CP15^*(CP10)^{(1.11)^*(4.32^*(1/3))})}{CP18^*0.631/2}$	$\frac{-(P/(70^*CQ15^*(CQ10)^{(1.11)^*(4.32^*(1/3))})}{CQ18^*0.631/2}$	$\frac{-(P/(70^*CR15^*(CR10)^{(1.11)^*(4.32^*(1/3))})}{CR18^*0.631/2}$
18	Nu=h/k	$-992.1^*CO13^*P/(CO11^2)/4$	$-992.1^*CP13^*P/(CP11^2)/4$	$-992.1^*CQ13^*P/(CQ11^2)/4$	$-992.1^*CR13^*P/(CR11^2)/4$
19	h	$-CO22/(CO20^*4179)$	$-CP22/(CP20^*4179)$	$-CQ22/(CQ20^*4179)$	$-CR22/(CR20^*4179)$
20	m	800	800	800	800
21	dT	$-CO22/(4179^*40)$	$-CP22/(4179^*40)$	$-CQ22/(4179^*40)$	$-CR22/(4179^*40)$
22	Q=IV	$-CO23/(CO14^*992.1)$	$-CP23/(CP14^*992.1)$	$-CQ23/(CQ14^*992.1)$	$-CR23/(CR14^*992.1)$
23	m=Q/cT	$\frac{-(1/(-1.8^*LOG((6.9/(CP10).10)))^2}{CO25^2/(0.02^*(CO24^2)/(2^*9.81))}$	$\frac{-(1/(-1.8^*LOG((6.9/(CP10).10)))^2}{CP25^2/(0.02^*(CP24^2)/(2^*9.81))}$	$\frac{-(1/(-1.8^*LOG((6.9/(CQ10).10)))^2}{CQ25^2/(0.02^*(CQ24^2)/(2^*9.81))}$	$\frac{-(1/(-1.8^*LOG((6.9/(CR10).10)))^2}{CR25^2/(0.02^*(CR24^2)/(2^*9.81))}$
24	V=m/AP	$-CO26^*992.1^*9.81$	$-CP26^*992.1^*9.81$	$-CQ26^*992.1^*9.81$	$-CR26^*992.1^*9.81$
25	f				
26	hf				
27	P				
28					

	A	B	C	D	E	F	G	H
1	Properties at 40°C							
2	cp	4179	-/kgK					
3	μ	0.000653	kg/ms					
4	k	0.631	W/mK					
5	ρ	992.1	kg/m3					
6	Pr	4.32						
7	flam	64/Re		=P/(E9^2)/4				
8								
9	Rough	20mm			0.02			
10	Re	500	600	700	800	900	1000	1100
11	D	0.02	0.02	0.02	0.02	0.02	0.02	0.02
12	A	=B11^2*P/(I)/4	=C11^2*P/(I)/4	=D11^2*P/(I)/4	=E11^2*P/(I)/4	=F11^2*P/(I)/4	=G11^2*P/(I)/4	=H11^2*P/(I)/4
13	E (m)	0.0002	0.0002	0.0002	0.0002	0.0002	0.0002	0.0002
14	E/D	=E13/B11	=C13/C11	=D13/D11	=E13/E11	=F13/F11	=G13/G11	=H13/H11
15	V	=E10*0.000653/(992.1*B11)	=C10*0.000653/(992.1*C11)	=D10*0.000653/(992.1*D11)	=E10*0.000653/(992.1*E11)	=F10*0.000653/(992.1*F11)	=G10*0.000653/(992.1*G11)	=H10*0.000653/(992.1*H11)
16	A	=P/(E9^2)/4	=P/(E9^2)/4	=P/(E9^2)/4	=P/(E9^2)/4	=P/(E9^2)/4	=P/(E9^2)/4	=P/(E9^2)/4
17	f	=64/B10	=64/C10	=64/D10	=64/E10	=64/F10	=64/G10	=64/H10
18	hf	=E17^2/(B11)*(B15^2)/(2*9.81)	=C17^2/(C11)*(C15^2)/(2*9.81)	=D17^2/(D11)*(D15^2)/(2*9.81)	=E17^2/(E11)*(E15^2)/(2*9.81)	=F17^2/(F11)*(F15^2)/(2*9.81)	=G17^2/(G11)*(G15^2)/(2*9.81)	=H17^2/(H11)*(H15^2)/(2*9.81)
19	P	=E18*9.81*992.1	=C18*9.81*992.1	=D18*9.81*992.1	=E18*9.81*992.1	=F18*9.81*992.1	=G18*9.81*992.1	=H18*9.81*992.1
20	Nu=hi/k	4.36	4.36	4.36	4.36	4.36	4.36	4.36
21	h	=E20*0.631/2	=C20*0.631/2	=D20*0.631/2	=E20*0.631/2	=F20*0.631/2	=G20*0.631/2	=H20*0.631/2
22	m	=E92.1*B15*P/(I)*(B11^2)/4	=C92.1*C15*P/(I)*(C11^2)/4	=D92.1*D15*P/(I)*(D11^2)/4	=E92.1*E15*P/(I)*(E11^2)/4	=F92.1*F15*P/(I)*(F11^2)/4	=G92.1*G15*P/(I)*(G11^2)/4	=H92.1*H15*P/(I)*(H11^2)/4
23	dT	=E24/(E22*4179)	=C24/(C22*4179)	=D24/(D22*4179)	=E24/(E22*4179)	=F24/(F22*4179)	=G24/(G22*4179)	=H24/(H22*4179)
24	Q=IV	1000	1000	1000	1000	1000	1000	1000
25	m=Q/CT	=E24/(4179*40)	=C24/(4179*40)	=D24/(4179*40)	=E24/(4179*40)	=F24/(4179*40)	=G24/(4179*40)	=H24/(4179*40)
26	V=m/AP	=E25/(E16*992.1)	=C25/(C16*992.1)	=D25/(D16*992.1)	=E25/(E16*992.1)	=F25/(F16*992.1)	=G25/(G16*992.1)	=H25/(H16*992.1)
27	f	=64/B10	=64/C10	=64/D10	=64/E10	=64/F10	=64/G10	=64/H10
28	hf	=E27^2/(0.02)*(E26^2)/(2*9.81)	=C27^2/(0.02)*(C26^2)/(2*9.81)	=D27^2/(0.02)*(D26^2)/(2*9.81)	=E27^2/(0.02)*(E26^2)/(2*9.81)	=F27^2/(0.02)*(F26^2)/(2*9.81)	=G27^2/(0.02)*(G26^2)/(2*9.81)	=H27^2/(0.02)*(H26^2)/(2*9.81)
29	P	=E28*992.1*9.81	=C28*992.1*9.81	=D28*992.1*9.81	=E28*992.1*9.81	=F28*992.1*9.81	=G28*992.1*9.81	=H28*992.1*9.81
30								

	A	CO	CP	CQ	CR
1	Properties at 40°C				
2	cp				
3	μ				
4	k				
5	ρ				
6	Pr				
7	flam				
8					
9	Rough				
10	Re	9600	9700	9800	9900
11	D	0.02	0.02	0.02	0.02
12	A	$=(CO11^2)*PI()/4$	$=(CP11^2)*PI()/4$	$=(CQ11^2)*PI()/4$	$=(CR11^2)*PI()/4$
13	E (m)	0.0002	0.0002	0.0002	0.0002
14	E/D	$=CO13/CO11$	$=CP13/CP11$	$=CQ13/CQ11$	$=CR13/CR11$
15	V	$=CO10*0.000653/(992.1*CO11)$	$=CP10*0.000653/(992.1*CP11)$	$=CQ10*0.000653/(992.1*CQ11)$	$=CR10*0.000653/(992.1*CR11)$
16	A	$=PI()*(0.02^2)/4$	$=PI()*(0.02^2)/4$	$=PI()*(0.02^2)/4$	$=PI()*(0.02^2)/4$
17	f	$=1/(-1.8*LOG(((6.9/CO10)+((CO14/3.7)^(1.11))),10)))^2$	$=1/(-1.8*LOG(((6.9/CP10)+((CP14/3.7)^(1.11))),10)))^2$	$=1/(-1.8*LOG(((6.9/CQ10)+((CQ14/3.7)^(1.11))),10)))^2$	$=1/(-1.8*LOG(((6.9/CR10)+((CR14/3.7)^(1.11))),10)))^2$
18	hf	$=CO17^2/CO11*(CO15^2)/(2*9.81)$	$=CP17^2/CP11*(CP15^2)/(2*9.81)$	$=CQ17^2/CQ11*(CQ15^2)/(2*9.81)$	$=CR17^2/CR11*(CR15^2)/(2*9.81)$
19	P	$=CO18*9.81*992.1$	$=CP18*9.81*992.1$	$=CQ18*9.81*992.1$	$=CR18*9.81*992.1$
20	Nu=h/k	$=(PI()/70)*CO17*(CO10^1.11)*(4.32^1/3)$	$=(PI()/70)*CP17*(CP10^1.11)*(4.32^1/3)$	$=(PI()/70)*CQ17*(CQ10^1.11)*(4.32^1/3)$	$=(PI()/70)*CR17*(CR10^1.11)*(4.32^1/3)$
21	h	$=CO20*0.631/2$	$=CP20*0.631/2$	$=CQ20*0.631/2$	$=CR20*0.631/2$
22	m	$=992.1*CO15*PI()*(CO11^2)/4$	$=992.1*CP15*PI()*(CP11^2)/4$	$=992.1*CQ15*PI()*(CQ11^2)/4$	$=992.1*CR15*PI()*(CR11^2)/4$
23	dt	$=CO24/(CO22*4179)$	$=CP24/(CP22*4179)$	$=CQ24/(CQ22*4179)$	$=CR24/(CR22*4179)$
24	Q=IV	1000	1000	1000	1000
25	m=Q/CT	$=CO24/(4179*40)$	$=CP24/(4179*40)$	$=CQ24/(4179*40)$	$=CR24/(4179*40)$
26	N=m/AP	$=CO25/(CO16*992.1)$	$=CP25/(CP16*992.1)$	$=CQ25/(CQ16*992.1)$	$=CR25/(CR16*992.1)$
27	f	$=1/(-1.8*LOG(((6.9/CP10)+((CP10/10))),10)))^2$	$=1/(-1.8*LOG(((6.9/CO10)+((CO10/10))),10)))^2$	$=1/(-1.8*LOG(((6.9/CQ10)+((CQ10/10))),10)))^2$	$=1/(-1.8*LOG(((6.9/CR10)+((CR10/10))),10)))^2$
28	hf	$=CO27^2/(0.02)*(CO26^2)/(2*9.81)$	$=CP27^2/(0.02)*(CP26^2)/(2*9.81)$	$=CQ27^2/(0.02)*(CQ26^2)/(2*9.81)$	$=CR27^2/(0.02)*(CR26^2)/(2*9.81)$
29	P	$=CO28*992.1*9.81$	$=CP28*992.1*9.81$	$=CQ28*992.1*9.81$	$=CR28*992.1*9.81$
30					

Appendix G: Data Sheets



The combination of chemical and physical properties of Teflon®/Neoflon is a result of its true fluorocarbon structure. This unusual structure leads to a material which has an almost universal chemical inertness; complete insolubility in all known solvents below 300°C (572°F); excellent thermal stability; and unsurpassed electrical properties including low dielectric loss, low dielectric constant and high dielectric strength. Furthermore, Teflon/Neoflon does not embrittle at very low temperatures.

Properties of Teflon® Insulation

General Properties of Neoflon and Teflon®

	Neoflon/Teflon® FEP	Neoflon/Teflon® PFA
Chemical Resistance: hydrocarbons, ethylene glycol, battery acid, brake fluids, other chemicals	NO EFFECT	NO EFFECT
Resistance to weathering	NO EFFECT	NO EFFECT
Water absorption (ASTM D570)	0.1%	0.1%
Flammability (UL 83, Vertical Wire Flame Test)*	NO AFTER BURN	NO AFTER BURN
Melting Point °F	518°F	590°F
Melting Point °C	270°C	300°C
Upper Service Temperature °C (°F) 1500 to 2000 hrs. estimated 20,000 hrs. Cold bend @ -65°C 2.5 K V for 5 min.	200°C (392°F) 177°C (350°F) PASS	288°C (550°F) 260°C (500°F) PASS
Specific gravity	2.15	2.15

Mechanical and Electrical Properties

	Neoflon/Teflon FEP	Neoflon/Teflon PFA
Tensile strength, psi 23°C (73°F) ASTM D638	3,000	4,000
Elongation, % 23°C (73°F) ASTM D638	300	300
Flexural modulus, psi 23°C (73°F) ASTM D790	95,000	95,000
Flex life, MIT (7 to 9 mils) 82°C (180°F) Flexes	100,000	200,000
Impact Strength, ft.lb/in.: ASTM D256 Room temperature	NO BREAK	NO BREAK
-54°C (-65°F)	10	10
Coefficient of friction, 10 fpm, 100 psi	0.3	0.2
Dynamic cut-through (lb) Instron ½" radius blade moving at 0.2"/min. (0.0031" insulation thickness) 23°C	118	
75°C	73	
Dielectric constant, ASTM D50	2.1	2.1
Volume resistivity, ohm-cm ASTM D257	10 ¹¹	10 ¹¹
Dissipation Factor, ASTM D150, 10 ³ - 10 ⁶ Hz	0.001	0.0004



**NOW!
AVAILABLE
IN PRE-
SPOOLED
LENGTHS**

Resistance vs. Wire Diameter (Resistance in ohms per double foot @ 20°C [68°F])

AWG No.	Diameter inches	Diameter mm	Type K ^{††} CHROME/ALUMINUM	Type J Iron/Constantan	Type T Copper/Constantan	Type E CHROME/ALUMINUM	Type S Pt/Pt10%Rh	Type R Pt/Pt13%Rh	Type R/SX Copper Alloy 11**	Type C [†] W5%Re/W26%Re	Type CX Alloy 405/Alloy 428	Type G [†] W/W26%Re	Type D [†] W3%Re/W25%Re	Type BX Copper/Copper
6	0.182	4.11	0.023	0.014	0.012	0.027	0.007	0.007	0.003	0.009	0.014	0.008	0.009	0.000790
8	0.129	3.25	0.037	0.022	0.019	0.044	0.011	0.011	0.004	0.015	0.023	0.012	0.015	0.001258
10	0.102	2.59	0.058	0.034	0.029	0.069	0.018	0.018	0.007	0.023	0.037	0.020	0.022	0.001998
12	0.081	2.06	0.091	0.054	0.046	0.109	0.028	0.029	0.011	0.037	0.058	0.031	0.035	0.00318
14	0.064	1.63	0.146	0.087	0.074	0.175	0.045	0.047	0.018	0.058	0.093	0.049	0.055	0.00505
16	0.051	1.30	0.230	0.137	0.117	0.276	0.071	0.073	0.026	0.092	0.148	0.078	0.088	0.00803
18	0.040	1.02	0.374	0.222	0.190	0.448	0.116	0.119	0.045	0.148	0.238	0.126	0.138	0.01277
20	0.032	0.81	0.586	0.357	0.298	0.707	0.185	0.190	0.071	0.235	0.371	0.200	0.220	0.02030
24	0.0201	0.51	1.490	0.878	0.7526	1.78	0.464	0.478	0.180	0.594	0.941	0.560	0.560	0.05134
28	0.0159	0.40	2.381	1.405	1.204	2.836	0.740	0.760	0.288	0.945	1.503	0.803	0.890	0.08162
30	0.0100	0.25	5.984	3.551	3.043	7.169	1.85	1.91	0.727	2.38	3.800	2.03	2.26	0.2064
32	0.0080	0.20	9.524	5.999	4.758	11.31	1.96	3.04	1.136	3.8	5.94	3.22	3.60	0.3282
34	0.0063	0.16	15.17	8.946	7.66	18.09	4.66	4.82	1.832	6.04	9.57	5.10	5.70	0.5218
36	0.0050	0.13	24.08	14.20	12.17	28.76	7.40	7.64	2.908	9.6	15.20	8.16	9.10	0.8296
38	0.0039	0.10	38.20	23.35	19.99	45.41	11.6	11.85	4.780	15.3	24.98	12.9	15.3	1.3192
40	0.00315	0.08	60.88	37.01	31.64	73.57	18.6	19.3	7.327	24.4	38.30	20.6	23.0	2.068
44	0.0020	0.051	149.6	88.78	76.09	179.20	74.0	76.5	18.18	60.2	95.00	51.1	56.9	5.134
50	0.0010	0.025	598.4	355.1	304.3	716.9	185	191	72.7	240	380.0	204	227	20.64
56	0.00049	0.012	2408	1420	1217	2816	740	764	302.8	1000	1583	850	945	86.38

* Increase the resistance by 19% for nickel plated, type RTD wire
† Not ANSI symbol

** Maximum Resistance of reviewed wire
†† Resistivity for Ni is 1.324 times type K values

Appendix H: Article